CHALMERS
UNIVERSITY OF TECHNOLOGY

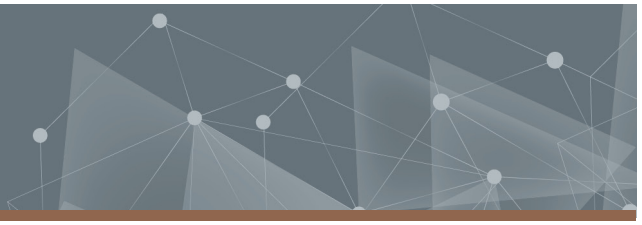

Converter Interaction Stability Analysis Tools

EENX30
Master's thesis in Sustainable Electric Power Engineering & Electromobility

Rasmus Andreasson & Victor Rasmusson

DEPARTMENT OF ELECTRICAL ENGINEERING

CHALMERS UNIVERSITY OF TECHNOLOGY
Gothenburg, Sweden 2026
www.chalmers.se

Master's thesis 2026

Converter interaction stability analysis tools

Victor Rasmusson and Rasmus Andreasson

CHALMERS
UNIVERSITY OF TECHNOLOGY

Department of Electric Power Engineering
Division of Electric Power Engineering
Chalmers University of Technology
Gothenburg, Sweden 2026

Converter interaction stability analysis tools
Victor Rasmusson
Rasmus Andreasson

Supervisor: Gustavo Pinares, Hitachi Energy
Examiner: Massimo Bongiorno, Department of Electric Power Engineering

Master's Thesis 2026
Department of Electrical Engineering
Division of Electric Power Engineering

Chalmers University of Technology
SE-412 96 Gothenburg
Telephone +46 31 772 1000

Typeset in LaTeX
Gothenburg, Sweden 2026

Abstract

As a result of efforts to reduce greenhouse gas emissions, the use of renewable energy has increased and, with these, power sources being integrated into the power system through power electronic interface devices (PEIDs). The dynamic behavior that PEIDs introduce has resulted in new stability challenges. Multiple cases of undamped oscillations originating from converters interacting with other grid elements has already occurred and understanding the instability mechanism is essential.

This thesis investigates methods and tools for converter interaction stability analysis and develops an automated tool for frequency domain stability assessment. Existing open source tools and different methodologies are evaluated with respect to their accuracy, computational efficiency and applicability. Requirements in the area from transmission system operators (TSO) are also reviewed.

The tool proposed in this thesis is based on sequence-domain frequency injections with multi-frequency perturbations to improve computational efficiency. Both Single-Input-Single-Output (SISO) and Multiple-input-Multiple-Output (MIMO)-based analysis methods are implemented and compared, including Nyquist-based criterion, disk margin evaluation and passivity-based a valuation. The tool is validated against an existing mathematical framework and benchmarked against already existing tools, as well as tested on a detailed MMC model.

The results show that the developed framework provides accurate, fast and detailed results when compared to established tools. The studies performed also show the importance of the perturbation magnitude when it comes to analyzing non ideal systems where insufficient or excessive injection magnitude can lead to noisy measurements or non-linear effects. The comparison between SISO and MIMO methods has provided similar results for a given system. The system under study has been varied to increase cross coupling on the converter admittance, and it has been found that SISO methods can provide inaccurate conclusions regarding system stability. The outcome from the review of the transmission system operator (TSO) requirements related to converter interaction stability is that, in general, there is no suggested method available, except for the Swedish TSO. Typically, the methodology and acceptance criteria regarding converter interaction stability is agreed with TSOs at the start of each project. With regards to stability margins, a more robust approach can be the use of a disk margin, due to its multi-loop capability in a MIMO system and the ability to analyze phase and gain at the same time.

Keywords: Small signal stability, Converter interaction analysis, Frequency analysis, Python, PSCAD, Impedance based stability analysis, Passivity-based approach, Converter admittance grid impedance, Positive sequence,Negative sequence

Acknowledgements

We would like to thank Gustavo Pinares, our supervisor, for his help and guidance during this thesis. Without his help this would not have been possible. We would like to thank our colleagues at Hitachi, for their help and input.

We would also like to extend our gratitude to Professor Massimo Bongiorno at Chalmers University of Technology, who served as our examiner during the thesis work.

Lastly, we would like to express our sincere gratitude to our family and friends for their unwavering support throughout these five years of study at Chalmers.

Victor Rasmusson, Rasmus Andreasson, Gothenburg, June 2026.

List of Acronyms

Below is the list of acronyms that have been used throughout this thesis listed in alphabetical order:

AC	Alternating Current
AVC	Automatic Voltage Control
DC	Direct Current
DGM	Disk based Gain Margin
DM	Disk Margin
DPM	Disk based Phase Margin
DUT	Device Under Test
DVC	Dynamic Voltage Control
ESCR	Equivalent Short Circuit Ratio
EMT	Electro Magnetic Transients
FFT	Fast Fourier Transform
GUI	Graphical User Interface
HVDC	High Voltage Direct Current
IMTB	Immitance Measurement Tool-Box
LHP	Left Half Plane
MFD	Mirror Frequency Decoupled
MMC	Modular Multilevel Converters
MIMO	Multiple input multiple output
NESO	National Energy System Operator
PBA	Passivity-Based Analysis
PEID	Power Electronic Interfaced Device
PLL	Phase Locked Loop
POC	Point Of Connection
PV	Photovoltaic
RES	Renewable-based Energy Sources
RHP	Right Half Plane
RMS	Root Mean Square
SI	Strength Indicator
SIAD-tool	Stability and Interaction Assessment in the frequency Domain tool
SISO	Single Input Single Output
Svk	Svenska Kraftnät
TSO	Transmission System Operator
VCC	Vector Current Controller

Contents

List of Figures

List of Tables

1
Introduction

In this section **Background** and **Aim** of the thesis will be presented. Further, the **Limitations** and **Specification of issue** that is to be investigated will be introduced.

1.1 Background

In recent years, the goals for greenhouse gas emissions reduction have led to the increase in renewable energy share in Europe. As of 2023, the share of wind and solar power (which are interfaced with the grid through power electronic converters) out of the total electricity generation has been 26.9 %, which is expected to increase in the future [1] . In addition to that, there has also been an increase in high voltage DC (HVDC) systems (which are based on power electronic converters), with a total of 16 dc-links being in service as of 2024 in European countries [2]. While power electronic based facilities bring in benefits to the power system operation, they also come with challenges. Examples are harmonics and undamped oscillations resulting from the interaction between the converter's control systems and the grid. These phenomena can cause disturbances that can affect the rest of the grid and can potentially cause blackouts if not accounted for [3]. Consequently, new requirements from Transmission System operators (TSOs) have come into effect to ensure that the grid remains stable after power electronic converters are connected into the system.

1.1.1 Converter Interaction Incidents

The first notice of difficulties regarding converters and AC grid interaction was for locomotives using high frequency converters. During the 90s, Swiss railway noticed very high current oscillations in the power system, which forced the protection system to shut down the locomotives. These high current oscillations could later be correlated with the high amount of converters integrated in the system [4]. Similar cases occurred in 2013 when oscillations at frequencies other than the nominal frequency caused the BorWin1 HVDC system to trip. This was a result of interactions between converters or converters and the network [5]

TenneT, the German and Dutch TSO, encountered challenges during the commissioning of its first offshore HVDC-connected wind farm, particularly due to stability

issues involving the converter systems. Consequently, the cable connection caused a change in the resonance frequency which led to unstable operation of the converter. Due to this being an unknown phenomenon at the time, the converter-grid interaction was not thoroughly investigated during the development of the project. Further investigation resulted in the discovery of a harmonic at a frequency of 451 Hz in the recorded voltages which was determined not be a result of the steady-state harmonics from the converters, thus the instability was attributed to the interaction between the controllers and the grid. In particular, the Phase-locked loop (PLL) and the current controller tuning together with the lack of connection to rotating mass were identified as the main cause of instability[4].

Other past incidents include the INELFE link between France and Spain that had a 1600 Hz oscillation and a 1550 Hz oscillation in the Dutch converter heavy power grid, that used both overhead lines and cables [6].

Another incident occurred in the South China power grid were the interaction of a static synchronous compensator (STATCOM) with a weak grid caused high frequency oscillations. The STATCOM had a negative impact on the severity of the oscillations. This could have been avoided in a grid with higher strength [4].

A commonality between these incidents mentioned above is the interaction between converters, the power grid and small changes in the grid impedance. Converter related stability issues are a relatively new phenomenon. Therefore, not enough research has been done on the subject and power system operators are finding challenges in dealing with this issue in respect to analyzing and setting standards for stability.

1.1.2 Converter interation analysis

In order to study the dynamic impact of the connection of power electronic converters and make sure that the system complies with the requirements, several studies must be performed before their connection to the grid. To identify undesired interactions, different methods such as time-domain simulations and frequency-domain analysis have been developed. Time domain simulations are rather straightforward to perform, however, they are based on a large number of simulations cases and often when issues are found it is difficult to identify which system component causes the issue. Frequency domain methods have been widely proposed and their main advantages is that they can give an insight into the possible causes of system instability, in case they are identified [4, 7, 8, 9, 10].

Therefore, there is a need to evaluate the developed tools and methods related to converter interactions studies in order to determine which one is the most suitable framework to perform studies, considering the different requirements from TSO's and availability of simulation models.

1.2 Aim

The aim of this thesis is to :

1. Evaluate different stability analysis methods and tools developed to study converter interaction stability. The advantages and limitations of the investigated methods and tools are determined.
2. Establish the requirements and methods proposed by TSOs related to converter interaction stability.
3. Develop a suitable framework and implement it in a computational tool to perform converter interaction stability analysis.

1.3 Limitations

This thesis is limited to only analyze stability related to converter control interaction. Other phenomenons such as frequency stability, transient stability are not in the scope of this thesis. TSO requirements such as compliance to fault-ride through, reactive power, harmonic distortion, are not covered in the thesis. Also, only methods regarding linear control are considered in the thesis, while methods based on non-linear control are not considered. Moreover the main focus will be on frequency domain methods meaning that time domain methods are not investigated.

The thesis will limit itself to the TSOs of Swedens, *Svenska Kraftnät*, Norway, *Statnet*, Denmark, *Energinet*, UK, *National Grid*, Germany, *TenneT*, Finland, *Fingrid*, Belgium *Elia*, and Spain *Red Electrica de España*.

1.4 Societal, ethical and ecological influence

The thesis deals with the topic of stability of power electronic converter integration which is necessary to ensure the safe operation of modern power systems. By ensuring the stable operation of power electronic converters in the power grid, the general public perception towards integration of renewable energy sources will change in a positive way. A more optimistic attitude towards wind turbines and solar power can accelerate the reduction of traditional energy sources and greenhouse gas emissions. [11].

This would generally have a positive effect on the environment and contribute on a more sustainable future for humans and animals on our planet. In addition, a greater understanding of the issue will help reduce the number of blackouts that occur, making electrical power more reliable and secure for the most critical loads in our society.

2

Converter interaction analysis methods and TSO requirements

A litterature review in the area of converter interaction stability has been carried out to gather knowledge and information required for the work of the thesis.

2.1 Stability analysis methods

To study the harmonic effects of the converters and ensure that the systems comply with the requirements, digital models are often utilized to test the systems before implementation into the grid. In order to identify undesired interactions, different methods such as time-domain and frequency-domain based methods have been developed and utilized. The most prominent methods among these being eigenvalue analysis as well as passivity-based and impedance based analysis [4].

Eigenvalue analysis is a linear system based method which can be used to determine a systems poles. The method itself studies the eigenvalues of a systems state space model and if said eigenvalues has a positive real part, i.e are in the right half plane, the system is unstable [12]. While this method is a very accurate way of determining stability it does however require detailed information about the system and it is difficult to tie the results to the cause of instability. A lot of converters are protected IP's which in turn makes a state space model hard to acquire, meaning this method cannot be applied to such cases [13].

Passivity and impedance based analysis are frequency domain methods that uses a systems impedance/admittance to determine stability. The main analysis tools used in these methods are either gain and phase-margins or the Nyquist stability criterion which can give a measure to the proximity of the system to instability [14]. Frequency domain methods do not require detailed state space models to be applied, hence they do not struggle with black box models [9, 15, 4]. These methods also split the system into a source and load meaning it is easier to distinguish which subsystem may be the cause of instability as well as which frequencies might be problematic.
Frequency domain methods are discussed in this chapter and are the main focus of the thesis.

2.1.1 Impedance based method

The impedance-based method is an approach where the system is divided into two subsystems, namely a generalized source and load system [7]. In [7] it is stated that in several cases the load can be modeled as a Norton equivalent current source and the grid can be represented as a Thevenin voltage source. An example of this type of system is shown in Figure 2.1.

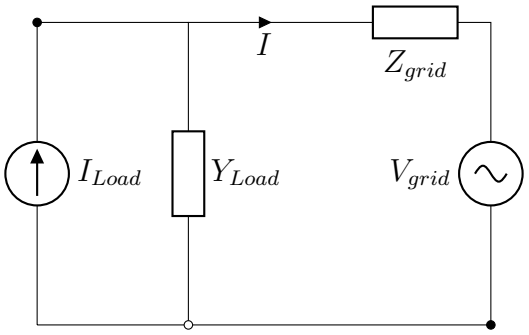

Figure 2.1: Norton and Thevenin-small signal representation of grid connected to converter

The current into the grid, I, can be expressed as (2.1).

$$I(s) = [I_{Load}(s) - V_{grid}(s)Y_{Load}(s)]\frac{1}{1 + Y_{Load}(s)Z_{grid}(s)} \tag{2.1}$$

The closed loop system stability can then be determined by the Nyquist stability criterion applied to (2.2) [4, 16].

$$L(s) = Y_{load}(s)Z_{grid}(s) \tag{2.2}$$

Note that (2.2) is a generalization, however most systems can be represented as sketched in Figure 2.1, i.e. one system grouping loads (and other devices) on one side, and another subsystem grouping sources (and other devices) on the other side.

2.1.2 Passivity-based method

The passivity based approach determines system stability by analyzing if all parts of a system is "passive". Passivity in this case means that the system is dissipating energy , and mathematically, a stable system $\mathbf{F}(s)$ is passive if it is positive semi-definite or if[17, 18, 19].

$$\mathbf{F}(jw) + \mathbf{F}(jw)^H \geq 0 \tag{2.3}$$

Where superscript H represents the *Hermetian conjugate* and $\mathbf{F}(j\omega)$ is a general expression that for the case of this thesis can be either impedances or admittances, and ω is frequency. If both systems fulfill the criterion shown in (2.3) the system is guaranteed stable. In addition, a feedback loop system, such as the one shown in Figure 2.2 is passive if $\mathbf{Y}(jw)$ and $\mathbf{Z}(jw)$ are passive. For a case of MIMO admittance, passivity-based analysis on the eigenvalues of (2.3) is instead done since that is equivalent [20]. However, if one system is non passive it does not mean the whole system is unstable it only means it is not guaranteed stable [10, 17].

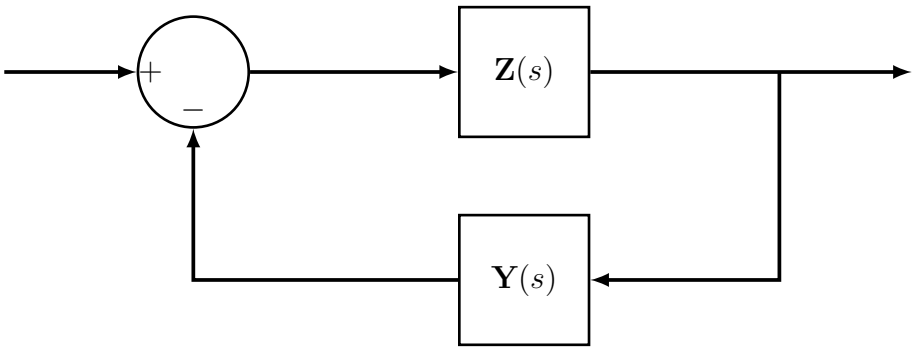

Figure 2.2: System containing the grid impedance and the converter admittance

2.2 Frequency domain Admittance/Impedance

Typically, converters are provided as black boxes which means detailed state space modeling cannot be performed [4, 9]. Stability analysis can instead be performed through frequency domain analysis which requires frequency responses of each subsystem in order to determine stability. In converter based stability studies, frequency responses are obtained through sinusoidal perturbations injected for a spectrum of frequencies. The perturbations are usually performed in the dq or sequence domain, which are going to be described in the following sections.

2.2.1 dq-Domain

Most power electronic converters (connected to a three-phase systems) have their control systems implemented in the dq-frame. The main advantage of transforming a three-phase system into dq-domain is that it becomes a two-phase dc system in steady state, therefore, it allows proportional integral control (PI-control) to be applied to the converter controller. The transformation is achieved by using a phase locked loop (PLL) to acquire the 'rotation' of the system and then transform it to dc values as follows[21, 22].

$$\begin{bmatrix} v_d \\ v_q \end{bmatrix} = \sqrt{\frac{2}{3}} \begin{bmatrix} \cos(\theta) & \cos(\theta - 120^o) & \cos(\theta + 120^o) \\ -\sin(\theta) & -\sin(\theta - 120^o) & -\sin(\theta + 120^o) \end{bmatrix} \begin{bmatrix} v_a \\ v_b \\ v_c \end{bmatrix} \tag{2.4}$$

$$\begin{bmatrix} v_a \\ v_b \\ v_c \end{bmatrix} = \sqrt{\frac{2}{3}} \begin{bmatrix} \cos(\theta) & -\sin(\theta) \\ \cos(\theta - 120^o) & -\sin(\theta - 120^o) \\ \cos(\theta + 120^o) & -\sin(\theta + 120^o) \end{bmatrix} \begin{bmatrix} v_d \\ v_q \end{bmatrix} \tag{2.5}$$

Where v_a, v_b, v_c all refer to the different phase-voltages, θ represents the transformation angle calculated by the PLL, v_d represents the voltage in the d-axis and v_q represents the voltage in q-axis.
The dq-sequence has been used extensively and it's implementation is inherently MIMO-defined which allows it to account for cross couplings. However, to be able to inject perturbations and analyze in the dq-sequence a reference frame is needed. As such the system relies on a PLL to resolve the angle which can make it more complex [21, 23, 4, 24].

2.2.2 Sequence domain

In power system theory an unbalanced three-phase system can be expressed as three separate balanced systems, namely:

- **Positive sequence**: A balanced system containing all three phasors aligned in the same sequence as the original three phase system (example in the order ABC).
- **Negative sequence**: A balanced system consisting of all three original phasors in opposite sequence of the original system (example in order ACB).
- **Zero sequence**: consists of the three phasors from the original sequence that are equal in magnitude and phase.

To go from the three phase domain to the sequence domain the relationship shown in (2.6) is applied. Note that α denotes a phase shift of 120^o ($\alpha = e^{j120^o}$) [22].

$$\begin{bmatrix} v_0 \\ v_p \\ v_n \end{bmatrix} = \frac{1}{3} \begin{bmatrix} 1 & 1 & 1 \\ 1 & \alpha & \alpha^2 \\ 1 & \alpha^2 & \alpha \end{bmatrix} \cdot \begin{bmatrix} v_a \\ v_b \\ v_c \end{bmatrix} \tag{2.6}$$

Where v_a, v_b, v_c represents the three-phase voltages, v_0 represents the zero sequence voltage, v_p represents the positive sequence voltage and v_n represents the negative sequence voltage. For converter interaction stability studies the positive and negative sequence networks are usually the only ones studied while the zero sequence network is ignored [21, 25, 17].

2.2.3 Mirror Frequency coupling effect

In an AC-DC converter, frequency coupling describes a phenomenon when the perturbation frequency intersects the grid frequency. In order to acquire the admittance and impedance of the system, a perturbation in either positive or negative sequence voltage is injected to obtain the response of a converter current. However, these perturbations will in some cases give a response in the opposite sequence due to being non mirror frequency decoupled(MFD). The frequency component for the positive sequence are presented in (2.7) and negative sequence component in (2.8) where the dq frequency represents the perturbation frequency and the base frequency is the frequency base of the system [16, 21].

$$f_{+pert} = f_{dq} + f_{base} \tag{2.7}$$

$$f_{-pert} = f_{dq} - f_{base} \tag{2.8}$$

A arbitrary positive-sequence voltage injection(v_p) at frequency (f_{+pert}) will yield a current response at the same frequency (i_p) but can also yield a negative sequence response (i_n) at frequency ($f_{+pert} - 2 \cdot f_{base}$) [26]. For this thesis the sequence domain impedances are plotted after the dq-frequencies to adhere to the modified sequence domain [21].

2.3 Stability analysis metrics

In this Section, methods for determining and analyzing stability in a closed loop system is introduced.

2.3.1 General Nyquist Stability Criterion

The Nyquist stability criterion is a method for determining the stability of a feedback loop system. For SISO, this method also provides the margin of stability at the systems current point of operation [12].

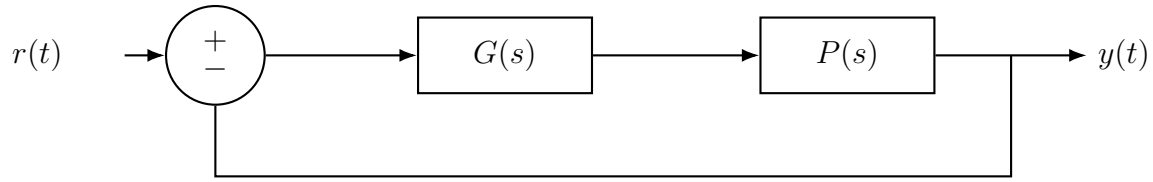

Figure 2.3: Description of a general SISO closed-loop system.

Consider the open-loop transfer function, $L(s)$, in (2.9), where $G(s)$ and $P(s)$ are the transfer functions indicated in Figure 2.3.

$$L(s) = G(s)P(s) \tag{2.9}$$

Then the number of unstable poles of the system in Figure 2.3 can be determined as

$$Z = P + N = 0 \tag{2.10}$$

Where Z is the number of Right Half plane (RHP) for the system shown in Figure 2.3.

P is the number of poles in the right half plane for $L(s)$.

N is the number of encirclements of $L(s)$ around the point -1 in the clockwise direction as the system $L(s)$ traverses the Nyquist contour [12]. In SISO systems, the closed loop system stability can also be determined through Bode plots if $L(s)$ is stable. Through the Bode plot, the classic gain and phase margins can be retrieved which represent how much gain magnitude and phase lag you can add before instability.
For MIMO systems, the Nyquist plot of (2.11) should follow the same criterion as above, except the observed encirclement should be around the origin.

$$\det(\mathbf{I} + \mathbf{L}(s)) \tag{2.11}$$

The Nyquist plot can also be determined through the Nyquist plots of the frequency dependent eigenvalues of the open loop transfer $\mathbf{L}$(s).

$$\lambda(\mathbf{L}(s)) \tag{2.12}$$

In this case, the number of frequency dependent eigenvalues that should fulfill the Nyquist Stability Criterion is equal to the order of $\mathbf{L}$(s).

When Y and Z are expressed in the sequence domain for a symmetrical AC-network, the expression in (2.11) is equivalent to (2.13) below.

$$\det(\mathbf{I} + \mathbf{Y}_{pn}\mathbf{Z}_{pn}) = 1 + S \tag{2.13}$$

With S being $S = z_p y_{pp} + z_n y_{nn} + z_n z_p \det(\mathbf{Y})$, where $z_p = z_{pp}$ and $z_n = z_{nn}$. For this case subscript pp and nn represents the diagonals in the matrices $\mathbf{Y}_{pn}$ and $\mathbf{Z}_{pn}$, [17]. This approach can be used for the purpose of investigating how each subsystem, in a MIMO system, contributes to the total system stability. Note that this applies only to AC grid impedances with no cross-coupling terms between positive and negative sequence, if not (2.11) should be plotted instead.

2.3.2 SISO margins

The SISO margins, which consist of gain and phase margins, are a metric that shows how close in either phase or gain a system is to instability. The gain margin measures the amount of tolerable disturbance in the plant, at the phase crossover frequency, and consists of an upper g_L and lower g_U gain limit (2.14). The phase crossover frequency is the frequency where the magnitude reaches 1.0 [27].

$$g_L < g < g_U \tag{2.14}$$

The phase margin in a system is the amount of tolerable deviation, at the gain crossover frequency, from the plant phase, before the system becomes unstable. The gain crossover frequency is the frequency where an angle of 180° is crossed [27]. A phase deviation can occur due to time delays in the feedback loop. The phase margins has an upper ϕ_U and lower ϕ_L phase limit where the closed loop system is stable for all angles according to (2.15) [28].

$$-\phi_L > \phi > \phi_U \tag{2.15}$$

However, SISO margins has the limitation that they are inaccurate when applied to MIMO systems, since they do not account for cross-coupling interactions [28].

2.3.3 Disk margins

Disk margin is a robust metric for stability that accounts for both gain and phase perturbations simultaneously. Gain and Phase are modeled as a complex factor, f, where the deviation from $f = 1$, acting on the open loop function as $L_f = f\mathbf{L}$ are the variation in gain and phase. The mathematical definition of the disk used in Disk Margin are presented in the (4) below.

$$f \in D(\alpha, \sigma) = \left\{ \frac{1 + \frac{1-\sigma}{2}\delta}{1 - \frac{1+\sigma}{2}\delta} : \delta \in \mathbb{C} \text{ with } |\delta| < \alpha \right\}. \tag{4}$$

α is the radius of the disk, δ is any complex number in the disk where the center is at 0 and σ is the skew parameter. A nonzero skew indicates a bias towards either gain decrease or gain increase.

Disk margins in the Nyquist plane implies that $1 + f\mathbf{L}(j\omega) \neq 0$, for all perturbations $f \in D(\alpha_{max}, \sigma)$ and for all frequencies ω. The stability condition is now $\mathbf{L}(j\omega) \neq -f^{-1}$ and can be interpreted as a Nyquist exclusion region. This means the Nyquist plot $L(j\omega)$ does not enter the disk, $D(\alpha_{max}, \sigma)$. The exclusion region is tangent of the Nyquist curve of $\mathbf{L}$ and contains the critical point $(-1, 0)$. By changing the skew σ, different exclusion regions are formed. For $\sigma = -0$ the disk is centered at the origin and both the perturbation and Nyquist exclusion sets are symmetric disks. If $\sigma = -1$, then the disk is centered at nominal $f = 1$ and α_{max} is the radius [28].
For $\sigma = +1$, the Nyquist exclusion disk is centered at -1, with α as the radius. This is defined as the S-based margin and α_{max} defines the minimum distance from the Nyquist curve of L to the critical -1 point. The expression for the minimum distance are shown below

$$\alpha_{max} = min_{\omega}|L(jw) + 1| \tag{2.17}$$

The disk margin consists of a combination of the disk based gain margin (DGM) and the disk based phase margin (DPM). DGM represents the lower and higher zero-crossing of the real axis of the disk in the complex plane while the disk based phase margin is the angle between the disk center and where the curve tangents the disk as shown in Figure. 2.4.

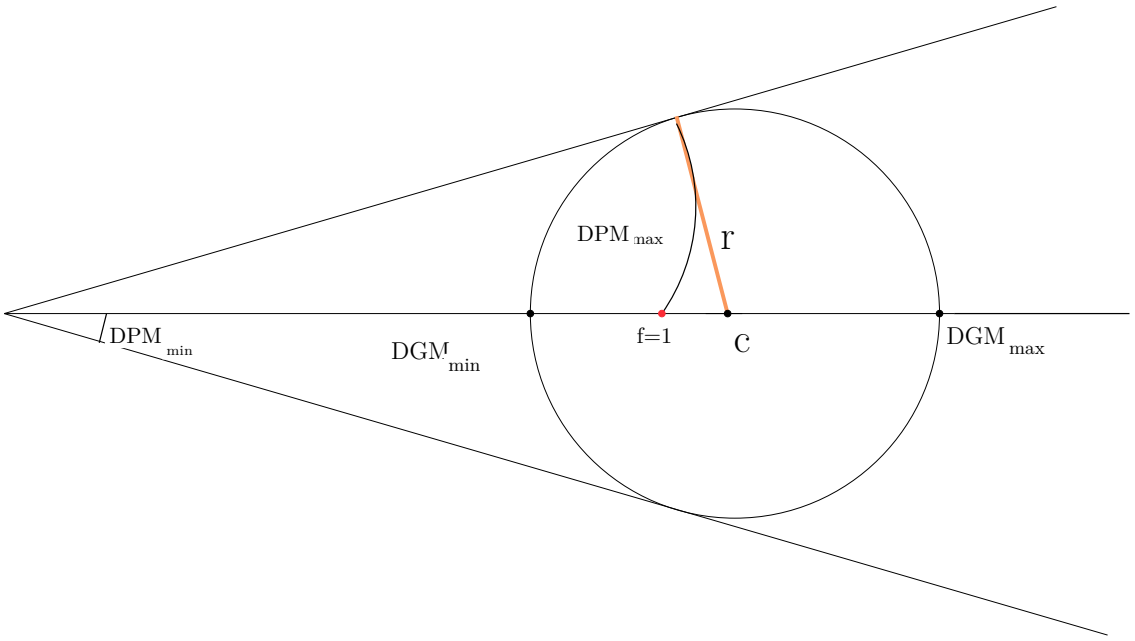

Figure 2.4: Disk representing the largest phase and gain margin for stability

In [29] it is proposed the method of a strength indicator (SI), for multi-converter power system, taking into account both phase and gain. From the disk based phase and gain margin the strength indicator, SI can be calculated as below

$$\text{SI} = \text{DGM*tan(DPM)} \tag{2.18}$$

The following classifications below are recomended in [29].

- **SI** < 0.2 Indicates a weak system with a high risk of oscillations and instability. An improvement in robustness is suggested.
- $0.2 <$ **SI** < 2 The system has moderate strength. Oscillations can be damped, although further adjustments of the control parameters can be made.
- **SI** > 2 The system is strongly stable with a low risk of oscillations. No further tuning of the controller is needed [29].

Disk margin are originally defined for SISO systems but can still be extended to MIMO systems by applying it to the frequency dependent eigenvalues of the transfer loop matrix. Each eigenvalue can be depicted as an equivalent SISO system with the eigenvalue that has the smallest disk margin being the indication of its stability margin. Disk margins, unlike SISO margins, handle multi-loop interactions in a MIMO system, meaning perturbations in gain and phase in multiple channels can be processed at the same time [28]. Disk margins also take into account all loop interactions and frequencies resulting in more guaranteed margins compared to classical phase and gain margins [30].

2.4 Converter stability methods and requirements by TSOs

2.4.1 ENTSO-E

According to the ENTSO-E guidelines for interaction studies between multiple HVDC links [31], the methodology states multiple modeling methods to analyze the system stability. Time domain simulations are suitable for simulations of non-linear HVDC systems and the grid for asymmetrical transients from disturbances. Time domain models alone is not sufficient but needs to be accompanied with a model in the frequency domain as it is the best method for studying instabilities. An alternative method is to use a state-space representation of the HVDC-system and the AC grid model, where the eigenvalues can be obtained to analyze the stability state of the system. A frequency scan followed by the impedance based approach is also suggested since it does not require much computation time and utilizes the Nyquist criteria to obtain stability margins [31].

2.4.2 Svenska Kraftnät

Svenska kraftnät (Svk) has proposed a method to perform stability assessment using frequency domain analysis [26]. The method is applied to a feedback system expressed in the positive- and negative sequence system, as shown in Figure 2.5. Thereafter, the Nyquist stability criterion is applied to sequence the stability of the system. The system feed-forward gain is the negative and positive sequence impedance's,Z_{gp}, Z_{gn} at the point of connection (POC). The, feedback gains are the self-admittances Y_{ap}, Y_{an} of the PEID. In order to obtain the admittances of the PEID, EMT simulation can be performed by using voltage perturbations, $\hat{v_p}$ and $\hat{v_n}$, respectively to perform the calculations below [26].

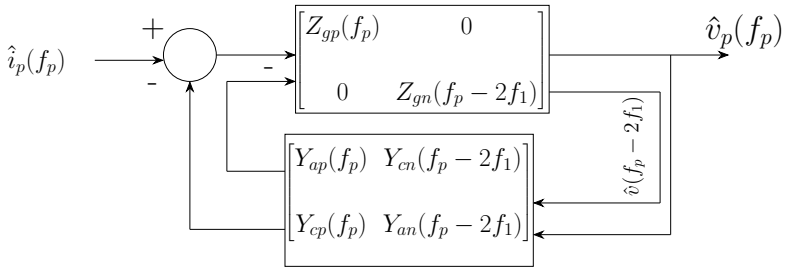

(a) Positive sequence.

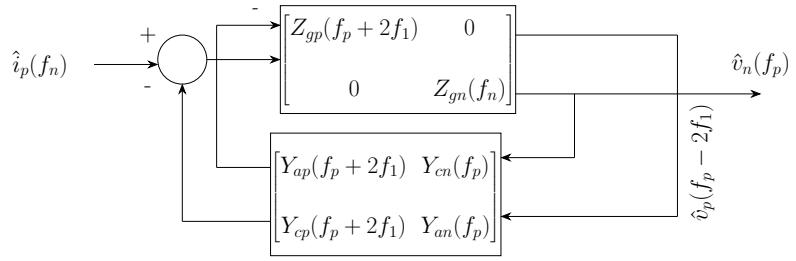

(b) Negative sequence.

Figure 2.5: Feedback system for positive and negative sequence.

$$Y_{ap} = \frac{\hat{i}_a(f_p)}{\hat{v}_p(f_p)}, \quad Y_{an} = \frac{\hat{i}_a(f_p)}{\hat{v}_n(f_p)}, \quad Y_{cp} = \frac{\hat{i}_a(f_p - 2f_1)}{\hat{v}_p(f_p)}, \quad Y_{cn} = \frac{\hat{i}_a(f_p + 2f_1)}{\hat{v}_n(f_p)} \tag{2.19}$$

The cross-coupling terms are denoted by Y_{cp} and Y_{cn}. The impedances and admittances in the POC and system are used to perform a impedance based stability analysis. In the frequency range of 1 to 250 Hz, the requirements that Svk provides, consists of a phase margin, which is presented in (2.20) and (2.21), where $\mu = 35°$ [32]

$$180° + \mu < \angle Z_{gp}(Y_{cp} + Y_{ap}) < 180° - \mu \tag{2.20}$$

$$180° + \mu < \angle Z_{gn}(Y_{cn} + Y_{an}) < 180° - \mu \tag{2.21}$$

In the frequency range of 250 to 2.5 kHz the effects of the cross-coupling are neglected. Only the self-impedance's of the converter are used. These converter

impedance's are required to have positive damping which means that the real part should be bigger than zero, according to (2.22) and (2.23).

$$Re\{Z_{ap}(f_p)\} > 0 \tag{2.22}$$

$$Re\{Z_{an}(f_p)\} > 0 \tag{2.23}$$

The plant owner is required to deliver the admittances of the PEID and a EMT model to Svk. Svk then performs a separate verification to confirm the results [26].

2.4.3 Fingrid

The Finish TSO, Fingrid, has had experience with converter related issues. Fingrid proposes the method of using the Equivalent Short Circuit Ratio (ESCR) metric, to decide if a system with a high share of converters requires further studies. A program developed by Fingrid calculates the ESCR for every converter, in a root mean square (RMS) model, and finds the one with the lowest N-1 contingency [33]. N-1 contingency means that the system must be stable after one contingency.

However, because of difficulties in defining an appropriate threshold for the ESCR due to differences in network topologies, Fingrid instead focuses on the accuracy of the Electromagnetic Transient (EMT) simulation, in the time domain, with a conservative ESCR value. With the use of a commercial conversion tool RMS models can be transferred to more accurate and detailed EMT models. If the simulation evaluations would conclude stability issues, Fingrid proposes curtailment of the maximum active power, control mode changes and grid topology changes to mitigate the issue [33].

2.4.4 National Energy system operator

The TSO of The United Kingdom, National Energy System Operator (NESO), has presented guidance on the assessment of inverter based resources in the power system. The techniques proposed to investigate converter behavior in a converter dominated power system are listed below [34].

- **Step change study**, where small step changes are applied to the grid voltage and phase angle to study the response of the system. This provides a good study of the scheme of interest. Acceptable response should be a response within the specified conditions from the grid code. Oscillation magnitude should not be more than 5% peak to peak, and settling time should be less than 2 s. Exceptions are sometimes made for the settling time [34].
- **Small signal injection study** uses EMT perturbation simulations to explore the behavior of a system. It is recognized as one of the best ways to explore the behavior of inverter based resources. For the studies the AC grid is represented as a Thevenin equivalent, while the converter under study will be represented using a detailed EMT model. The desired frequency oscillations are injected into the system to evaluate the behavior. An example setup are shown in Figure 2.6. Acceptable responses according to NESO should ideally be, no increase in magnitude of injected oscillations with positive damping. No

instability, during different oscillation injections or change in active or reactive power. The system should return to normal conditions after the injection [34].

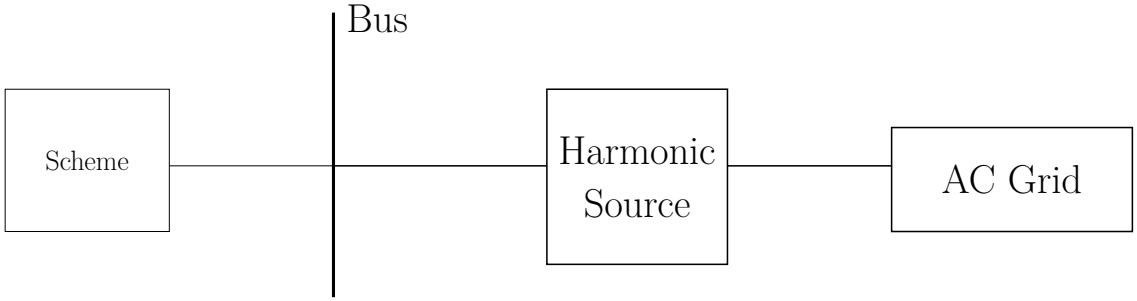

Figure 2.6: Example of study setup for limited time domain simulation.

- **Active frequency scans** are a method to study the impedance and phase angle of a converter. For the study the AC grid is represented as a Thevenin equivalent, like the small signal injection study and thereafter a range of frequencies are injected into the converter to obtain the characteristics. To improve the frequency scan analysis, the use of the MIMO approach is suggested rather than the SISO one, because it provides a more accurate analysis since it accommodates multiple interactions which are present in a real world system. The small signal injection can be either be performed through series voltage injection or shunt current injection. The acceptable response according to NESO is that the assessment of the small signal stability should demonstrate stable operation. The system is considered stable if the eigenloci do not encircle the critical point $[-1, 0]$ in the complex Nyquist plot [34].
- **Eigenvalue analysis** is becoming one of the preferred ways to study interaction phenomena. The method uses a detailed EMT model for the converter, where the linear state space model together with a Thevenin equivalent as the AC grid are used to determine the eigenvalues of the full system. Not the frequency dependent eigenvalues, like other methods suggest. This provides oscillation modes, frequency of oscillation and damping co-efficient. Acceptable responses are that all closed-loop eigenvalues are expected to be in the left-hand plane of the Laplace plane. A minimum of 10% damping ratio is required for all oscillation modes [34].

  It uses a frequency scan with detailed assumptions for the EMT model of the converter. The connected AC grid is represented as a Thevenin equivalent, and the system as a linear state space representation. These are used to determine the eigenvalues of the system, and provide oscillation modes, frequency of oscillation and damping co-efficient.

2.5 Stability analysis tools

This section summarizes the stability analysis tools investigated for this thesis.

2.5.1 Z-tool

Z-tool is an automated tool developed in Python at KU Leuven to obtain frequency dependent admittances from different subsystems in the grid and analyze their stability. Z-tool connects the perturbation sources directly by connecting the source and load subsystems to a shunt voltage source that recreates the prior circumstances while applying perturbations, see Figure 2.7 [13]. This implementation allows both sides of the POC to be scanned at same time without the risk of instability disrupting the results. In [9] they mention that stability is determined both by the impedance and the passivity based methods. For the impedance-based method it splits the system into sources and loads as shown in Figure 2.1 and utilizes the admittance ratio between the two systems to do stability evaluation using the Nyquist criterion [9]. As for the passivity based method it plots the measured response as their eigenvalues over a frequency spectrum. Z-tool performs both the injections and the post process analysis in the dq domain. It also has the feature of multiple scan blocks being active at the for the same simulation, as shown in Figure 2.8. Further, it utilizes PSCADs built in multi-core function to run multiple simulations at the same time to speed up the process. It also utilizes multi-frequency injection where multiple perturbation signals are sent in to the same simulation to further save time. However, the multi-frequency perturbation injection is limited to sending in 8 simultaneous injections or a single one [9, 35].

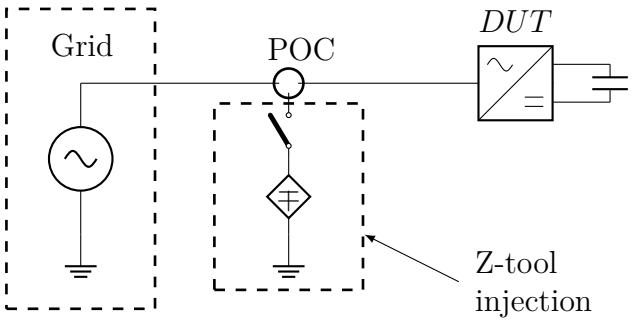

Figure 2.7: Simple example showing the Z-tools connection at the POC of a simple grid and converter system

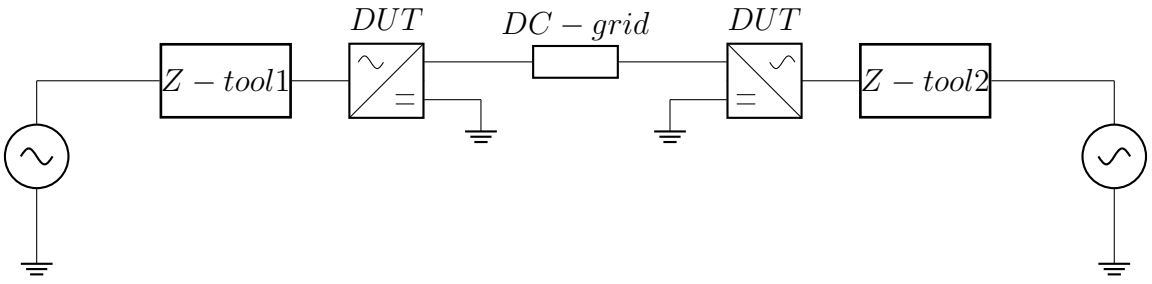

Figure 2.8: Example of system with multiple points being measured at the same time

2.5.2 IMTB

IMTB (Immitance Measurement ToolBox) is an impedance analysis tool developed in Python by Energinet. The tool utilizes the frequency scan method described in Section 2.1 to obtain the frequency dependent impedances of the system under study. However, unlike Z-tool, IMTB does not provide stability assessment tools, instead, the user needs to perform such evaluations post scan using the resulting impedance [15]. IMTB allows for injections in both the sequence domain as well as the dq domain, the post processing can be done in dq-domain where it is MIMO defined or in the classical SISO sequence-domain. In addition, IMTB has a graphical user interface which makes it accessible for users with limited Python experience. The script also utilizes the multi-core capabilities provided by PSCAD meaning the scanning can be sped up [15].

2.5.3 SIaD-tool

The SIaD (Stability and Interactions assessment in the frequency-Domain) Tool is a admittance scan and stability assessment tool developed in Spain as a collaborative effort between multiple universities. It utilizes both passivity-based analysis and impedance-based analysis with the Nyquist criterion on system stability. It also offers modal analysis as well as phase and gain margin analysis. The Modal analysis allows the user to find resonances in the system using the eigenvalues of the admittance/impedance characteristics shown in (2.24).

$$\mathbf{Y}_{sys}(jw) = \mathbf{Y}_{sys1}(jw) + [\mathbf{Z}_{sys2}(jw)]^{-1} \tag{2.24}$$

The phase and gain margin implementation show the phase and gain evaluation for a full MIMO matrix so the cross couplings are also evaluated unlike classical SISO phase and gain evaluation. It's compatible with both power systems implemented in PSCAD and MATLAB models [18]. The tool shares similarities with Z-tool, however, SIAD does not exploit the full capability of PSCAD with regards to multicore simulations. One thing to be noted is that the tool works under the assumption that the systems under analysis will reach a stable state which means that the impedance scan may fail if the system is unstable. The tool does however offer multiple different injection types such as PN, abc as well as dq. The PN analysis is MIMO defined and its definition is close to what is presented in (2.19) [18].

3
Tool development

To study converter and grid interactions, a tool has been developed in PSCAD and Python to automate the stability analysis. As stated before, there are already existing tools, however, they come with their own pros and cons in terms of analysis capabilities, execution time and adaptability. This tool means to compensate on the other tools shortcomings. The implementation of the tool is explained in this chapter.

3.1 PN-injection

The primary perturbation type to determine the frequency response of the converter has been performed in the modified sequence domain, proposed in [21]. The sequence domain is chosen because it is simpler and easier to implement compared to the dq-sequence. Injections are performed in both the positive and negative sequence domains. As stated earlier, results from injections in either positive or negative sequence can yield responses in both domains if the system is non MFD which will need to be adhered to in the post processing [21]. The injection is defined using (2.6) and utilizes the frequency definition that has been shown in Section 2.2.3 as well as in [21].

3.2 PSCAD Block

To perform frequency injection and measurements using an automated script for different systems, a PSCAD block has been developed that can be connected at different points in the system, as shown in Figure 3.1.

The perturbation injection defined in the block can be either shunt current injection or series voltage. The injection for each phase has been formulated as shown in (3.1) where positive sequence is shown and then negative sequence injection is formulated as shown in (3.2)

$$\begin{bmatrix} V_{ap} \\ V_{bp} \\ V_{cp} \end{bmatrix} = V_{Inj-amp} \cdot \begin{bmatrix} \cos(\omega_p) \\ \cos(\omega_p - \frac{2\pi}{3}) \\ \cos(\omega_p + \frac{2\pi}{3}) \end{bmatrix} \tag{3.1}$$

$$\begin{bmatrix} V_{an} \\ V_{bn} \\ V_{cn} \end{bmatrix} = V_{Inj-amp} \cdot \begin{bmatrix} \cos(\omega_n) \\ \cos(\omega_n + \frac{2\pi}{3}) \\ \cos(\omega_n - \frac{2\pi}{3}) \end{bmatrix} \tag{3.2}$$

In this, the injection is performed individually to each subsystem in order to avoid the grid affecting the converter under study or vice versa [25]. When the converter is measured, the grid is replaced by an ideal voltage source, this to guarantee no interaction. When measuring the grid, the converter is then instead completely disconnected and replaced by the perturbation source. The implementation in PSCAD is depicted in Figure 3.1 and 3.2. The switches shown in Figure 3.1 are turned on or off from inputs when running the Python script, where SW2 decides if the grid or the ideal source is to be connected and SW1 decides if the DUT is to be connected or not. In the context of this thesis the DUT represents the converter under study.

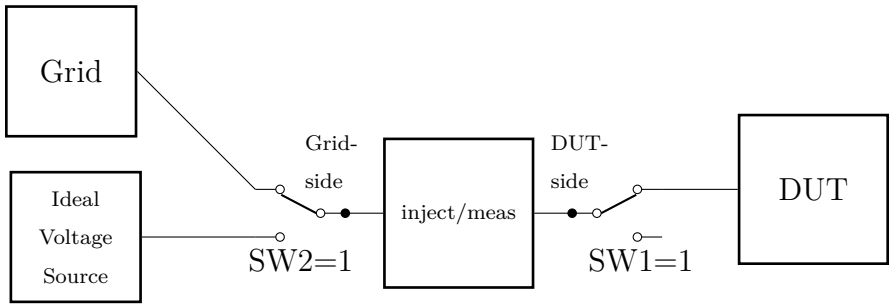

Figure 3.1: Component disconnection for separate analysis.

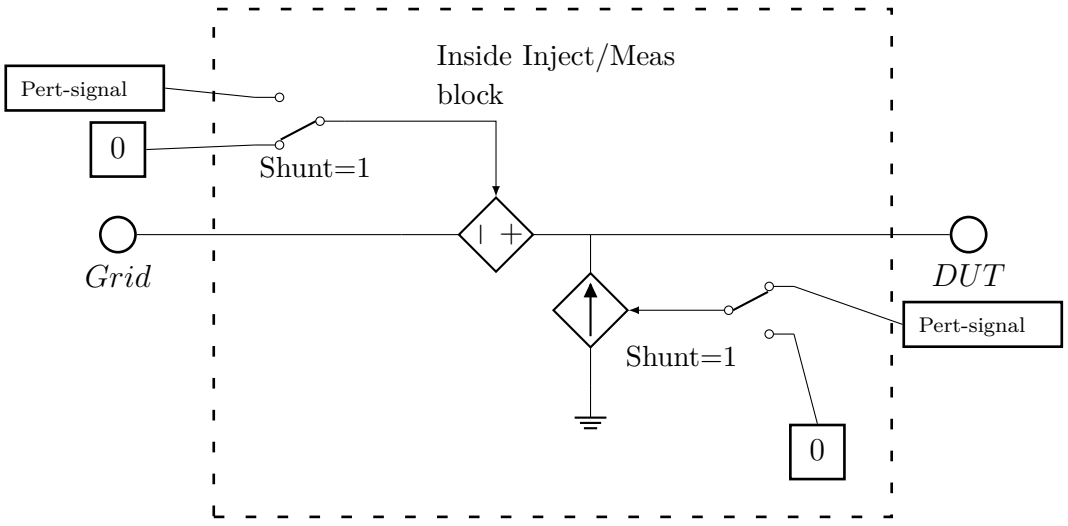

Figure 3.2: Perturbation method for arbitrary phase

Figure 3.2 shows the content of the inject/meas block, where one phase is shown. The injection type is decided by one variable labeled as shunt in Figure 3.2. This variable makes the amplitude zero for either the current perturbation source or the voltage depending on it's value.

3.3 Multi-frequency injection

To decrease simulation time, the possibility to inject multiple frequencies simultaneously has been investigated. For example instead of running 50 simulations to

obtain impedances/admittances for 50 frequencies, 10 injections can be done at the same time hence only requiring 5 simulations. The approach followed in this thesis is to split the original frequency spectrum list into smaller lists. Then, the injection is performed sequentially for each item in every list. Ideally, each response should be obtainable accurately through a Fast Fourier Transform (FFT). However inaccuracies may appear due to spectral leakage. Spectral leakage in this case refers to frequency bins of the FFT leaking "energy" into neighboring frequency bins. The challenge lies in the proximity these frequencies have to each other which could cause spectral leakage in the FFT to affect the end results [36]. Because of this, two methods for injection has been implemented in this thesis, namely a linear and spaced method. The frequencies of the perturbation signals to be injected can be arranged in a matrix where the column values are the frequencies to be injected simultaneously. The linear method in short fills the columns linearly with the frequencies. An example of how the injection matrix is created is shown in (3.3).

$$\begin{matrix} \\ \downarrow \\ \end{matrix} \begin{bmatrix} 20 & 35 & 50 \\ 15 & 30 & 45 \\ 10 & 25 & 40 \end{bmatrix} \tag{3.3}$$

For the spaced method the rows are filled instead with an example matrix being shown in (3.4).

$$\begin{matrix} \\ \downarrow \\ \end{matrix} \begin{bmatrix} 40 & 45 & 50 \\ 25 & 30 & 35 \\ 10 & 15 & 20 \end{bmatrix} \tag{3.4}$$

The arrow in both (3.4) and (3.3) represents the first column of frequencies to be injected. The latter method allows for less risk of spectral leakage that affects the results. However, it is important that the columns does not contain values that have two times the base system frequency of spacing between each other to avoid injecting signals at the mirror frequencies. For example if a list of simultaneous perturbations would contain both a positive sequence injection of 40 Hz and 140 Hz, then when the negative sequence response from the 140 Hz injection is analyzed the positive sequence response from the 40 Hz case will be picked up as well meaning inaccurate values.

3.4 Post-processing

Before each analysis a steady-state measurement is always performed, where no perturbation signal is injected. The steady-state measurements are then removed from the perturbation measurements to acquire only the perturbation response, as follows

$$\Delta v(t) = v_{measured}(t) - v_{ss}(t) \tag{3.5}$$

Where $\Delta v(t)$ represents the voltage measurements with the steady state removed, $v_{measured}(t)$ is voltage from the perturbation measurements and $v_{ss}(t)$ is the steady state voltage without any perturbation. Then, an FFT has been performed on $\Delta v(t)$ to acquire the frequency spectrum for each phase. The spectral components can then be transformed to their respective positive and negative components following the Fortesque transform (2.6). The developed tool has been defined so that for each response in the positive and negative sequence, the tool would pick the response at the expected frequency. For example, when handling a positive sequence injection, into a 50 Hz system with a frequency injection of f_p the script would look at the value at this frequency to acquire, i_{pp} but would also look at $f_p - 100$ to acquire the negative response, i_{np}, caused by cross coupling. Then the opposite is performed for the negative injection, where the negative response, i_{nn}, is acquired at f_n and the positive sequence response, i_{pn}, caused by cross coupling is acquired at $f_n + 100$. Subsequently, with the current and voltage responses, the admittance matrix $\mathbf{Y}_{PN}$ were calculated using the 2×2 matrices of the PN voltage and currents according to (3.6)

$$\begin{bmatrix} Y_{pp} Y_{pn} \\ Y_{np} Y_{nn} \end{bmatrix} = \begin{bmatrix} i_{pp} & i_{pn} \\ i_{np} & i_{nn} \end{bmatrix} \times \begin{bmatrix} v_{pp} & v_{pn} \\ v_{np} & v_{nn} \end{bmatrix}^{-1} \tag{3.6}$$

The elements in (3.6) are explained as follows:

- v_{pp} and i_{pp} are the positive sequence voltage and current response from a positive sequence injection. Y_{pp} represents the admittance that causes a positive sequence current response from a positive sequence voltage injection.
- v_{np} and i_{np} represent the negative current and voltage response from a positive sequence injection. Y_{np} is the admittance that causes a negative sequence current response from a positive sequence injection
- v_{pn} and i_{pn} represent the positive current and voltage response from a negative sequence injection. Y_{np} is the admittance that causes a positive sequence current response from a negative sequence injection
- v_{nn} and i_{nn} represent the negative current and voltage response from a negative sequence injection. Y_{nn} is the admittance that causes a negative sequence current response from a negative sequence injection

The acquired PN domain admittance matrix in (3.6) can be transformed into the dq domain, as follows [21, 17].

$$\mathbf{Y}^{dq} = \mathbf{T}^{-1} \times \mathbf{Y}^{pn} \times \mathbf{T} \ \text{, with } \ \mathbf{T} = \frac{1}{\sqrt{2}} \begin{bmatrix} 1 & j \\ 1 & -j \end{bmatrix} \tag{3.7}$$

3.5 Passivity and Stability analysis

Following the calculation of the admittances, an investigation of the system stability using the impedance and passivity-based method, was performed.

3.5.1 Passivity-based analysis module

As mentioned before, through the passivity-based analysis, it can be concluded that the system is stable if both the converter and the grid are passive. For this investigation, the eigenvalues of (2.3) has been used to determine if the system is passive. The passivity check module has been implemented in Python were the script returns a message to notify the user if the system is passive or not. The script also plots the real parts of the eigenvalues (2.3) over the frequency spectrum for the user to inspect. Similarly a passivity check for the grid was also implemented.

3.5.2 Nyquist criterion module

(2.11) was plotted in order to investigate the closed loop system stability using the impedance-based method. As described in Section 2.3.1 and 2.1.1, the system stability can be determined by following the Nyquist criterion applied to (2.11). In addition, to gain further understanding of the impact each subsystem component, (2.13) was applied.

To obtain a further view of the system stability margins, the S-based disk margin, from Section 2.3.3, was applied using (2.17). The margin has also been plotted in the complex plane, together with the closed loop system Nyquist plot, to provide an estimate of how close the system is to the critical point -1. This implementation was done for the purpose of comparing the stability margins between different test cases.

3.6 Structure of the tool

A general flow of the tool and all of its modules is shown in Figure 3.3

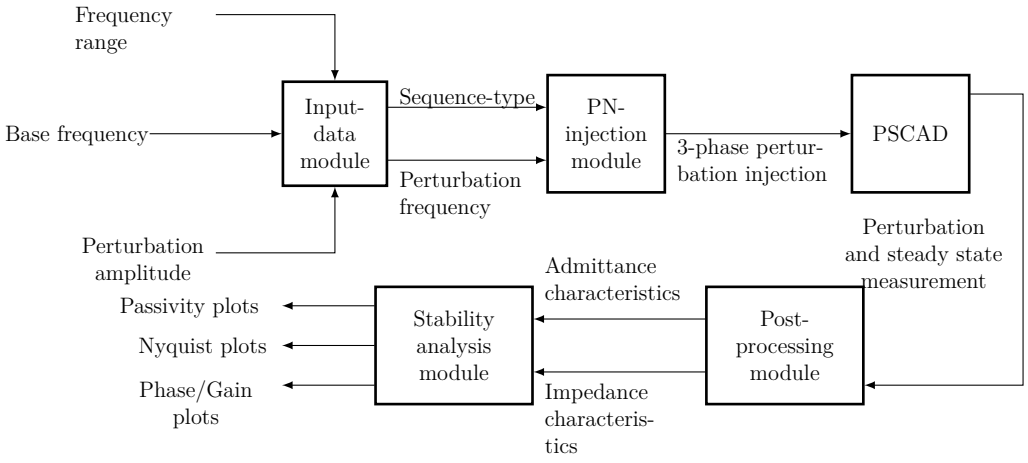

Figure 3.3: Tool workflow

3.6.1 SISO, MIMO and Svenska Kraftnät comparisson

Since MIMO-based analysis of converter interactions is still a relatively new approach, it is of interest to compare it with traditional SISO stability analysis. In addition to applying the SISO method, this thesis also considers the method proposed by Svk, which computes admittances according to (2.19).

In the SISO stability analysis method, admittances has been calculated by taking Ip/Vp and In/Vn, ignoring cross-coupling elements, and then performing a Bode plot and Nyquist plot to investigate the stability condition of the system. In the Bode plot the distance to $\pm 180°$ in unit with a gain magnitude of 1, in combination with checking the gain margin at ± 180, is verified in order to determine the system stability. Furthermore, the Svk approach has been implemented in the developed tool by following (2.19). A comparison has been made between the SISO and MIMO approaches to investigate where SISO approaches can be a good approximation to MIMO approach.

3.7 Test systems

In this section the systems that the developed tool has been verified against are presented.

3.7.1 Ideal converter model

To be able to verify the performance of the tool, an ideal EMT model has been provided. The model is sketched in Figure 3.4 and it consists of an ideal converter connected to an ac grid through a cable. The converter is ideal meaning that the power electronic bridges are modelled as an ideal voltage source on the ac side, and an ideal current source on the dc side, as shown in Figure 3.5. The converter controls dc side voltage and reactive power exchange at the converter POC. The reactive power exchange is regulated directly through the current reference in the q axis, i_f^{qref}. Thus, the converter aims to represent a reactive power compensation device, such as a STATCOM. The parameters of the ac grid and cable are shown in Table 3.1, and the converter parameters are shown in Table 3.2. Figure 3.5 presents a screenshot of the model build in PSCAD showing also the "measurement point", which is where the perturbations are going to be injected. In addition to the ideal EMT model, a linearized model of the EMT system has been provided. Section 3.7.2 presents an analytical derivation of the converter admittance matrix, Y, and the grid impedance matrix Z.

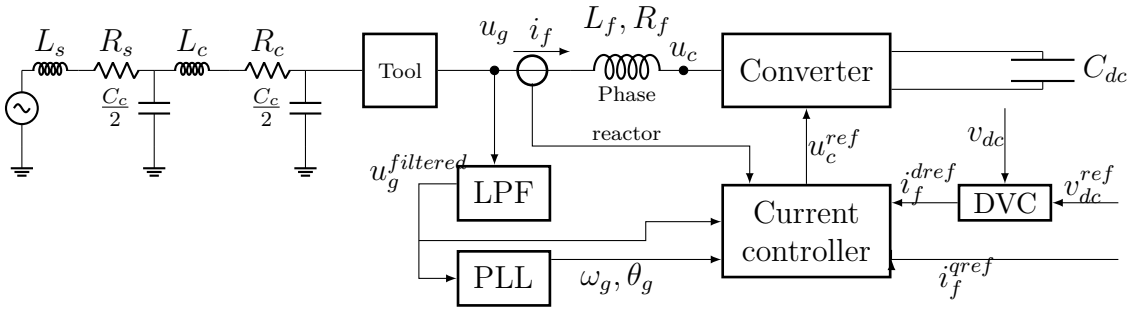

Figure 3.4: PSCAD equivalent model.

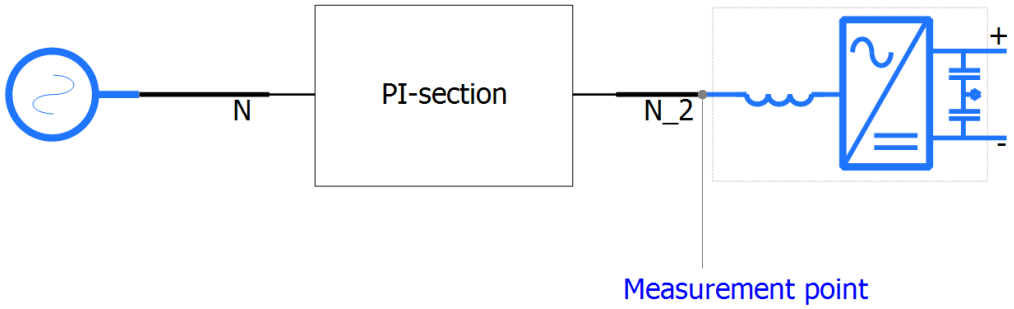

Figure 3.5: Screenshot of the PSCAD implementation.

Table 3.1: Table of parameters and corresponding values for the grid side equivalent.

Parameter	Value
V_s	66 $[kV]$
L_s	0.26 $[H]$
R_s	8.1677 $[\Omega]$
L_c	0.44 $[mH/km]$
R_c	0.28 $[\Omega/km]$
C_c	0.17 $[\mu F/km]$

Table 3.2: Converter settings and ratings

Parameter	Value
Rated frequency f	50 $[Hz]$
Rated dc-side voltage V_{dc}	132 $[kV]$
Rated ac-side voltageV_{ac}	66 $[kV]$
$L_{reactor}$	0.260 $[H]$
$R_{reactor}$	0.817 $[\Omega]$
Dc link capacitor C_{dc}	9.183 $[\mu F]$
Control mode	DC voltage control
Voltage proportional gain, kp_{vdc}	1.154 p.u
Voltage integrator gain, ki_{vdc}	0.1731 p.u
Voltage integrator time constant, ti_{vdc}	0.018 p.u
Current proportional gain, kp_i	0.75 p.u
Current integrator gain, ki_i	0.0075 p.u
Current integrator time constant, ti_i	0.424 p.u
PLL Bandwidth, α_{pll}	0.2 p.u
PLL proportional gain, kp_{pll}	0.4 p.u
PLL integrator gain, ki_{pll}	0.04 p.u

Note that the system is only meant for testing purposes and does not represent a real system. Cable length or resonance peaks might be exagerated for the purpose of demonstrating the instability phenomenon under investigation.

3.7.2 Linearized state-space model

The state space model of the converter, shown in Figure 3.4, is presented in this Section. In this case, two rotating frames are considered, as described in [17]. One is the dq frame defined by the angle estimated by the converter PLL and the other one is the synchronous dq frame, which rotates at a constant speed. The linearized phase-reactor current, i_f, can be described in dq frame as (3.8) and (3.9).

$$\frac{d\Delta i_f^d}{dt} = \frac{-Rf}{Lf}\Delta if_f^d + \omega_0 \Delta i_f^q + i_{f0}^q \Delta\omega + \frac{\Delta u_g^d}{L_f} - \frac{\Delta u_c^d}{L_f} \tag{3.8}$$

$$\frac{d\Delta i_f^q}{dt} = -\frac{R_f}{L_f}\Delta i_f^q - \omega_0 \Delta i_f^d - i_{f0}^d \Delta\omega + \frac{\Delta u_g^q}{L_f} - \frac{\Delta u_c^q}{L_f} \tag{3.9}$$

Δ indicates variables that are deviations from the initial operating point and subscript "0" indicates that the variable has taken the value of the initial operating point [17]. R_f and L_f are the resistance and inductance of the phase reactor, respectively. The dq phase reactor currents and the POC voltages are represented through i_f^d,i_f^q and u_g^d, u_g^q respectively. u_c^d and u_c^q represent the converter dq voltages, and ω_0 the steady-state frequency. The Vector Current Controller (VCC) dynamics can be described by (3.10), (3.11), (3.15) and (3.14), and the low pass filter by (3.12) and 3.13.

$$\frac{\mathrm{d}m^d}{\mathrm{d}t} = k_i(\Delta i_f^{dref} - \Delta i_f^d), \tag{3.10}$$

$$\frac{\mathrm{d}m^q}{\mathrm{d}t} = k_i(\Delta i_f^{qref} - \Delta i_f^q), \tag{3.11}$$

$$\frac{\mathrm{d}u_{gfl}^d}{\mathrm{d}t} = -\alpha_f u_{gfl}^q + \alpha_f \Delta u_g^d, \tag{3.12}$$

$$\frac{\mathrm{d}u_{gfl}^q}{\mathrm{d}t} = -\alpha_f u_{gfl}^q + \alpha_f \Delta u_g^q, \tag{3.13}$$

$$\Delta u_c^d = -k_p(\Delta i_f^{dref} - \Delta i_f^d) - m^d + \omega_0 \Delta i_f^q + i_{f0}^q \Delta\omega + u_{gfl}^d, \tag{3.14}$$

$$\Delta u_c^q = -k_p(\Delta i_f^{qref} - \Delta i_f^q) - m^q + \omega_0 \Delta i_f^d + i_{f0}^d \Delta\omega + u_{gfl}^q, \tag{3.15}$$

where m^d and m^q are integral states, i_f^{dref} and i_f^{qref} are current references, k_p and k_i are the proportional and integral gains of the VCC, respectively and α_f is the voltage filter bandwidth. The PLL dynamics are described by

$$\frac{\mathrm{d}n_\omega}{\mathrm{d}t} = k_{il} u_{gfl}^q \tag{3.16}$$

$$\frac{\mathrm{d}\Delta\theta_g}{\mathrm{d}t} = n_\omega + k_{pl} u_{gfl}^q \tag{3.17}$$

where k_{il} and k_{pl} are the proportional and integral gains, respectively, of the PLL. The dc-side voltage controller are described by (3.18) and (3.19) below

$$\frac{\mathrm{d}n_{u_{dc}}}{\mathrm{d}t} = k_{ie}(\Delta u_{dc}^{ref} - \Delta u_{dc}) \tag{3.18}$$

$$i_f^{dref} = k_{pe}(\Delta u_{dc}^{ref} - \Delta u_{dc}) + n_{u_{dc}} \tag{3.19}$$

$n_{u_{dc}}$ is an integrator state, u_{dc}^{ref} is the dc voltage controller input reference and k_{pe} and k_{ie} are the proportional and integral gains of the controller.
The two rotational frames (the converter dq frame and the synchronous dq frame) are related to each other as follows

$$\begin{bmatrix}\Delta i^d \\ \Delta i^q\end{bmatrix} = \begin{bmatrix}\Delta i^{sd} \\ \Delta i^s q\end{bmatrix} + \begin{bmatrix} i_0^q \\ -i_0^d\end{bmatrix} \Delta\theta_g \tag{3.20}$$

$$\begin{bmatrix}\Delta u_g^d \\ \Delta u_g^q\end{bmatrix} = \begin{bmatrix}\Delta u^{sd} \\ \Delta u^{sq}\end{bmatrix} + \begin{bmatrix} u_0^q \\ -u_d^0\end{bmatrix} \Delta\theta_g \tag{3.21}$$

$$\mathbf{I}_f^s = \mathbf{Y}\mathbf{u}_g^s + \mathbf{F}\mathbf{r} \tag{3.22}$$

where, $[\Delta i_f^{sd} \Delta i_f^{sq}]$, $\mathbf{u}_g = [\Delta u_g^{sd} \Delta u_g^{sq}]$ and $\mathbf{r} = [\Delta i_f^{dref} \Delta i_f^{qref}]$. $\mathbf{Y}$ is the input of the converter.

$$\mathbf{F} = \begin{bmatrix}\frac{\alpha}{s+\alpha} & 0 \\ 0 & \frac{\alpha}{s+\alpha}\end{bmatrix}, Y = \begin{bmatrix} y(s) & 0 \\ 0 & y(s)\end{bmatrix} + \begin{bmatrix} 0 & (yu_{g0}^{sq} + i_{f0}^{sq} f_{pll}(s)) \\ 0 & -(yu_{g0}^{sd} + i_{f0}^{sd}) f_{pll}(s)\end{bmatrix} \tag{3.23}$$

and

$$y(s) = \frac{-s^2}{(sL_f + R_f)(s+\alpha)(s+\alpha_f)}, f_{pll}(s) = \frac{\alpha_f u_{g0}^{sd}}{s^2 + k_{pl} u_{g0}^{sd} s + k_{il} u_{g0}^{sd}} \tag{3.24}$$

Where α is the VCC bandwidth, and $k_p = \alpha L_f$ and $k_i = \alpha R_f$, are the VCC proportional and integral gain, respectively. The definition of the AC grid can be defined by the following transfer function (3.25). The transfer function for the grid impedance can be explained by (3.26) and (3.27).

$$\mathbf{u}_g^s = -\mathbf{Z}\mathbf{i}_f^s \tag{3.25}$$

$$Z_{grid}(s) = \frac{1}{\frac{1}{Z_{cap}(s)} + \frac{Z_{source}(s)+Z_{cap}(s)}{Z_{source}(s)Z_{cap}(s)+Z_{cable}(s)(Z_{source}(s)+Z_{cap})(s)}} \tag{3.26}$$

$$Z_{cap}(s) = \frac{2}{sC_c}, Z_{source}(s) = R_s + sL_s, Z_{cable}(s) = R_c + sL_c \tag{3.27}$$

Here R_s and L_s represents the source resistance and inductance, L_c, R_c and C_c represent the ac cables inductance, resistance and capacitance. If the AC-grid is symmetric, the impedance is the diagonal in the sequence domain. By combining (3.22) and (3.25) a feedback system can be formed as the one in Figure 3.6, [17].

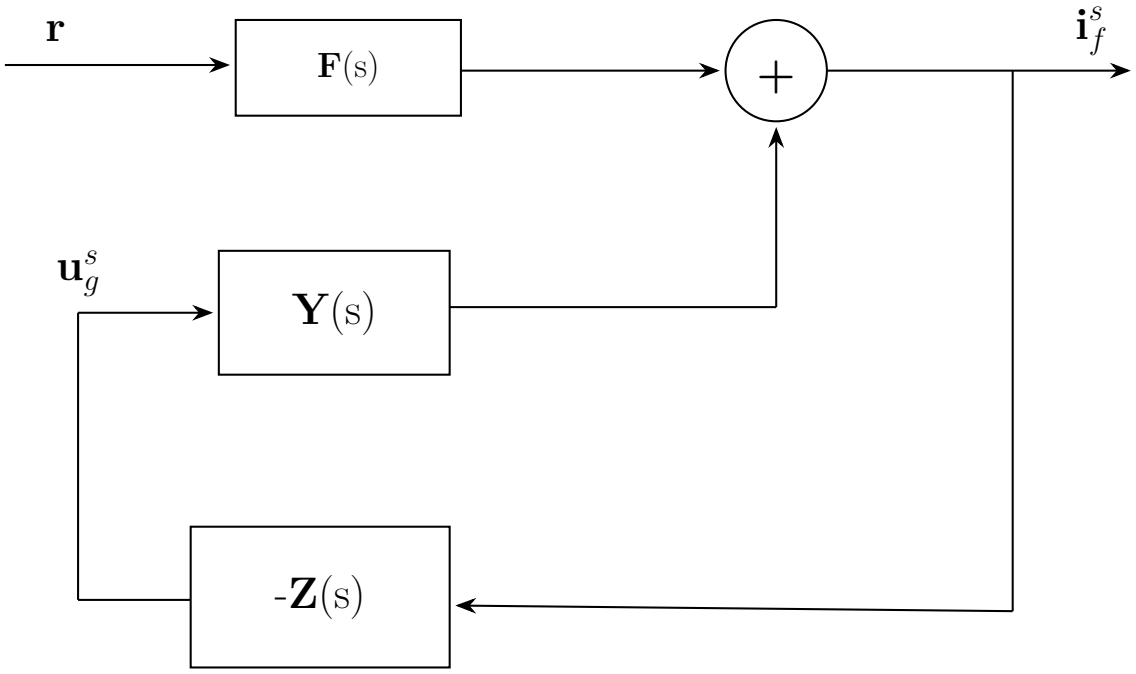

Figure 3.6: Feedback loop of the system.

3.7.3 PSCAD MMC Network testing

To test the system on a non ideal model a MMC model provided in the examples from PSCAD has been used. The measurement tools are connected to the converter where the base frequency is 60 Hz, voltage base is 230 kV and the power base is 1500 MW. A simple representation of the system is shown in Figure 3.7 and is further explained in [37]. Note that the MMC includes power electronic bridges, so some harmonic distortion is expected in the simulations.

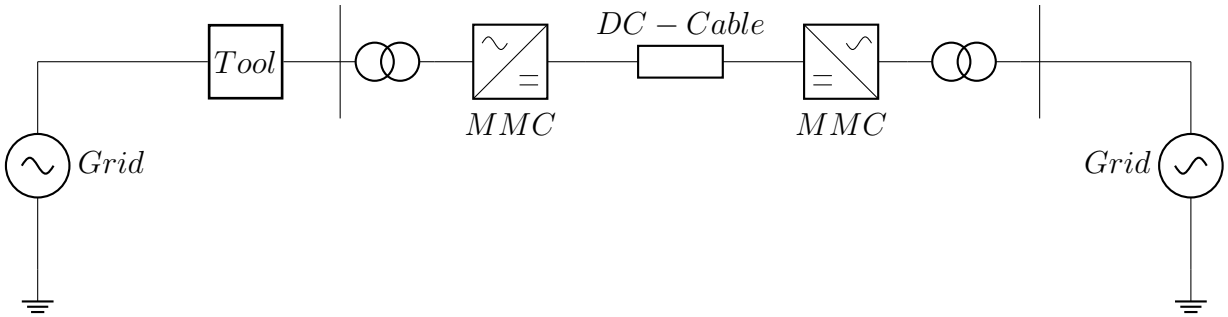

Figure 3.7: PSCAD MMC example.

4

Results and analysis

In this chapter, the results from the different studies performed in the thesis are summarized.

4.1 Tool test and verification

In this Section, the results from the frequency scans performed from the different tools are presented, to verify if the results align well with the frequency responses obtained from the mathematical model. Table 4.1 shows the different cases applied to the mathematical model where the system parameters to be varied are the cable length and the reactive power injection by the converter.

Table 4.1: Simulation cases

case:	cable length (km)	q (reactive power flow in p.u)
1	20	0
2	20	-0.5
3	20	-1
4	30	0
5	30	-0.5
6	30	-1

4.1.1 20 km cable result

For the 20 km cable length, the elements of the PN admittance matrices for a reactive power flow case of 0, -0.5 and -1 p.u are presented in Figure 4.1 and Figure 4.2 respectively. The elements of the grid side impedance characteristics are presented in Figure 4.3. Lastly, the passivity and the Nyquist plots for the different power flow cases are presented in Figure 4.4 and 4.5, respectively.

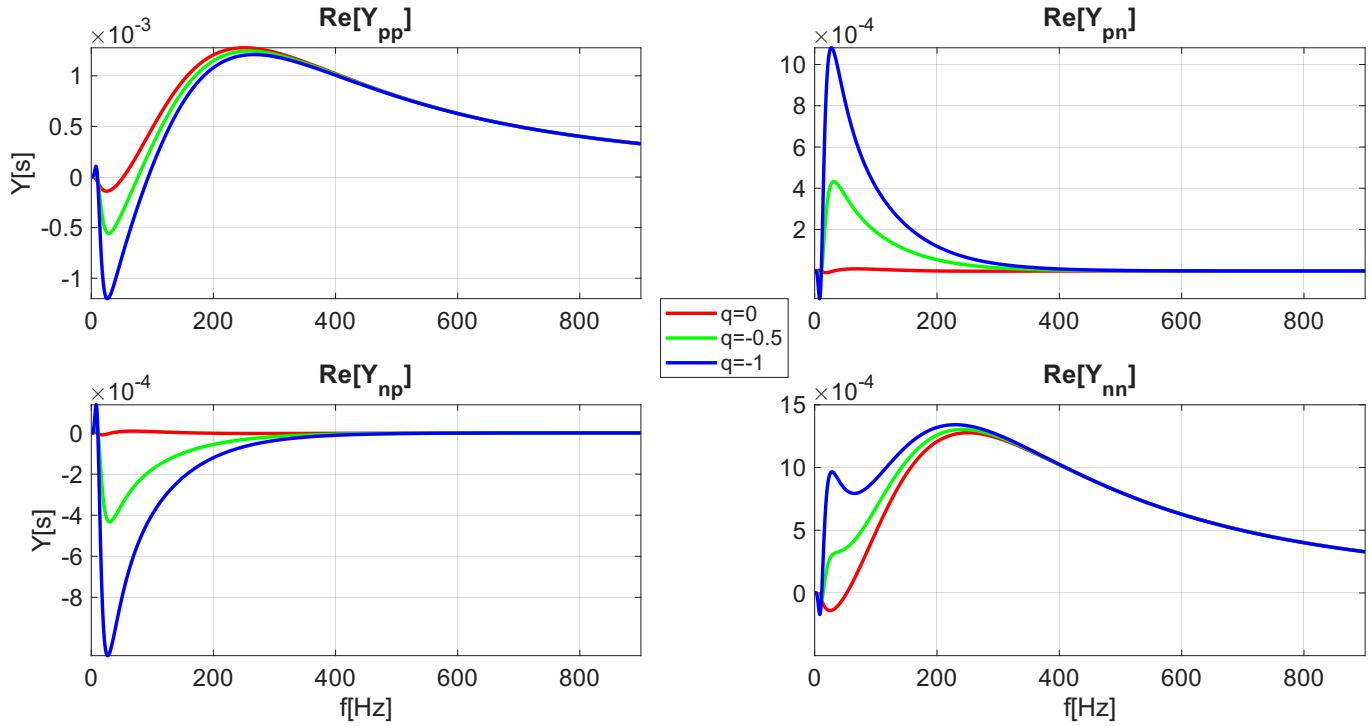

Figure 4.1: Real parts of the elements of the converter PN admittance matrix in siemens Cases corresponds to converter connected to a 20 km cable.

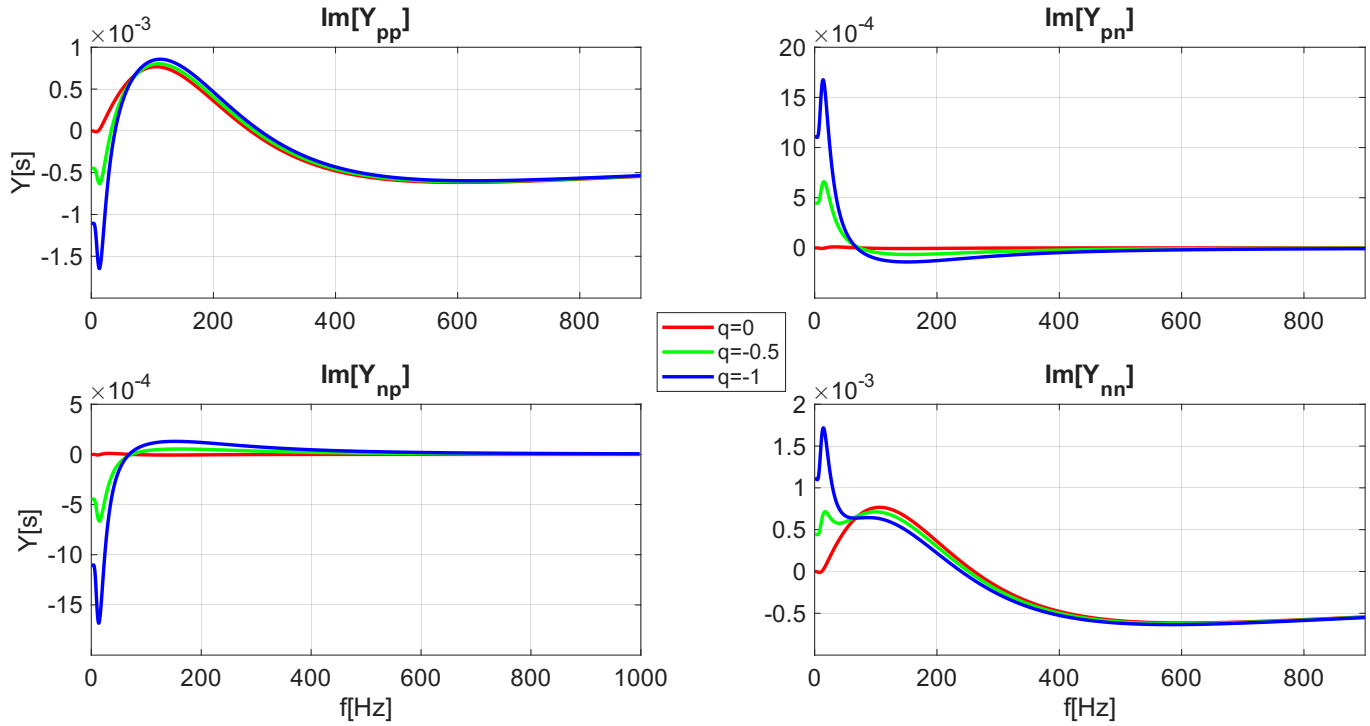

Figure 4.2: Imaginary parts of the elements of the converter PN admittance matrix in siemens Cases corresponds to converter connected to a 20 km cable.

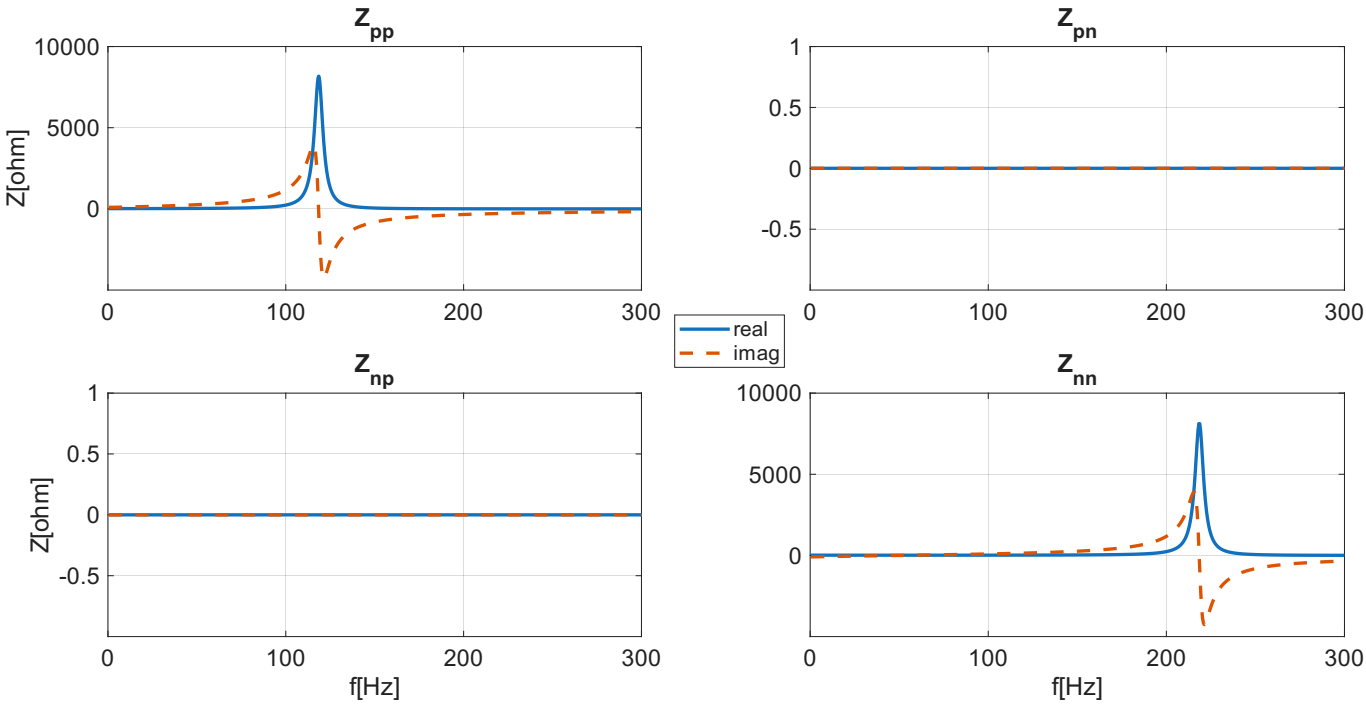

Figure 4.3: Elements of the grid side sequence domain impedance from the mathematical model for a 20 km cable.

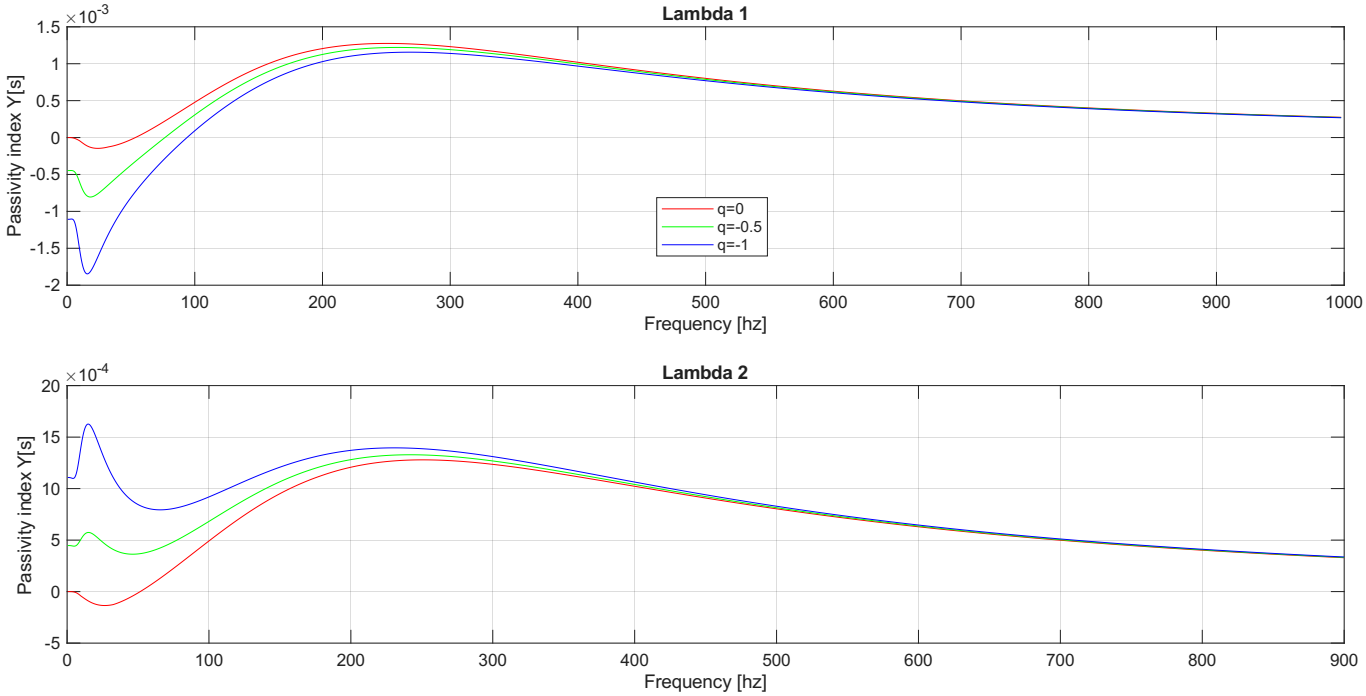

Figure 4.4: Passivity indices λ_1 and λ_2 for the converter connected to a 20 km long cable from the mathematical model

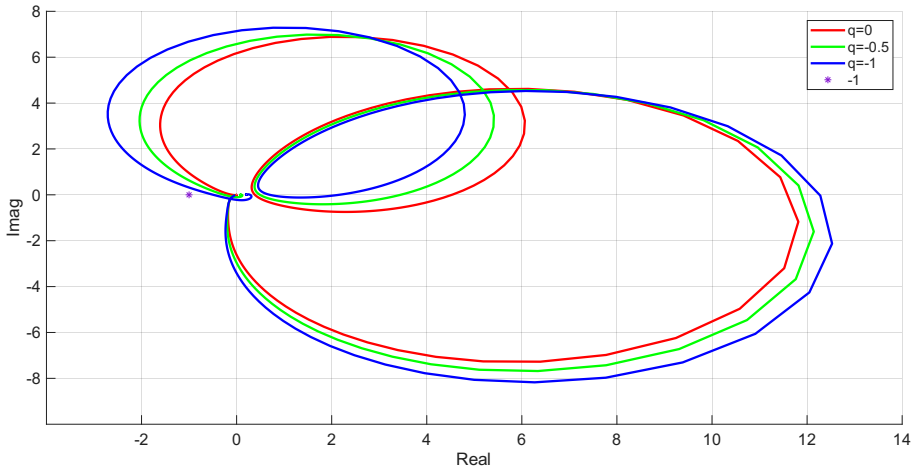

Figure 4.5: Nyquist plot for the open loop system connected to the 20 km cable

The ac resonance can be approximately calculated as follows

$$f_{\text{res}=\frac{1}{2\pi\sqrt{\text{LC}}}} \tag{4.1}$$

Which, with the reactance stated in Section 3.7.1, results in a grid resonance frequency of 167 Hz. This means, that in the sequence domain the resonance peaks appears around 117 Hz in positive sequence and 217 Hz in the negative sequence, as expected considering the mirror frequency effect explained in Section 2.2.3. This coincides with the peaks observed in Figure 4.3. Furthermore, it can also be seen that the Nyquist plots in Figure 4.5 shows stability for all power flow cases. It can also be seen that the higher the reactive power consumed by the converter, the closer the system moves to instability.

4.1.2 30 km long cable

For the 30 km cable length, the real parts of the elements of dq and PN plots for a reactive power flow case of 0, -0.5 and -1 p.u are presented in Figure 4.6 and Figure 4.7, respectively. The corresponding imaginary parts are presented in Figure 4.3 and 4.4. The elements of the grid side impedance are presented in Figure 4.8 for the PN domain. Lastly, the passivity and the Nyquist plots for the different power flow cases with a 30 km grid is presented in Figure 4.9 and 4.10.

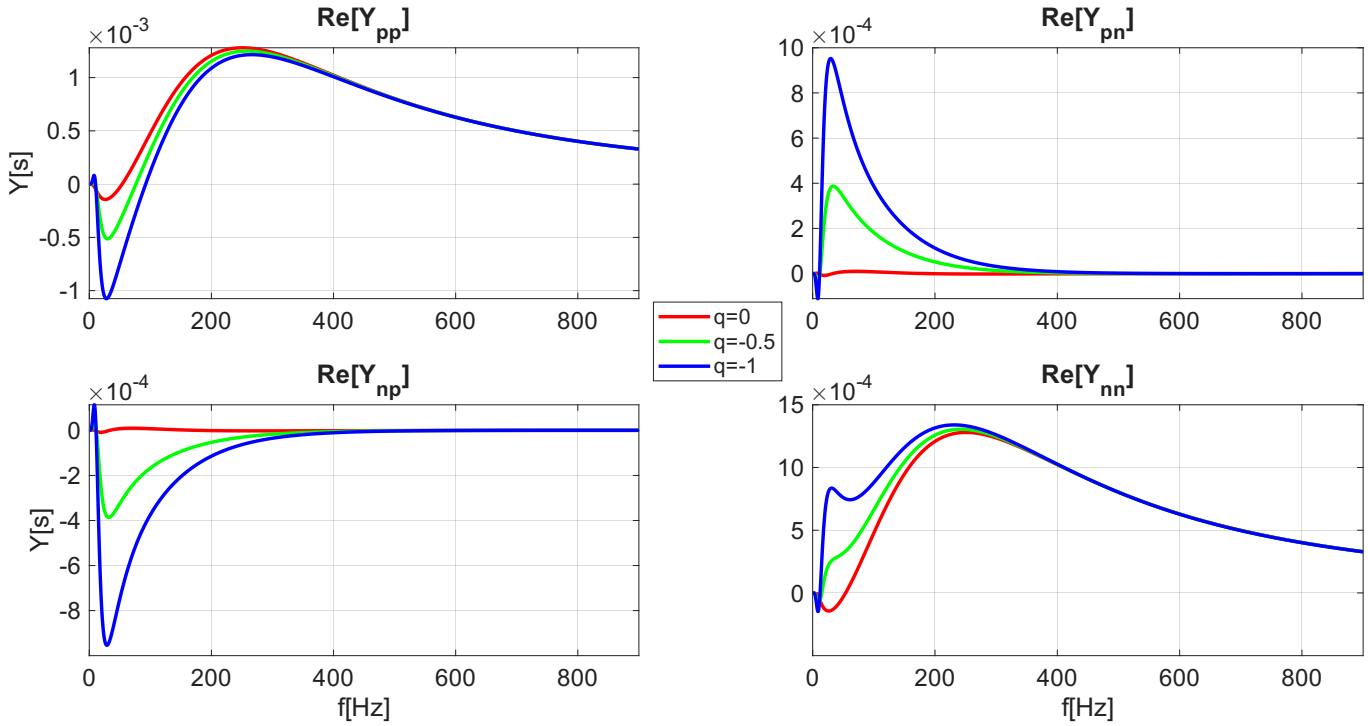

Figure 4.6: Real PN domain admittance results from the mathematical model for a 30 km cable.

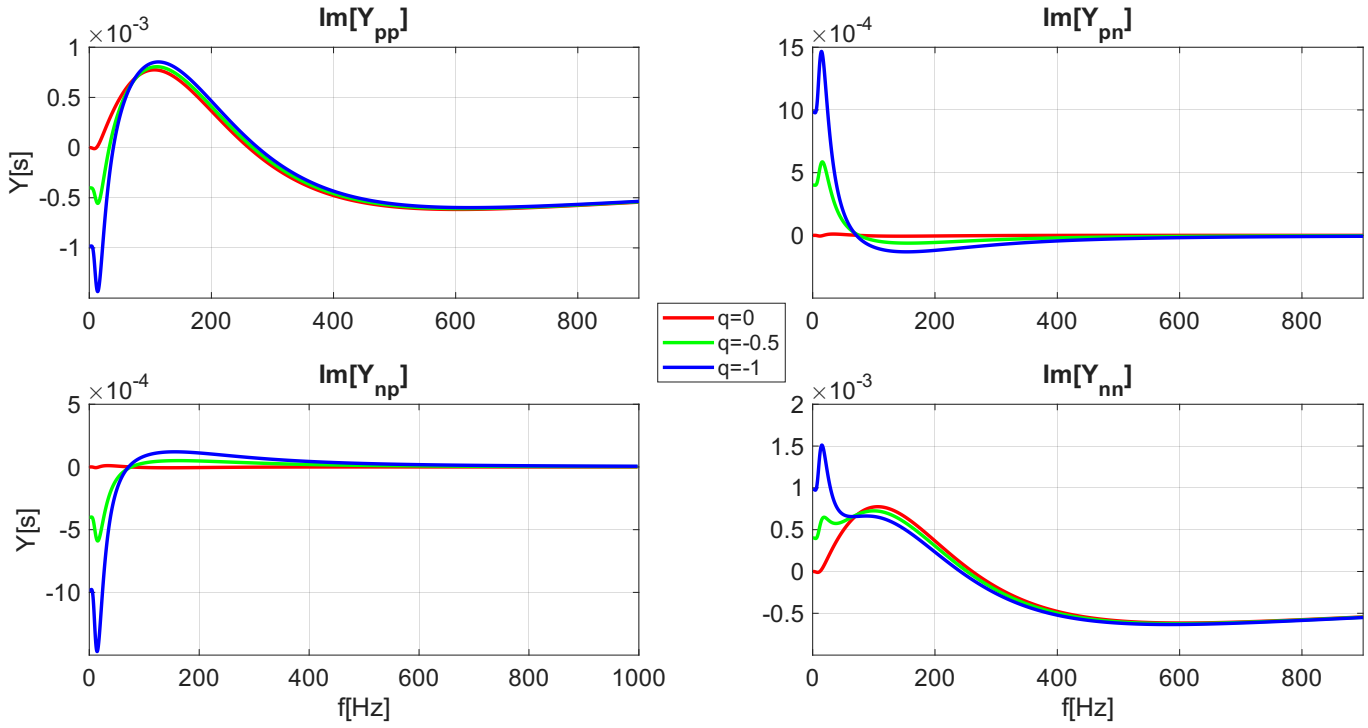

Figure 4.7: Imaginary PN domain admittance results from the mathematical model for a 30 km cable.

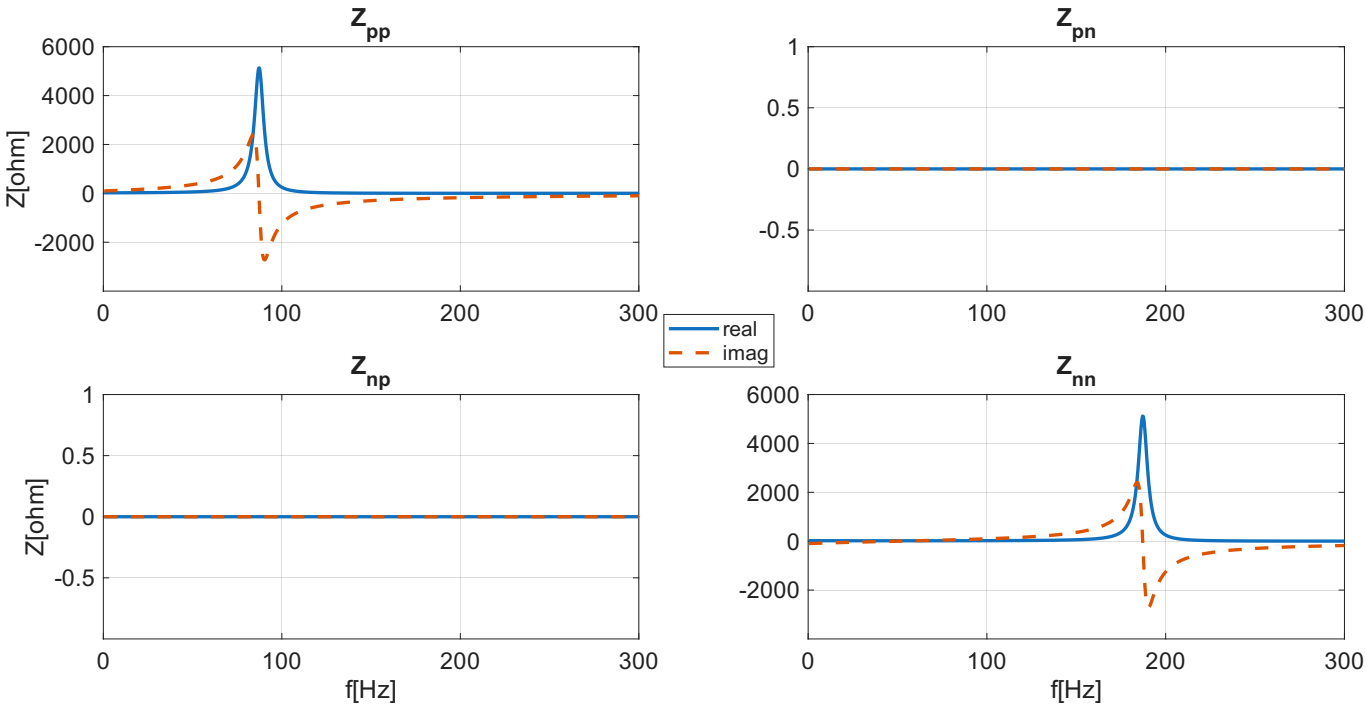

Figure 4.8: Mathematical grid equivalent impedance characteristics in PN domain for a 30 km cable.

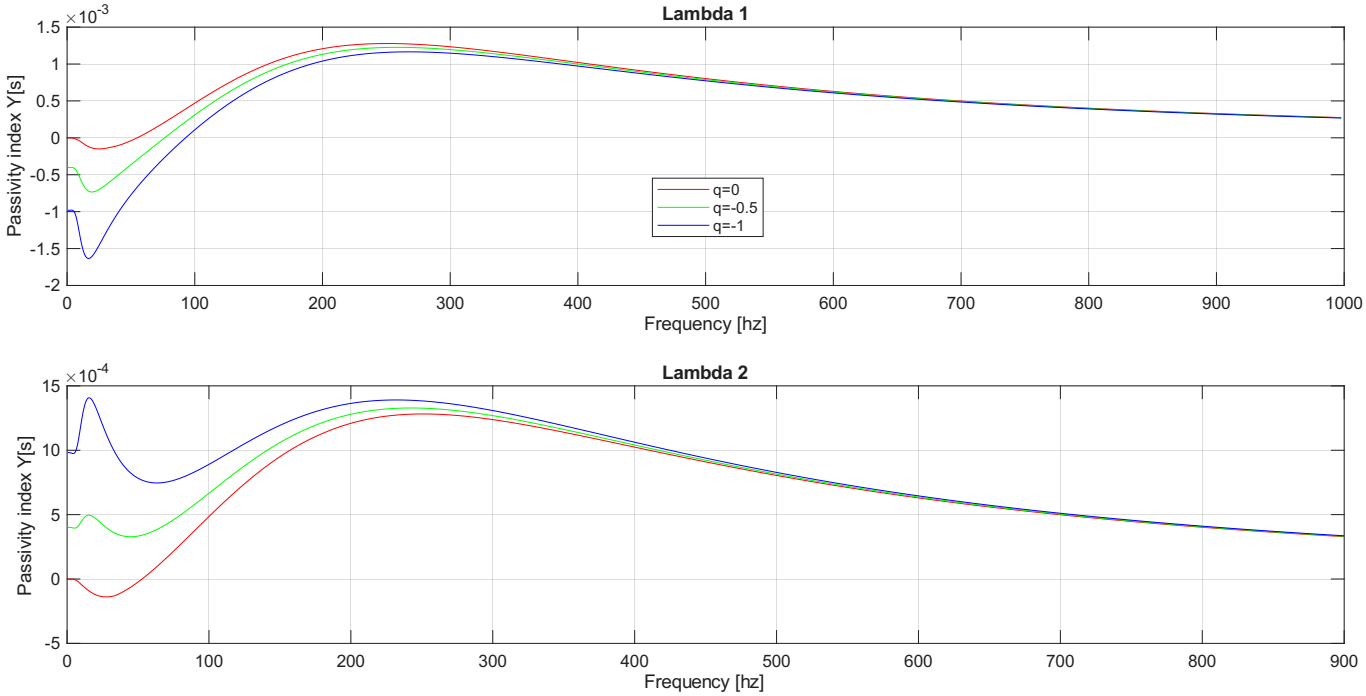

Figure 4.9: Passivity analysis for the case of 30 km long line from the mathematical model for a 30 km cable.

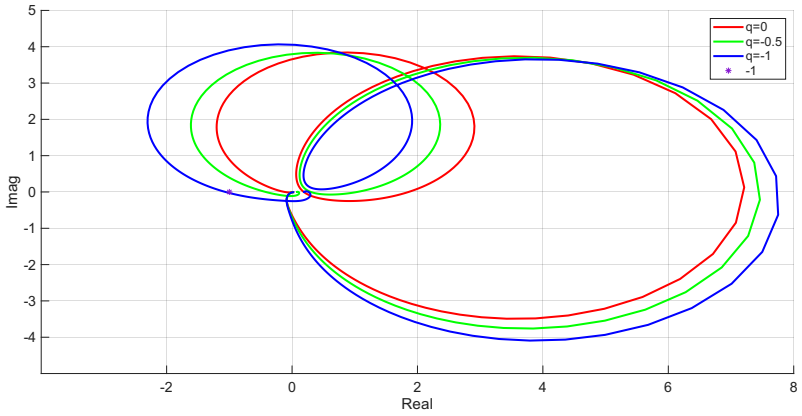

Figure 4.10: Nyquist plots for the previously shown admittance characteristics of the system for a 30 km cable.

Using the same approach as in Section 4.1.1, the expected resonance frequency was found at 136 Hz. This means expected resonance peaks at 86 Hz in the positive sequence and 186 Hz in the negative sequence, which corresponds well with the resonance peaks from Figure 4.8. Further, what is specifically of interest for this case is that the system becomes unstable when the power flow is q=-1 as can be seen in the Nyquist plot, as shown in Figure 4.10. Time domain simulation have been run to verify the results of the Nyquist stability criterion. The simulation consists of decreasing the current reference in the q-axis (regulating the reactive power exchange) from 0, -0.5 and then to -1. p.u, for both cable lengths, 20 km and 30 km. The results are presented in Figure 4.11a and 4.11b
As can be seen in the results, the converter reaches instability when connected to the 30 km line, which confirms the theoretical analysis.

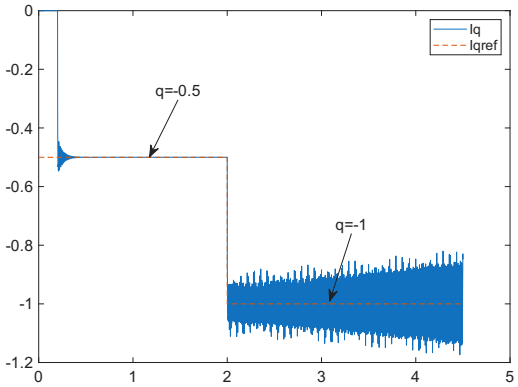

(a) q-current from converter connected to a 30 km pi-section cable.

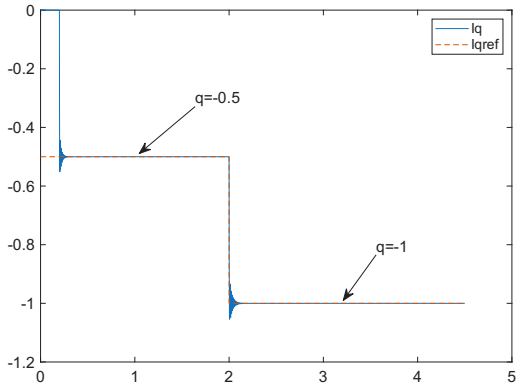

(b) q-current from converter when connected to a 20 km pi-section cable.

Figure 4.11: Time domain characteristics from the PSCAD model.

4.2 Tool Validation

The validation of the thesis tool is performed through a multi-frequency injection of 10 simultaneous perturbations. The grid and converter are measured separately to avoid interference. The converter is measured using a series voltage perturbation and the grid is measured using shunt current injection. In order to obtain the initial operating points for the converter, a load flow simulation is performed for each case. The respective cable lengths, reactive power flow and operating point at the converter terminal are presented in Table 4.2

Table 4.2: Table presenting the changing parameters for the test cases.

case:	cable length (km)	q (reactive power flow in p.u)	Terminal voltage, u_c (p.u)
1	20	0	1.097
2	20	-0.5	1.013
3	20	-1	0.910
4	30	0	1.155
5	30	-0.5	1.069
6	30	-1	0.966

For each case a multi-frequency perturbation is injected and the frequency injections are shown in Table 4.3

Table 4.3: Injected frequencies.

Simulation	Frequencies to be injected simultaneously (Hz)									
1	2	92	182	272	362	452	542	632	722	812
2	3	93	183	273	363	453	543	633	723	813
3	4	94	184	274	364	454	544	634	724	814
.	.	.	.	.	.	.	.	.	.	.
.	.	.	.	.	.	.	.	.	.	.
.	.	.	.	.	.	.	.	.	.	.
88	89	179	269	359	449	539	629	719	809	899
89	90	180	270	360	450	540	630	720	810	900
90	91	181	271	361	451	541	631	721	811	901

4.2.1 Grid measurement

The thesis tool was applied to the PSCAD model mentioned earlier and set up to measure the grid for a cable length of 20 km and 30 km. Both results are shown in Figure 4.12 and 4.13. Comparing these plots with the ones shown in Figure 4.3 and 4.8 shows that the tool manages to capture the grid with good accuracy.

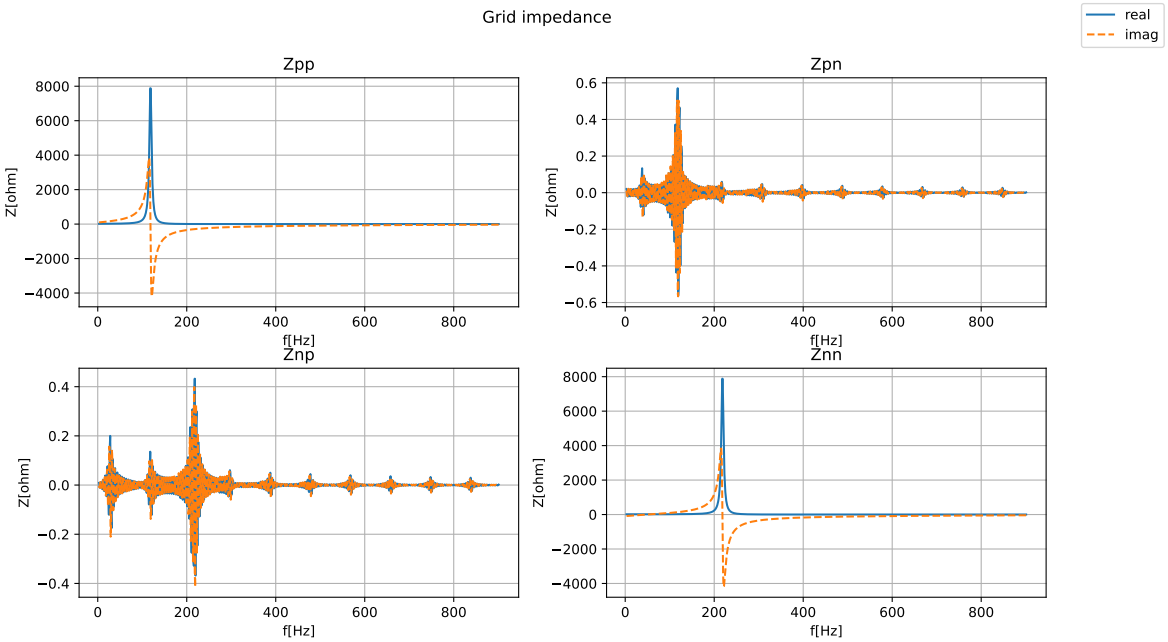

Figure 4.12: Grid impedance characteristics captured by the thesis tool for a 20 km long cable

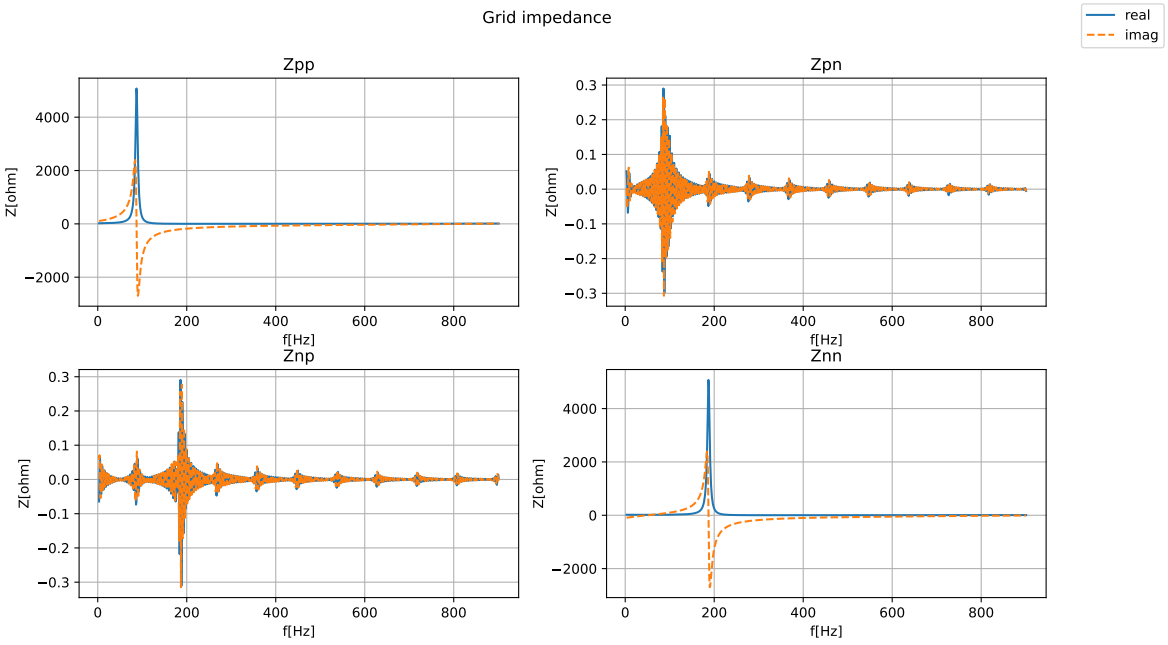

Figure 4.13: Grid impedance characteristics captured by the thesis tool for a 30 km long cable

4.2.2 Converter admittance scan

The tool analysis of the converter yielded, similar to the grid impedance, very accurate results. The admittance matrix elements for a reactive power flow of $q = -1$ are shown in Figure 4.14 and 4.15. The only impact that the grid has on the converter admittance in this case is that the different voltage operating points give a change in amplitude which can be seen in Figure 4.14 and Figure 4.15. A direct comparison between the measurements of the thesis tool and the mathematical model results are shown in Figure 4.16 where minor differences are observed.

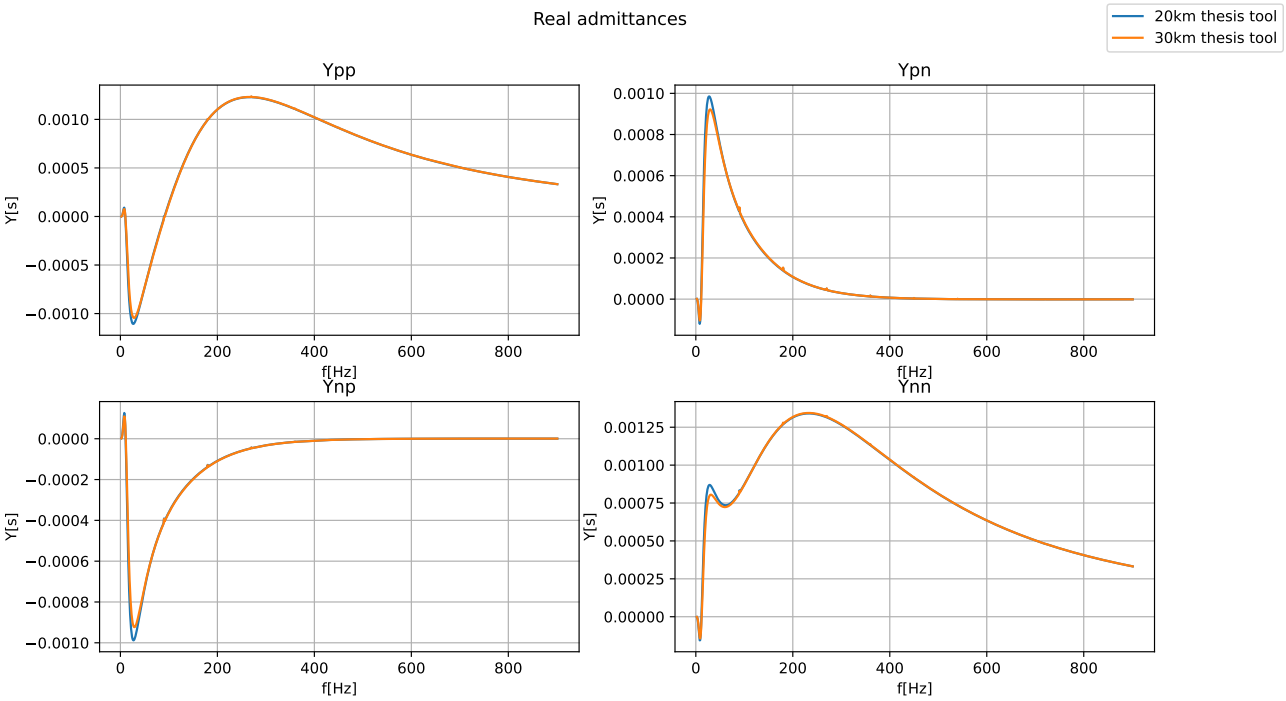

Figure 4.14: Real converter admittance characteristics captured by the thesis tool.

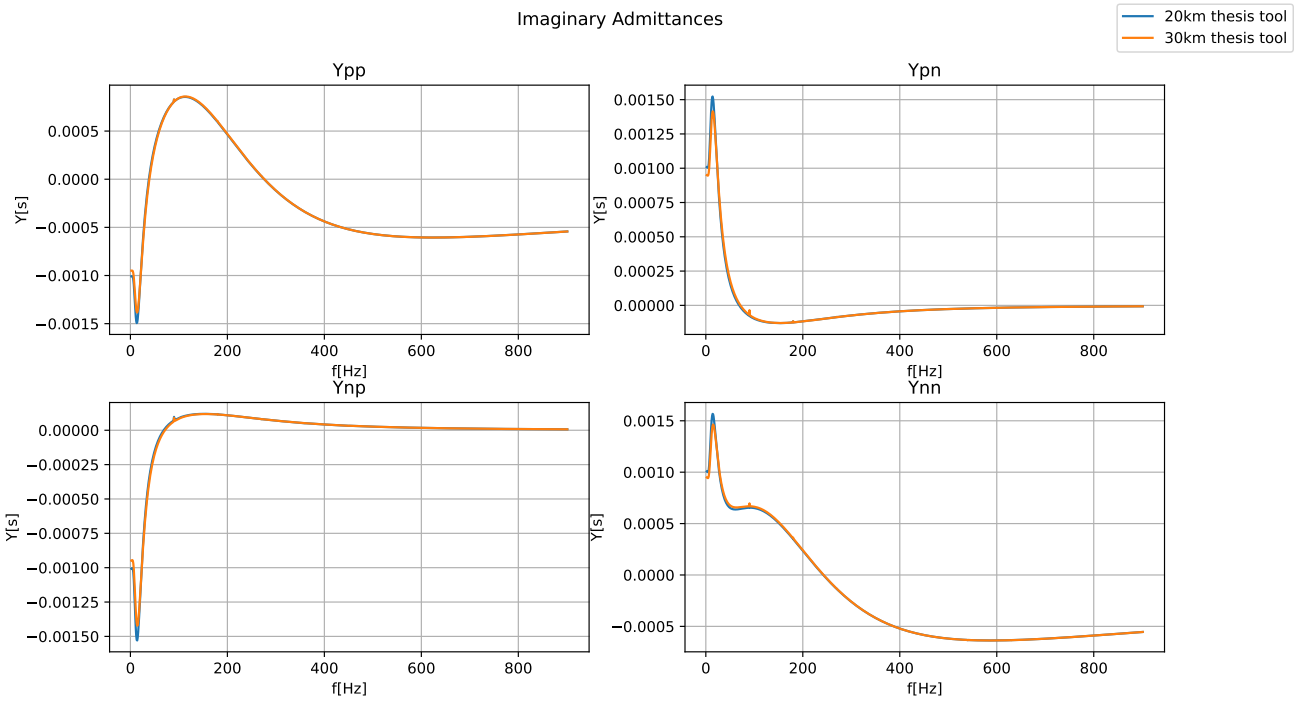

Figure 4.15: Imaginary converter admittance characteristics captured by the thesis tool.

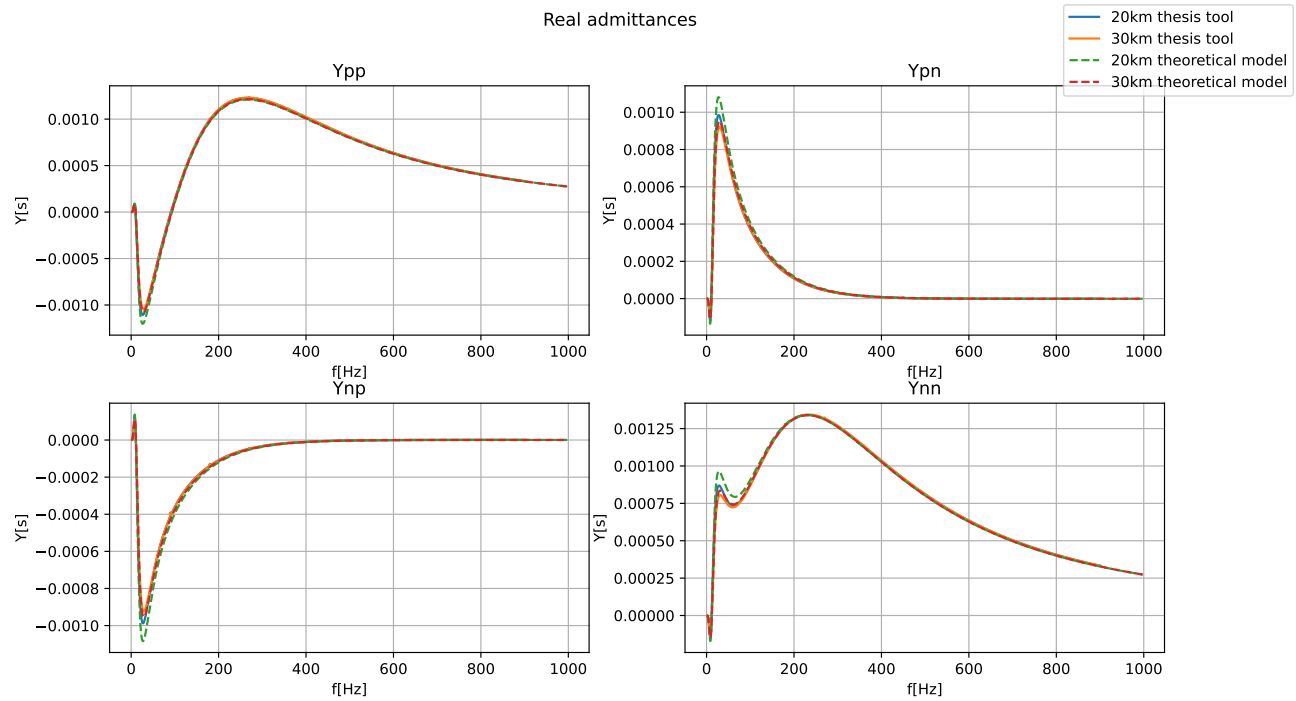

Figure 4.16: Real converter admittance characteristics captured by the thesis tool and the mathematical model.

4.2.3 Tool notes

The Nyquist plots are not presented, but they yielded the same conclusion as the mathematical model. The multi-frequency perturbation implementation did not yield any errors in the plots and it also managed to cut down the simulation times from 2 hours and 10 minutes to approximately 14-16 minutes.

4.3 Validation of other tools

Admittance and impedance scans have been performed for the system described in Section 3.7.1 with the tools presented in Section 2.5. General comments about the tools with regards to modification or similar things are introduced in the following sections and then all tools are compared in the same plot.

4.3.1 IMTB

The results from IMTB are primarily presented in dq-domain since that is the main sequence the tool is built for. Worth noting for this tool is that it gives the results as impedances and not admittances so to be able to measure and compare with the other characteristics it has therefore been altered to show admittance matrices from the converter instead. IMTB lacks any form of further stability analysis other than impedance measurement. As such, impedance and admittances are the only things that will be discussed.

4.3.2 Z-tool

Z-tool gives all results from the scan in dq-domain admittance form so to be able to compare with the earlier models the admittance characteristics of the grid has as such been transformed to impedances for the sake of comparison. Z-tool uses the Nyquist plots of the eigenvalues of the open loop transfer function, while the thesis tool uses the determinant of $\mathbf{I}+\mathbf{L}(s)$, however, conclusions are the same. The passivity analysis also yielded the same conclusion.

4.3.3 SIaD

Similar to Z-tool, SIAD also provides all results in admittances, so for the grid characteristics these admittances have been transformed into impedances. It plots the Nyquist stability plots as well as the passivity plots the same way as Z-tool does it and for the 20 km q=-1 case the results are very much the same. However, for the 30 km q=-1 case the tool was not able to capture a stable admittance plot of the system, hence they are not shown.

4.3.4 Tool comparison

A more direct comparison between the tools and the mathematical model are presented in the following sections. Note that unlike the previous comparison between

the thesis tool and the mathematical model this analysis is done in dq since the majority of the tools are defined in the dq-domain.

4.3.4.1 20 km line q=-1

The results for the real values of each tool measurement is presented in Figure 4.17 and the imaginary plots are presented in Figure 4.18.

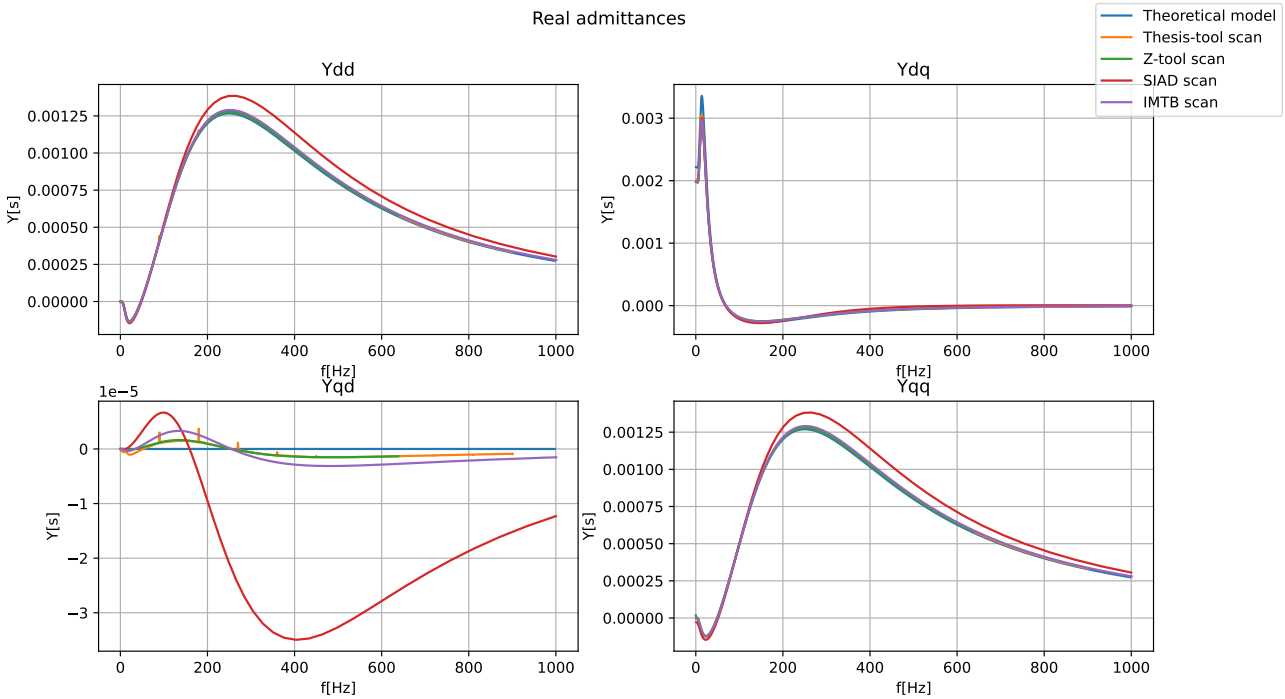

Figure 4.17: Real values from all the tools and the mathematical model.

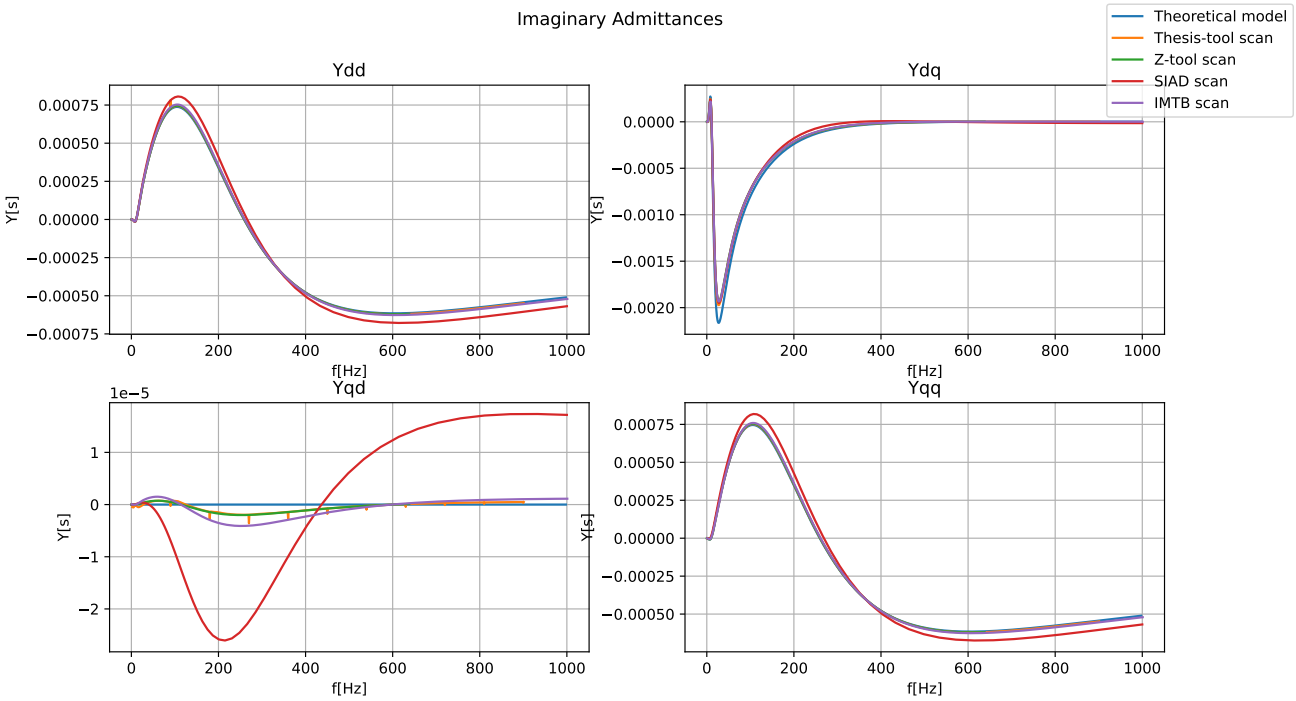

Figure 4.18: Imaginary values from all the tools and the mathematical model.

4.3.4.2 30km line q=-1

The results for the real values of each tool measurement are presented in Figure 4.19 and the imaginary plots are presented in Figure 4.20.

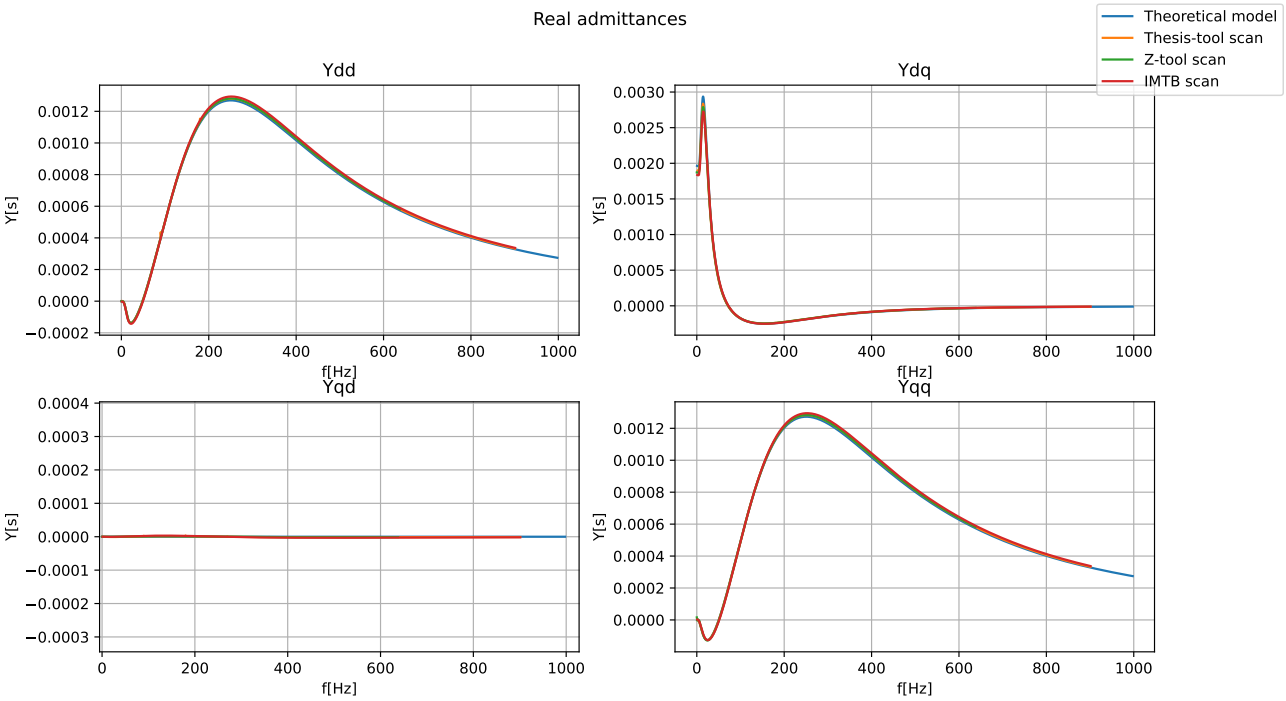

Figure 4.19: Real values from all the tools and the mathematical model.

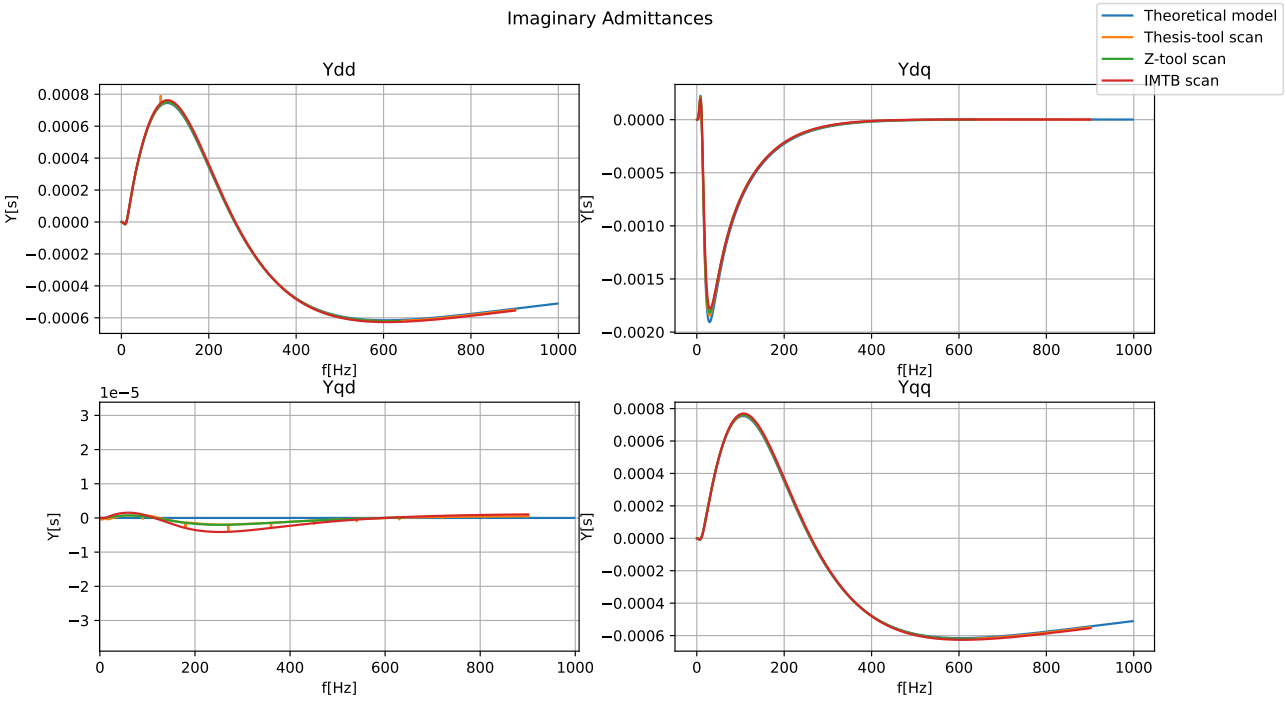

Figure 4.20: Imaginary values from all the tools and the mathematical model.

As can be seen, each tool show similar accuracy. Z-tool, the thesis tool and IMTB all have approximately the same error compared to the mathematical model which

shows that the tools are relatively reliable. SIaD could however not capture the 30 km cable case since the system was unstable and for the 20 km case it has also been seen that the tool has differing amplitudes compared to the other tools, however the difference is not that large.

4.3.5 PSCAD MMC model

Admittance scans has been performed using both Z-tool and the tool developed for this thesis, in order to to identify the challenges that might appear when performing the scans on a more detailed model. It has been found from initial scans that the system gives extremely small current responses indicating high impedance as well as having steady state noise. As such, three cases have been tested with a perturbation magnitude of 5%, 1% and 0.1%. The real part of the admittance in the dq domain for the two injection cases are presented in Figure 4.21. The thesis tool and the Z-tool showed similar results and as such only the results from the thesis tool are shown here.

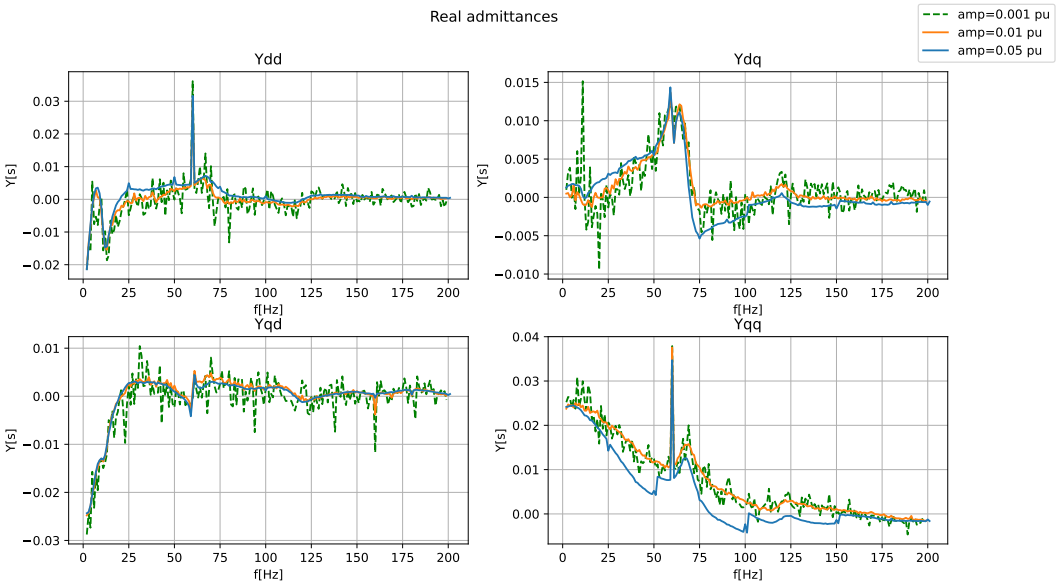

Figure 4.21: MMC dq analysis acquired from the developed tool.

From Figure 4.21, the injection that has 1% and the injection with 5% differed a bit from each other in amplitude, the same phenomena could be seen for Z-tool as well. Note that an amplitude of 2% was also injected which yielded the same amplitude as injecting 1%. The 0.1% shows very noisy measurements compared to the other two measurements. A steady state analysis of the RMS voltage of the system was also performed which is shown in Figure 4.22 where the average deviation casued by the noise was appreciated to be 0.7 kV.

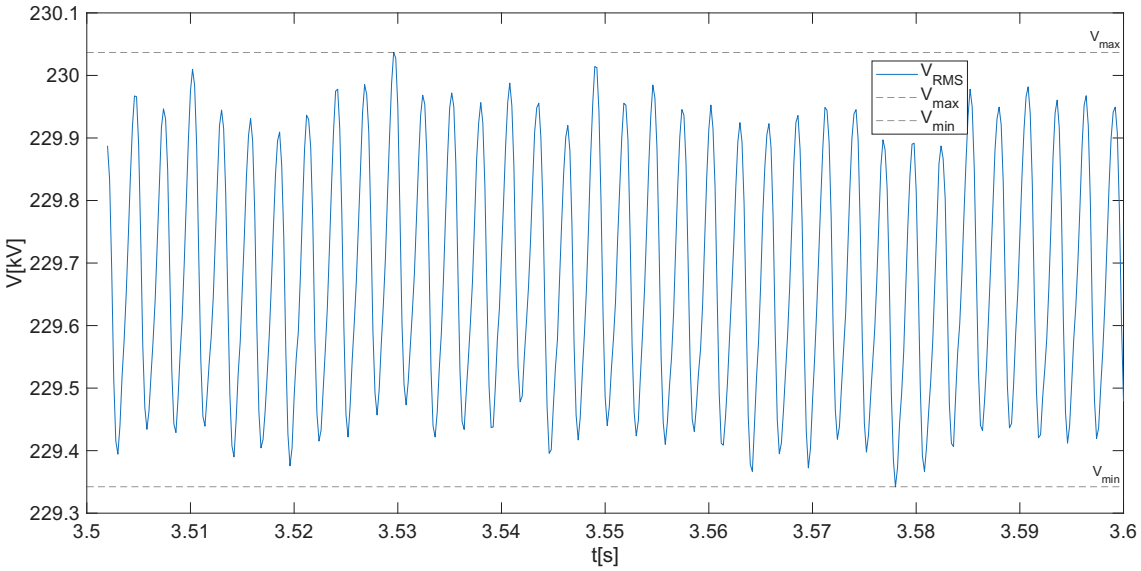

Figure 4.22: RMS voltage variation of the MMC when no disturbance is applied.

4.3.6 Disk margin implementation

For the implementation of the disk margin in the Nyquist plot, the S-based disk margin from Section 2.3.3 was used. A circle was plotted with the center at -1 and radius as the minimum distance to the $L(s)$ curve. The disk represents all simultaneous gain and phase perturbations that the system could handle while maintaining stability. A stable case of the S-based disk margin is shown in Figure 4.23.

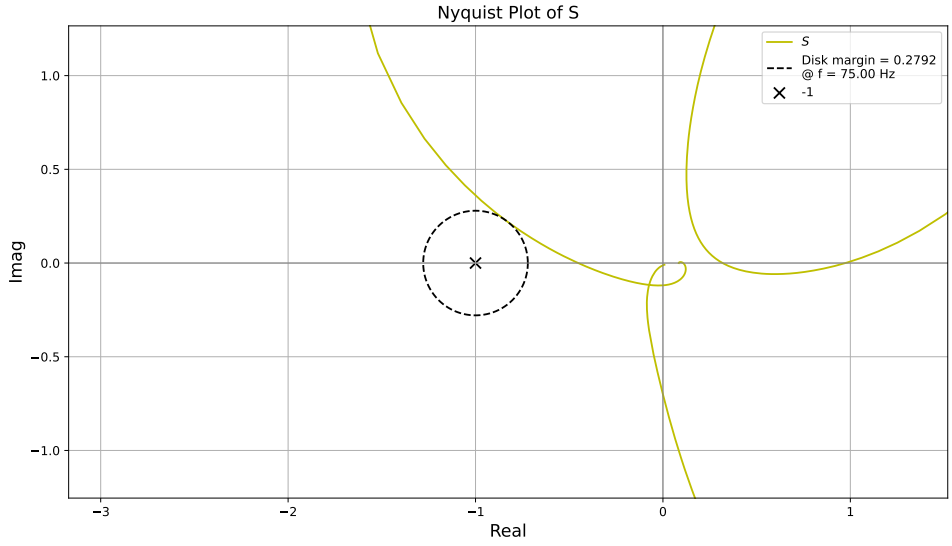

Figure 4.23: Disk margin plotted in the complex plane for the case with 30 km cable and q=-0.5.

The plot and its radius are mainly to give an graphical indication of how close

the system is to instability. The disk margin is also used for means of comparison between different cases.
For a reference of how the system is performing, the classification from [29] using (2.18) is applied. The results are shown in Table 4.4 below.

Table 4.4: Strength index of the system for the thesis test cases.

cable length(km)	Reactive power flow (q)	S-based Disk margin	Strength Index (SI)
20	0	0.5668	0.4391
20	-0.5	0.4438	0.3430
20	-1	0.2948	0.2051
30	0	0.5136	0.3955
30	-0.5	0.2792	0.2273
30	-1	unstable	unstable

The SI values shows that a reactive power flow of 0 and -0.5 for both cable lengths and -1 for 20 km cable length describes the system as moderately stable, according to the definitions stated in Section 2.3.3. For a reactive power flow of -1 and cable length of 30 km the system is at risk of being unstable and having oscillations, according to Section 2.3.3.

4.4 SISO, MIMO and Svenska kraftnät approach comparison

The SISO method where cross-coupling is neglected gilded the following results for the case $q = -1$ for 30 km.

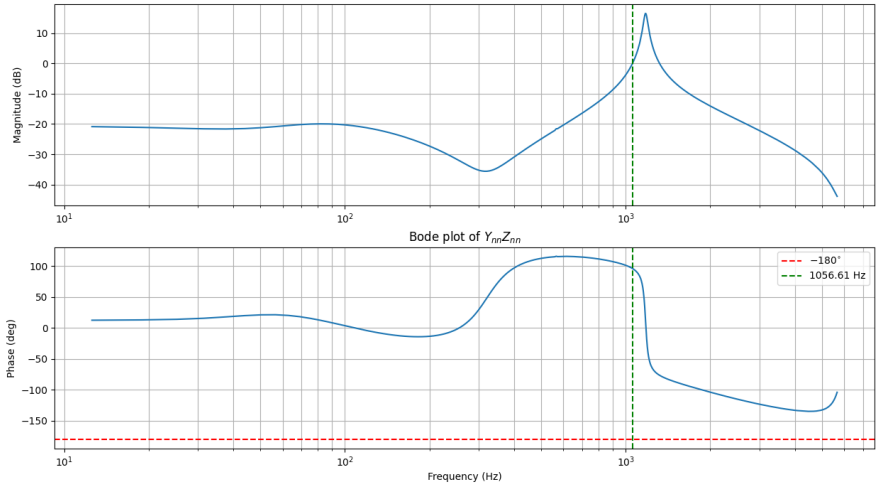

Figure 4.24: Bode plot of negative sequence open loop function.

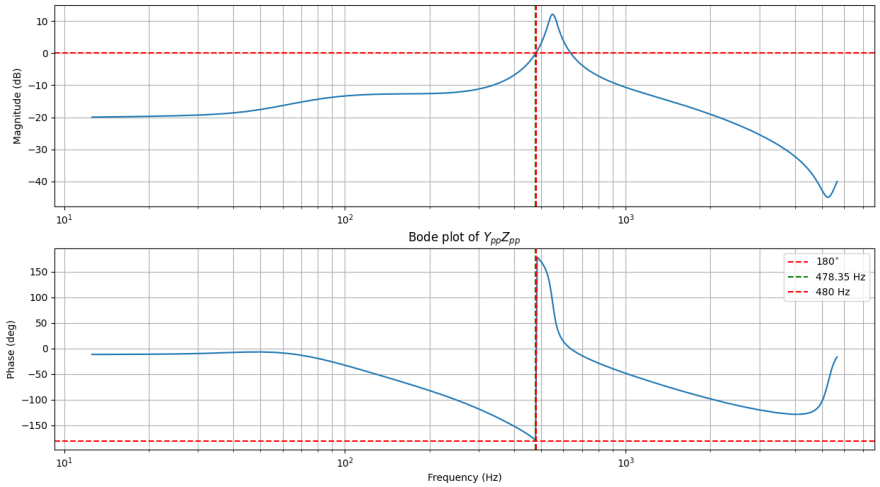

Figure 4.25: Bode plot of Positive sequence open loop function.

From Figure 4.25, it can be concluded that the system is unstable since it supersedes a phase angle of $\pm 180°$ in unity with a gain greater than 1, at the observed crossover frequency of ≈ 479Hz which means the system is unstable.

As mentioned during the test cases for the developed tool, the stability analysis for the $q = -1$, 30 km cable, case is expected to have an unstable condition, as shown in Figure 4.26.

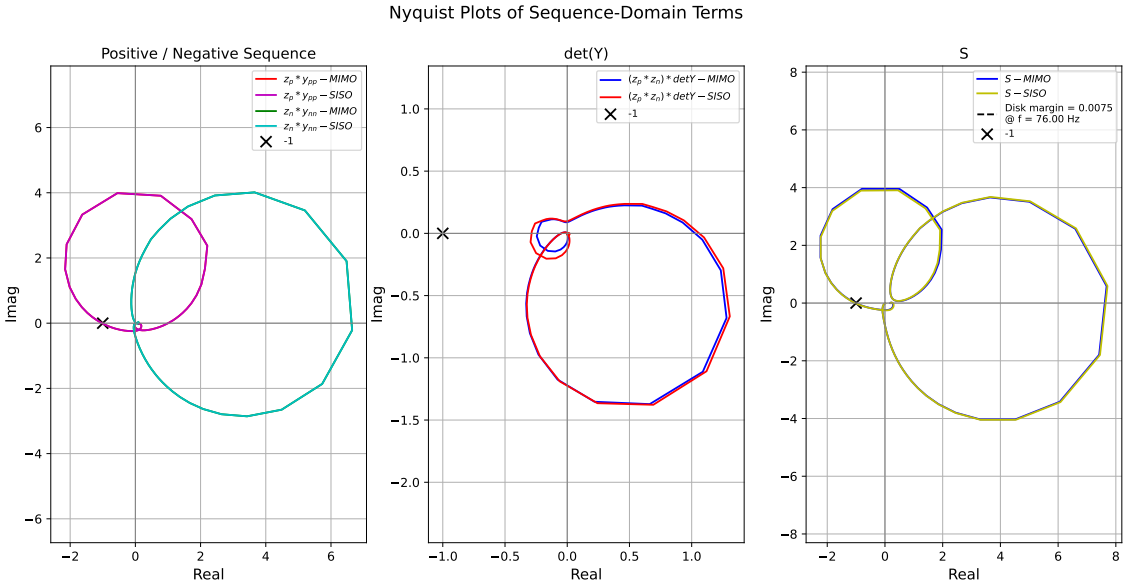

Figure 4.26: Nyquist plot of the open loop function from both the MIMO and SISO calculation.

According to the test model, the case $q = -1$ should be unstable according to the mathematical model. The Bode plots show a phase margin of $\varphi_m = -0.782°$ and gain margin of $A_m = -0.228$, which shows that the system is unstable. A comparison between the SISO Nyquist plots and the $y^{pp}z^p$ and $y^{nn}z^n$ are shown in Figure

4.26. For this particular case, small difference can be shown between the two approaches.

The phase and gain margins for the different test cases are presented in Table 4.5 and 4.6.

Table 4.5: Phase and gain margin for positive sequence.

cable length(km)	Reactive power flow (q)	Phase margin (φ_m)	Gain Magnitude (A_m)
20	0	42.17°	19.07
20	-0.5	31.86°	11.7
20	-1	20.5°	6.57
30	0	36.3°	16.9
30	-0.5	19.25°	7.5
30	-1	-0.782°	-0.228

Table 4.6: Phase and gain margin for negative sequence.

cable length(km)	Reactive power flow (q)	Phase margin (φ_m)	Gain Magnitude (A_m)
20	0	79.17°	∞
20	-0.5	82.35°	∞
20	-1	85.54°	∞
30	0	80.4°	∞
30	-0.5	80.02°	∞
30	-1	84°	∞

Table 4.5 shows that the margins decreases with a decrease in reactive power flow, making the system closer to instability. This compares well with the disk margin results from Table 4.4, where it also decreases with decrease in power flow.

4.4.1 PLL bandwidth increase

A new test case has been performed where a PLL bandwidth of 32 Hz (equal to 0.64 in p.u) is applied. The Nyquist plots are shown in Figure 4.27. When the PLL bandwidth is increased, the cross-coupling effect increase their magnitudes, as can be seen in the admittance amplitudes for the converter with the original bandwidth and the increased one, as shown in Figure 4.28 and 4.29. Thus, the main intention with this additional case is to test the impact of high cross couplings in the admittance matrix.

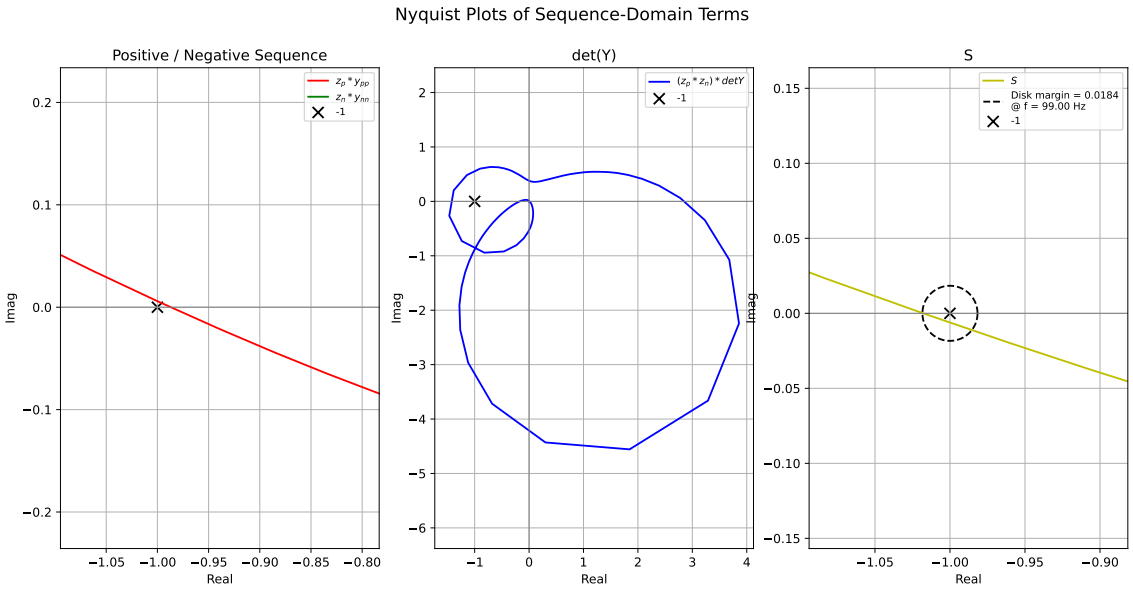

Figure 4.27: Nyquist plot of SISO and MIMO systems, for a 20 km system, q = -0.5 and PLL bandwidth $\alpha_{pll} = 0.64$p.u.

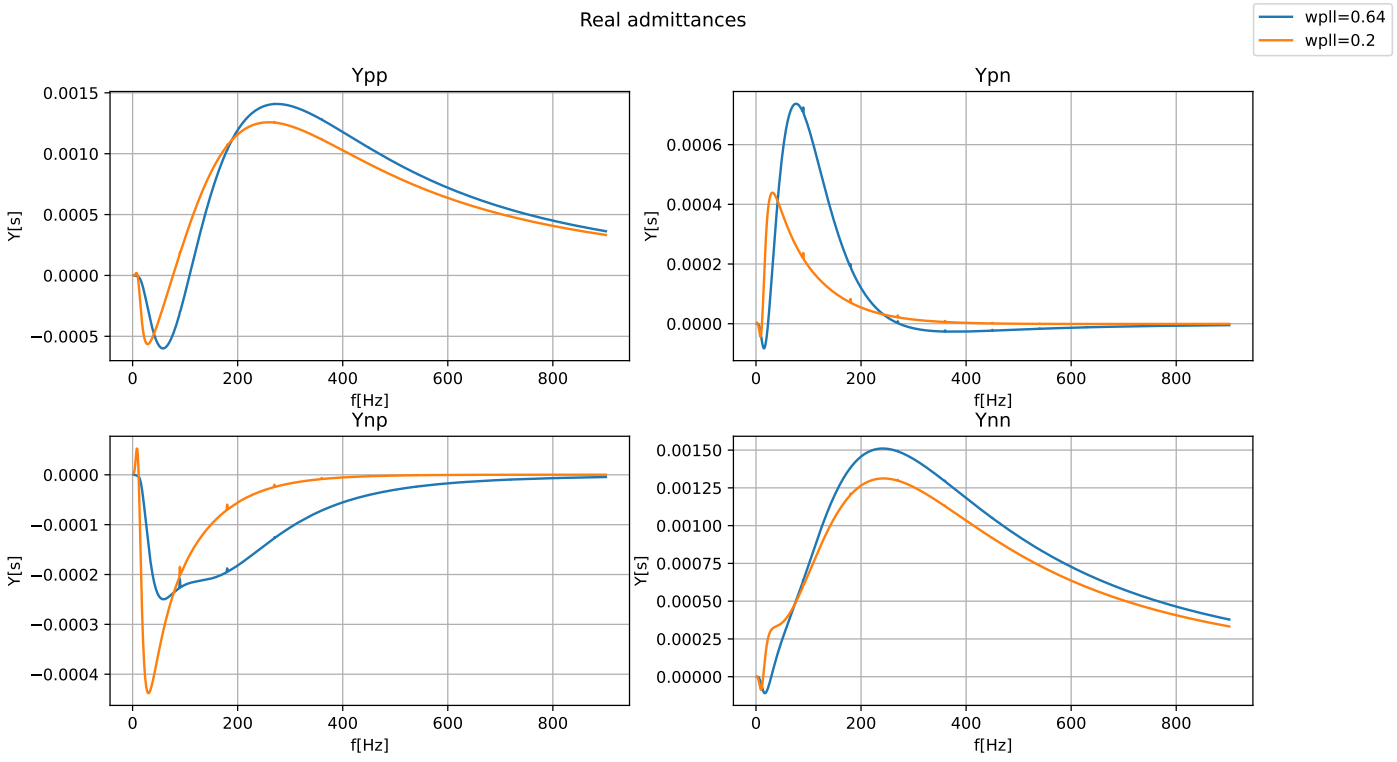

Figure 4.28: Real values for a PLL bandwidth of α_{pll}= 0.2 p.u and 0.64 p.u.

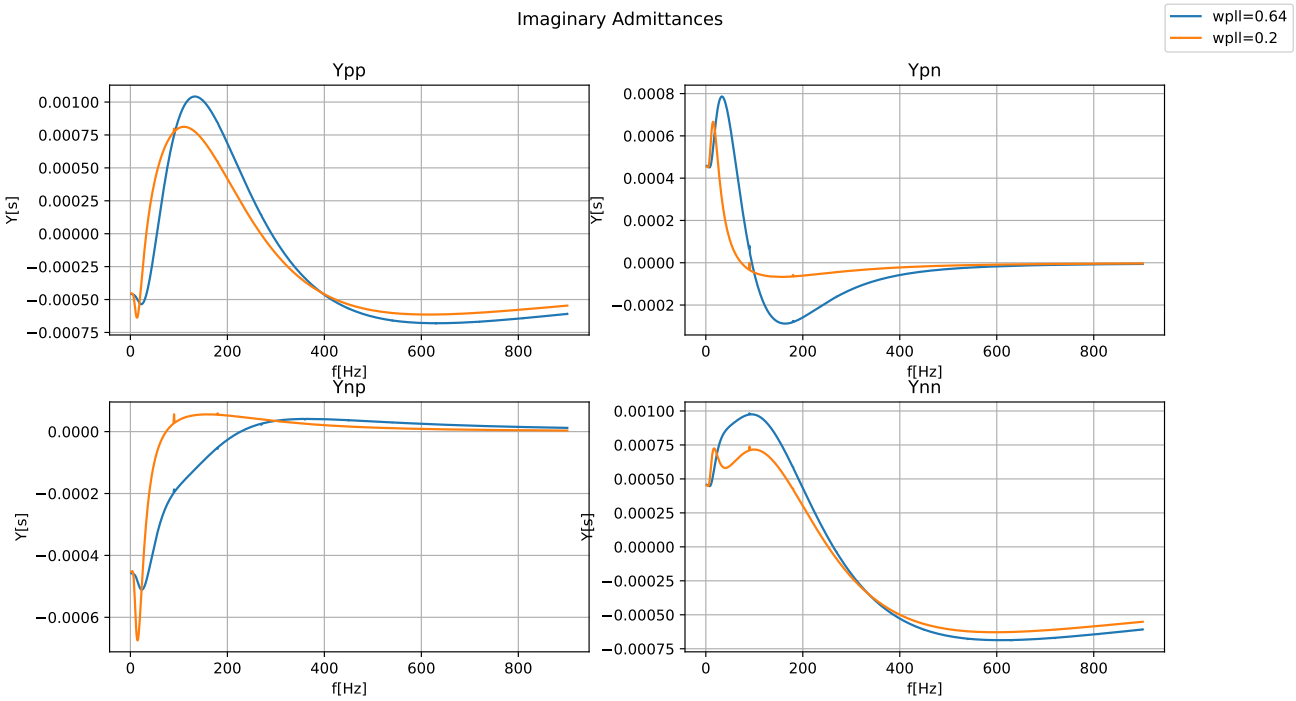

Figure 4.29: Imaginary values for a PLL bandwidth of α_{pll}= 0.2 and 0.64.

even though the Nyquist plots of the SISO and MIMO systems appear to be similar, the increased cross-coupling has a critical effect on the final conclusion, leading to different stability assesment between the SISO and MIMO approach.
The approach performed by Svk, which is described in Section 2.4.2, has also been carried out. Note that in the Svk approach the equivalent admittances are calculated in order to utilize the requirement proposed by Svk. Namely, the phase margin requirement for low frequencies (2.20) and (2.21) and high frequencies (2.22) and (2.23).

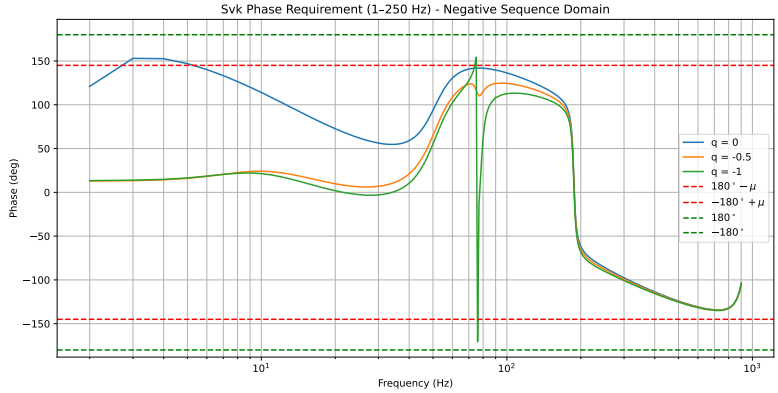

(a) Negative sequence phase criteria for low frequencies

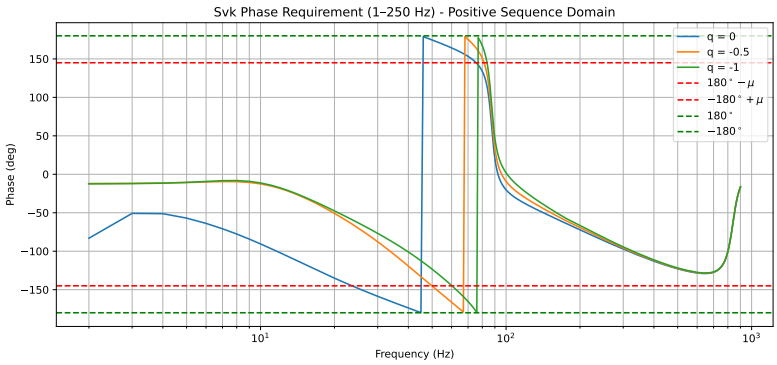

(b) Positive sequence phase criterion for low frequencies

Figure 4.30: Svk phase criterion for a 30 km cable length

Figure 4.30 presents Bode plots using admittances calculated through the Svk approach. For the positive sequence it can be concluded that the phase margin is not fulfilled since the phase margin of $\varphi_m \approx -35°$ is exceeded for all three cases. For the negative sequence a peak can be observed for the case with reactive power flow q=-1, not fulfilling the margin. This is suspected to come from a resonance from the AC grid.

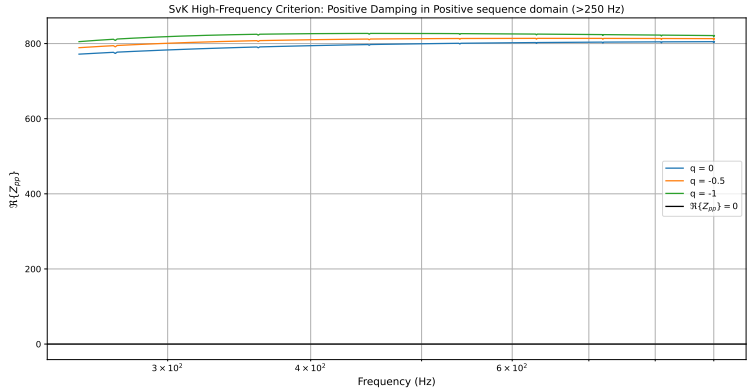

(a) Positive sequence Svk phase criterion at high frequencies

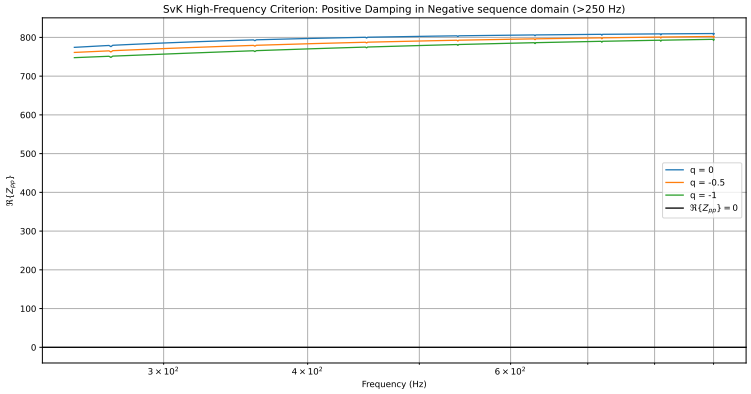

(b) Negative sequence Svk phase criterion at high frequencies

Figure 4.31: Svk phase criterion for real converter impedance at high frequencies.

For frequencies above 250 Hz they can be observed to always be above 0 for both cases, hence they fulfill the requirement.

4.5 Discussion

Discussion about the different topics investigated in this chapter are presented next.

4.5.1 Tool-comparison

Table 4.7 presents an assessment of the used tools for different criteria. The next Sections present details on the assessment.

Table 4.7: Assessment of the used tools on a scale of 1-5 with 5 being the best and 1 being the worst

Tool	IMTB	SIAD	Z-tool	Thesis tool
Time performance	3	1	5	4
User experience	5	3	3	3
Stability analysis	1	5	3	5
Tool adaptability	5	3	4	5

4.5.1.1 Time performance

Simulation times can become critical if the system under study has high complexity. An ideal system can yield results for a full frequency scan in a couple of minutes but for more realistic and detailed models the simulation time can extend up to several days. Therefore, the tool performance with respect to time required to perform the frequency scans are discussed in this section. All tools measured where set up so they had a simulation time step of 5 μs and a channel sample interval of 100 μs. The tools that had the capability for it utilized 8 simultaneous simulations for the analysis and the frequencies where scanned over a spectrum of 1-900 Hz with a frequency step baseline of 1 Hz.

- **IMTB**'s time performance is middle of the line when it came to time consumption. It utilizes PSCADs built in parallel simulation capabilities, which means simulation time can decrease in relation to the amount of parallel simulations that are active. After that, the results are handled by the post processing within a reasonable time which scale up with the total number of frequencies analyzed. The time to complete a scan for each case overall was around 2 hours and 30 minutes.
- **SIaD**'s time performance has been the poorest among all the used tools since at the time of writing this thesis, it performs one simulation for each frequency and does not utilize the earlier mentioned parallel simulation functionality of PSCAD. Compared to the other tools this severely limits it's time performance so that in some cases, to achieve better execution times, the frequency step interval has been lowered. In the SIAD documentation regarding its capabilities it is claimed that it should be able to handle multi-frequency injections which could improve its time performance. However, as of this moment, it has not been implemented. The average time to perform a scan according to the set-up described in this Section has been 18 and a half hours approximately, before lowering frequency step.
- **Z-tool**'s time performance is the fastest compared to all other tools. It utilizes both PSCADs parallel simulation method and multi-frequency injection which further decreases simulation time. Its post processing of the measured results is faster than any of the other tools tested. The time consumption in total is overall for all cases around 13-16 minutes.
- **Thesis tool**'s time performance tied with Z-tools, with Z-tool having faster post processing. It utilizes both parallel simulations and multi-frequency injection much like Z-tool. This leads to relatively fast simulation times. The average time to execute each case for the thesis tool is around 14 minutes to

16 minutes.

4.5.1.2 User Experience

Here the tools are evaluated for their ease of use which includes setting up the tools and running simulations.

- **IMTB**'s user experience is extremely good compared to the other tools covered in this thesis. The tool came with a manual set up in PSCAD which is easily explained in their user guide on GitHub. IMTB is the only tool out of the ones tested that has its own built in graphical user interface (GUI) which simplifies the frequency scan progress immensely. Since this user interface comes pre-packaged with the necessary dependencies, minimal knowledge about Python is needed to run it.
- **SIaD**'s user experience is quite good for users with prior programming knowledge, and it is slightly superior to Z-tool and the Thesis tool in the form of simplicity. When utilized in the context of this thesis, the tool has a standard Python script template that the user can utilize to set up the parameters of the frequency scan.
- **Z-tool**'s user experience is good for a user with prior knowledge about programming but is not as good as SIaD's mostly because it is not clear for the user how to get started. The tool is very versatile in regards to how it allows the user to write their own code and sequences from for the stability analysis. However, for a user with limited prior programming experience setting up these sequences can be very difficult. The simplest way to utilize it is to instead download the examples that they have on GitHub and rewrite their example script. However, at the time of writing this thesis, it is mentioned on the tool's GitHub page that a GUI is in development.
- **Thesis tool**'s user interface performs also slightly below SIAD's but mostly due to the relatively short time frame given for the development of the tool. Like SIaD it uses a main input script where parameters are entered to perform the analysis. Although, unlike SIaD all functions for running the analysis and post processing are not bundled together in one script and is instead split up into different scripts that handle different parts of the analysis. While this gives a more controlled experience for each part, it can make it more confusing for potential users.

4.5.1.3 Stability analysis

This chapter describes in detail the different capabilities the tools have for stability analysis. This includes how well the results from the tools are presented or which stability criteria and capabilities each tool can analyze.

- **IMTB** provides the user the impedance in dq, alpha-beta and the Jacobian matrix form or it gives SISO PN impedance results. It can scan either the grid, converter or both at the same time. The impedances are presented in interactive plots, which the user can use to study the different characteristics of the subsystem under study. However, if the user would like to perform

Nyquist stability or passivity-based analysis, they need to perform such analysis separately.

- **SIAD**'s post scan stability analysis is the most detailed from all tested tools. It offers impedance based stability analysis with Nyquist plots, phase and gain analysis for (SISO), passivity-based analysis as well as modal analysis. The only issue comes from the fact that the tool expects/needs the two systems to be stable when measuring them since it needs to capture the steady state of the system. This means that, if the grid and converter are unstable when connected together, measurements will be distorted by the sustained oscillations and the admittance or the stability analysis will be non conclusive.
- **Z-tool**'s post process analysis allowed for both MIMO Nyquist plots of the eigenvalues and passivity analysis. It did also contain the capability to do gain evaluation of eigenvalues which interestingly enough is a MIMO-gain analysis. However, no phase plots are provided so margins cannot be extracted. Note that Z-tool by default, shows the phase and gain in each impedance plot separately but it does not provide it for the whole system.
- **Thesis tool** provides both the function of performing the impedance based method's of stability analysis and passivity analysis. The impedance based analysis is visualized through a Nyquist plot in the sequence domain. A Nyquist plot of the frequency dependent eigenvalues of the systems open loop transfer function are also provided. With the Nyquist plots, a S-based disk margin is provided to the user pointing out the critical frequency and "distance" to instability. The passivity-based analysis is performed on both the grid and converter. Furthermore, a Bode plot considering only the SISO approach are also provided to observe phase and gain behavior. The tool allows Nyquist plots in both SISO and MIMO definition and the plot is a bit easier to read since it only plots 1 curve for each case instead of two.

4.5.1.4 Tool adaptability

A discussion on the adaptability of each tool is presented here. This refers to how well a tool works in a new environment and if said environment needs changes for the tool to work.

- **IMTB** has worked quite well with the thesis test model provided due to the tools simplicity. While in the early tests it has been affected by the instability of the system at the 30 km grid and power flow of q=-1 this has been due to them being interconnected. IMTB has the ability to measure the converter with no grid connected and vice versa. The tool documentation suggests this as the preferred scan method and following that procedure yields good measurements.
- **SIaD** has some issues regarding the adaptability to new systems. The tool itself has some variable names that could commonly already exist in the model that it is being tested on, which could lead to problems in the postprocessing. Further, the tool needs to have a connection to the grid and if said grid is infinite the tool has been experienced to crash, at least from cases performed in this thesis. Since the tool needs a grid to evaluate the power flow and steady state it becomes problematic when the system is unstable. While it is stated

in the documentation related to this tool that it should be used on systems that are stable this limits its possibility of identifying unstable cases.

- **Z-tool** has similar issues to SIaD tool when it comes to performing impedance scans on infinite AC grids as it also has crashed when used for this thesis. Unlike SIaD, while Z-tool is connected for the last unstable case it still managed to acquire the admittance characteristics of the system without seeing any noise or artifacts. The reason for this is probably due to the systems disconnection method and it having a more robust steady state source recreation. Another metric that was not explored for this thesis but still deserves to be mentioned is the fact that Z-tool can measure multiple POC's at the same time. As long as proper naming of the tool is given to it when implemented into the system, multiple analysis blocks can be active on both the DC and AC side of converters.
- **Thesis tool** works much like IMTB in the sense that it is recommended to measure the grid and converter independently of each other. Like IMTB and unlike SIAD and Z-tool this tool also works with an infinite grid connected if that is sought after, and similar to IMTB this is sometimes even recommended.

4.5.2 TSO converter stability methods and requirements.

The investigation into the requirements for converter interaction stability has led to the conclusion that most of the TSOs do not have any public information about preferred methods or acceptance criteria for converter interaction stability. Moreover, most TSOs agree on methods and requirements for converter interaction stability on a case to case basis. Methods for studying converter interaction stability are suggested by ENTSO-E, Svk, Fingrid and NESO. Entso-E, NESO and Svk suggests EMT simulations and a stability analysis in the frequency domain to study the characteristics of the converter. NESO and ENTSO-E suggests the use of the Nyquist criterion for providing stability margins, while Svk has the most detailed explanation of the requirements for converter interaction stability, with a phase margin limit for low frequencies and full passivity requirement for high frequencies. The method in [26], suggests a way of calculating the admittances using a semi-SISO approach while still taking into account the cross-coupling effect.

Fingrid uses another method of using the ESCR and the N-1 contingency, which is different from the analysis performed using the frequency domain proposed by Svk and NESO. This is a method for the identification of possible instability caused by a converter in a large system. However, for more detailed studies of local interactions between a converter and the grid, the approach is not sufficient, since it does not provide detailed characteristics of the converters behavior but only suggest a possible instability depending on its ESCR. It does not provide any stability margins either, it solely locates the most critical converter with risk of instability in the system.

It is widely regarded that a stability analysis in the frequency domain is the most convenient way of studying converter interaction stability since it provides infor-

mation about the impact of each subsystem on the overall system stability. The stability of the converter interaction is still a relatively new concept, and therefore, many TSOs have not yet established general methods and set standards. Typically, regarding converter interaction stability, requirements are agreed with the connectees upon the start of the connection application process.

4.5.3 SISO vs MIMO calculation method

When the comparison of MIMO and SISO analysis is performed in Figure 4.27, it is noticed that the investigated system did not show much difference in results when comparing the stability analysis of the two calculation methods. The reason for the similarity between the SISO and MIMO comparison is that the grid impedance magnitude is low for the whole frequency range, except around the resonance frequency, meaning that the term $z_p y_{pp}$ is dominant at the positive sequence grid impedance resonance frequency. Note that the positive and negative sequence resonance frequencies are spaced by 100 Hz.
For the case presented in Figure 4.26, both the SISO results and the MIMO results are shown. It is discovered that with the use of a PLL bandwidth of 0.64 p.u different stability outcomes are shown from the Nyquist plots with the use of each approach. The SISO Nyquist plot indicates a stable system while the MIMO Nyquist plot shows an unstable system. With the change of PLL bandwidth, a state was reached where the cross-coupling effect has a more significant impact in the Nyquist plots. Although, the cross coupling impact in this particular case is very small, this highlights the importance of accounting for the cross-coupling effect and to consider the use of a full MIMO stability analysis approach.

4.5.4 Disk vs SISO margin comparison

The use of SISO phase and gain margins presented for both the SISO and Svk approaches, showed accurate interpretations of the system stability. However, the use of phase and gain margins in MIMO systems can be misleading since it does not account for the impact of loop interactions [28].
The use of a Disk margin provides a more robust stability measure, accounting for both phase and gain perturbations simultaneously. Disk margin is also a more appropriate way of computing stability margins in MIMO systems, with multi-loop capability where the impact of loop interactions is considered at the same time. In MIMO systems, perturbations in gain may result in phase shifts hence the importance of considering simultaneous perturbation in both phase and gain. Disk based margins also take into account all frequencies and loop interactions and is not limited to only the crossover frequency, making the margins more reliable. The disk margin applied in the thesis tool is an S-based margin, which means that it has a skew parameter $\sigma = +1$. The strength indicator (SI) has been calculated for the studied systems and it has given a assessment on the system strength, informing that the systems are either weak or of moderate strength.

4.5.5 Admittance scan of an MMC and steady state effects

As stated before, an admittance scan has been performed on the PSCAD example model of an MMC-based HVDC-converter to observe the impact of a more detailed converter model on the frequency scan. The primary effect is the impact of the perturbation magnitude on obtained admittances. As can be seen in Figure 4.21, different amplitudes showed differing effects on the results. A simulation without perturbation has been run and the steady state variation in RMS voltage has been found to be approximately 0.7 kV (see Figure 4.22). Thus the pre injection noise is around 0.2% which is larger than the 0.1% injection magnitude resulting in the noisy measurement. The other two perturbations with magnitudes of 1% and 5% give less noisy results since their amplitudes are larger than the amplitude of the noise. However, it can be seen that the injection amplitude of 5% started to deviate from the other measurements, most likely, due to the fact that the large perturbation started to excite non-linearities of the converter. The main finding of the MMC study is that for a more complex system is that the injection amplitude must be adjusted according to the background noise while not becoming so large as to excite the non-linearities of the converter.

4.5.6 Frequency resolution

For the initial analysis of the system, a frequency step of 5 Hz was applied. However, the low frequency resolution resulted in measured admittances and impedances being largely different compared to the linearized converter and ac grid models. This is because, the low frequency resolution missed the resonance peaks, especially in the case studied in this thesis where the ac grid resonance is very high. A comparison between the accuracy of two different resolutions are shown in Figure 4.32 and in Figure 4.33.

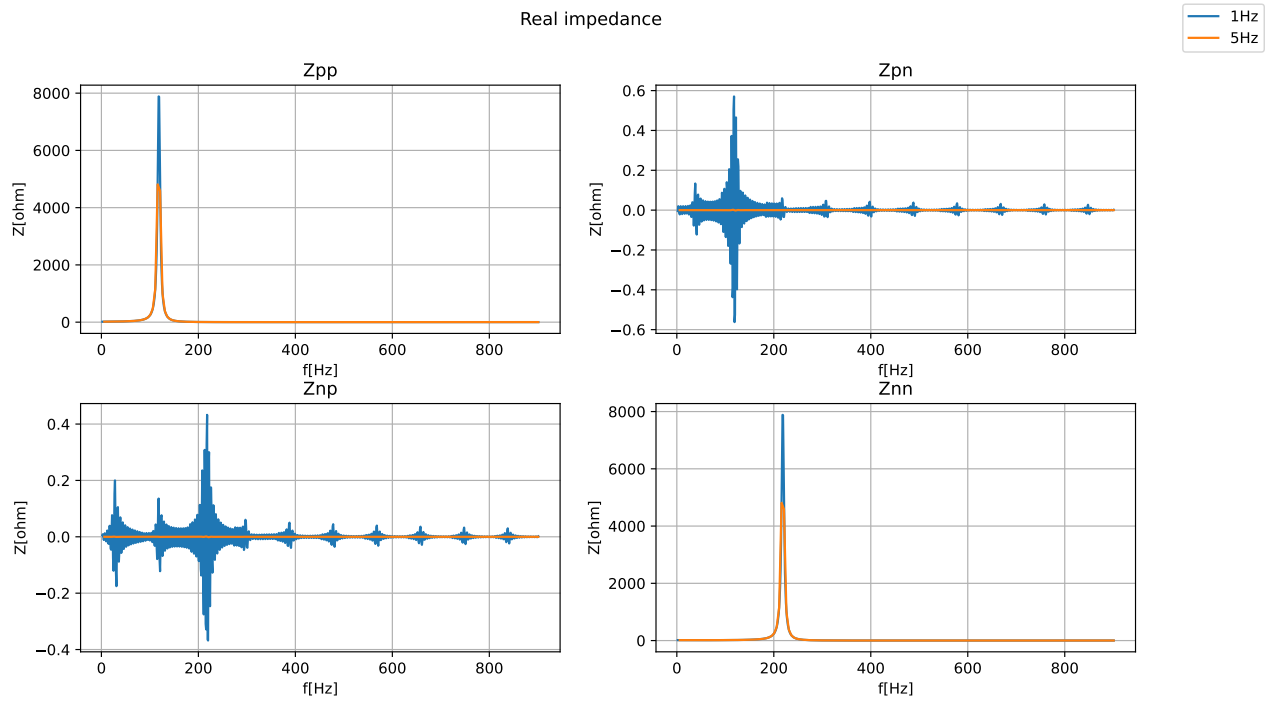

Figure 4.32: Grid real impedance scan for a 20 km long cable for injections with frequency steps of 1Hz and 5Hz.

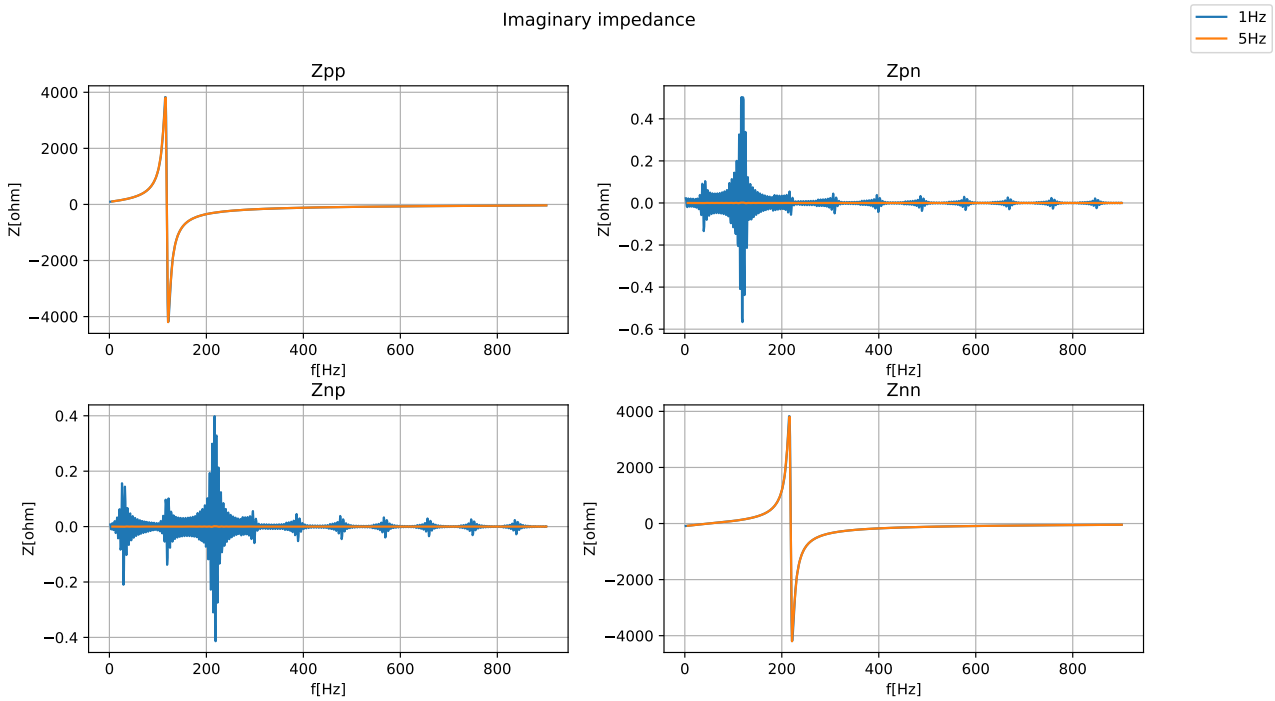

Figure 4.33: Grid imaginary impedance scan for a 20 km long cable for injections with frequency steps of 1Hz and 5Hz.

As can be seen in the plots above, impedance measurements with injections of 5 Hz step manages to measure the impedance well throughout the whole frequency range, except at the resonance, where the measured peak is significantly lower compared to impedance of the linearized model. Due to this phenomena there is a need for higher frequency resolution around the resonance frequency for these cases, when post analysis is performed the converter admittance can be solved by interpolation during said resonance points

5
Conclusion

This thesis investigates converter interaction stability methods, tools and challenges with a converter integrated power system. The theory and methods behind these tools have been studied for better understanding, along with current methods and requirements by TSOs in the industry.

This thesis has investigated different approaches for impedance calculation. Svk's proposed approach for computing the admittances has been tested and compared with the MIMO and SISO approaches. The result of the comparison yielded minor differences between the prior mentioned approaches, due to small cross-coupling effect of the system in consideration. This indicates that with weak cross-coupling effect SISO analysis can provide good stability approximations. For assessment of stability margins in MIMO systems, the disk margin approach is appropriate, as it is capable of multi-loop interactions and consider both phase and gain perturbations simultaneously.

Among the evaluated sources for TSO requirements, only Svk provides clear guidelines for converter interaction stability analysis. A possible explanation for this is that converter interaction stability is a relatively new phenomenon, and therefore requirements are set by TSOs on a case-by-case basis. General methods are discussed by ENTSO-E, Fingrid and NESO, and these include a frequency injection followed by an impedance based stability assessment, as well as ESCR evaluation and timed domain evaluation.

The tools investigated in this thesis all showed reliable performance when admittance scans are carried out. However, they differ in terms of computational efficiency, stability assessment, adaptability, and ease of use. The thesis tool attempts to address for these different shortcomings by achieving performance comparable to the most efficient tools thanks to multi-frequency injections while providing improved adaptability and enhanced post-processing capabilities compared to existing solutions. The thesis also contributes by providing insight into the established analysis methods as well as the exploration of new ones in respects to margin analysis and stability evaluation.

The findings of this thesis show that methodological choices and tool implementation plays a large role regarding stability assessment conclusions. With the rise of converter integration the need for robust and reliable analysis methods and tools will be increasingly important to ensure stable system operation.

5.1 Future work

Although this thesis has performed various tests and investigation there is still some further points that would be interesting to continue on:

1. Deeper analysis of grids with large cross-coupling terms to further see eventual differences between MIMO and SISO analysis.
2. Stability analysis with multiple converters.
3. Aggregation of system impedances. In several cases the frequency admittances/impedances from different components are provided separately. As such a way to aggregate these components together is of interest
4. Further analysis of perturbation size and multi-frequency perturbations to see if there are any issues that could be caused by too high an injection amplitude or too many multi-frequency injections.
5. Investigation on selection of appropriate margins for stability analysis.

Bibliography

[1] Eurostat, "Shedding light on energy in europe – 2025 edition." `https://ec.europa.eu/eurostat/web/interactive-publications/energy-2025`, 2025. Interactive publication.

[2] ENTSOE, "Entso-e hvdc utilisation and availability statistics 2024," tech. rep., European Network of Transmission System Operators for Electricity, 2025.

[3] M. Beza and M. Bongiorno, "Impact of converter control strategy on low- and high-frequency resonance interactions in power-electronic dominated systems," *International Journal of Electrical Power Energy Systems*, vol. 120, p. 105978, 2020.

[4] M. A. Quester, *Investigating Converter Control Interactions in the Transmission Grid*. Doctoral dissertation, RWTH Aachen University, Aachen, Germany, July 2021. Approved by the Faculty of Electrical Engineering and Information Technology.

[5] V. Yellisetti and A. Moser, "Complexity reduction for converter-driven stability analysis in transmission systems," *Electronics*, vol. 14, no. 1, 2025.

[6] C. Carlsson and E. Larsson, "Detection of emerging stability phenomena in the future swedish power system – comparing rms-based and waveform-based detection techniques for power systems dominated by power electronics," master's thesis, Linköping University, Department of Electrical Engineering, Linköping, Sweden, 2024. LiTH-ISY-EX–24/5678–SE.

[7] J. Sun, "Impedance-based stability criterion for grid-connected inverters," *IEEE Transactions on Power Electronics*, vol. 26, no. 11, pp. 3075–3078, 2011.

[8] T. Roose, D. Lee, and J. Beerten, "Hybrid mimo method for impedance-based stability analysis of mtdc systems," *International Journal of Electrical Power Energy Systems*, vol. 172, p. 111254, 2025.

[9] F. J. Cifuentes Garcia, T. Roose, C. Sakinci, D. Lee, L. Dewangan, E. Avdiaj, and J. Beerten, "Automated frequency-domain small-signal stability analysis of electrical energy hubs," in *2024 IEEE PES Innovative Smart Grid Technologies Europe (ISGT EUROPE)*, pp. 1–6, 2024.

[10] G. Wu, Y. He, H. Zhang, X. Wang, D. Pan, X. Ruan, and C. Yao, "Passivity-based stability analysis and generic controller design for grid-forming inverter," *IEEE Transactions on Power Electronics*, vol. 38, no. 5, pp. 5832–5843, 2023.

[11] E. M. Schöll and U. Nopp-Mayr, "Impact of wind power plants on mammalian and avian wildlife species in shrub- and woodlands," *Biological Conservation*, vol. 256, p. 109037, 2021.

[12] B. Lennartsson, *Reglerteknik: Grundläggande teori*. Lund, Sweden: Studentlitteratur, 3 ed., 2006.

[13] F. J. Cifuentes Garcia and J. Beerten, "Z-tool: Frequency-domain characterization of emt models for small-signal stability analysis," *Electric Power Systems Research*, vol. 252, p. 112405, 2026.
[14] J. Wang, A. R. Zamani, M. Beza, M. Bongiorno, A. Narula, and J. R. Svensson, "A frequency-domain stability margin indicator for grid-connected converter systems," in *2025 IEEE Energy Conversion Conference Congress and Exposition (ECCE)*, pp. 1–8, 2025.
[15] ENERGINET, "Imtb-github," 2025.
[16] J. Sun, "Frequency-domain stability criteria for converter-based power systems," *IEEE Open Journal of Power Electronics*, vol. 3, pp. 222–254, 2022.
[17] G. Pinares, "Pv tool deliverable 2.2." 2019.
[18] L. A. Garcia-Reyes, O. Gomis-Bellmunt, E. Prieto-Araujo, V. A. Lacerda, and M. Cheah-Mañe, "Siad-tool: A comprehensive frequency-domain tool for small-signal stability and interaction assessment in modern power systems," 2026.
[19] M. Beza and M. Bongiorno, "Identification of resonance interactions in offshore-wind farms connected to the main grid by mmc-based hvdc system," *International Journal of Electrical Power Energy Systems*, vol. 111, pp. 101–113, 2019.
[20] MathWorks, "Passivity indices," n.d. MATLAB Control System Toolbox Documentation.
[21] A. Rygg, M. Molinas, C. Zhang, and X. Cai, "A modified sequence-domain impedance definition and its equivalence to the dq-domain impedance definition for the stability analysis of ac power electronic systems," *IEEE Journal of Emerging and Selected Topics in Power Electronics*, vol. 4, no. 4, pp. 1383–1396, 2016.
[22] O. P. Prabha S.Kundur, *Power System Stability and Control, Second edition.* McGraw Hill, 2022.
[23] A. Rygg, M. Molinas, C. Zhang, and X. Cai, "On the equivalence and impact on stability of impedance modeling of power electronic converters in different domains," *IEEE Journal of Emerging and Selected Topics in Power Electronics*, vol. 5, no. 4, pp. 1444–1454, 2017.
[24] S. Shah, "Impedance of three-phase systems in dq, sequence, and phasor domains." IEEE PES Webinar, National Renewable Energy Laboratory (NREL), 2020. NREL/PR-5D00-77669, August 18, 2020.
[25] G. Pinares and M. Bongiorno, "Independent channel design approach for stability analysis of grid-connected converters," *Electric Power Systems Research*, vol. 189, p. 106774, 2020.
[26] O. Lennerhag, "Managing stability in the future converter-dominated swedish power system," *CIGRE NRCC paper*, 2025.
[27] MathWorks, "Gain Margin, Phase Margin, and Crossover Frequencies." `https://se.mathworks.com/help/control/ref/dynamicsystem.margin.html`, 2026. Accessed: 12 May 2026.
[28] P. Seiler, A. Packard, and P. Gahinet, "An introduction to disk margins [lecture notes]," *IEEE Control Systems Magazine*, vol. 40, no. 5, pp. 78–95, 2020.
[29] H. Zou, Z. Tang, T. Hu, and G. Todeschini, "A disk-based margin indicator for stability assessment of multiconverter power systems," *IEEE Journal of*

Emerging and Selected Topics in Power Electronics, vol. 14, no. 2, pp. 1685–1696, 2026.

[30] MathWorks, "Disk-based gain and phase margins," n.d. Accessed: 2026-05-25.

[31] ENTSO-E, "Interactions between hvdc systems and other connections," implementation guidance document, European Network of Transmission System Operators for Electricity (ENTSO-E), Brussels, Belgium, Mar. 2018.

[32] Svenska kraftnät, "Vägledning – utökade systemstudier vid risk för oönskad interaktion," tech. rep., Svenska kraftnät, 2025. Intern publikation. Tillhandahålls på begäran via Svenska kraftnät.

[33] R. Korhonen, V. Hytti, P. Partinen, and M. Lindroos, "Tso experience with converter driven stability management in outage planning," in *23rd Wind Solar Integration Workshop (WIW 2024)*, vol. 2024, pp. 383–388, 2024.

[34] National Energy System Operator (NESO), "Guidance on oscillation assessment for inverter based resources (ibrs)," tech. rep., National Energy System Operator, September 2025. Accessed: 2026-05-18.

[35] Electa-Git, "Z-tool: A python-based implementation for the frequency-domain stability analysis of modern power systems." `https://github.com/Electa-Git/Z-tool`, 2026. Version v0.1.40.

[36] B. P. Lathi and R. Green, *Signal Processing and Linear Systems*. New York: Oxford University Press, 2nd ed., 2021.

[37] PSCAD Inc., "Pscad knowledge base article 234." `https://www.pscad.com/knowledge-base/article/234`. Accessed May 8, 2026.

A

Appendix 1

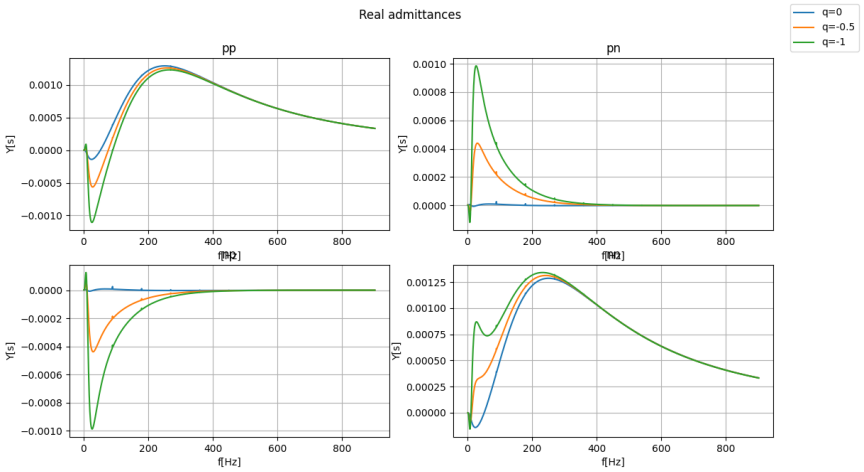

Figure A.1: Real sequence domain converter admittance characteristics from the thesis tool for a 20km long line

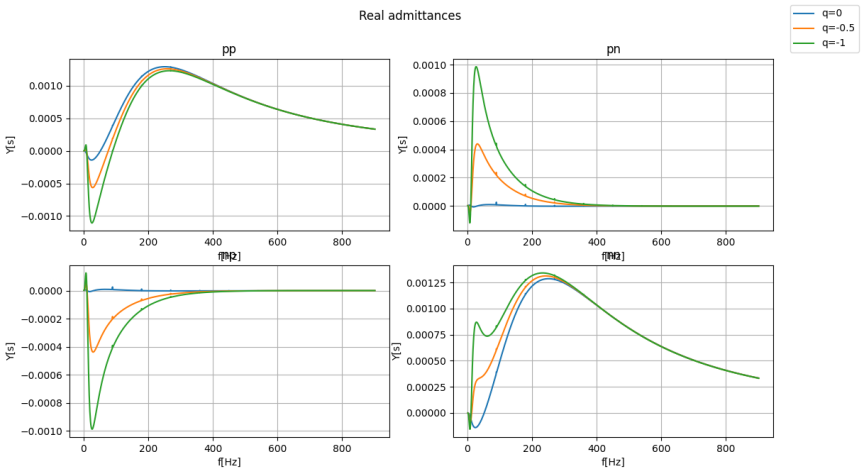

Figure A.2: Imaginary sequence domain converter admittance characteristics from the thesis tool for a 20km long line

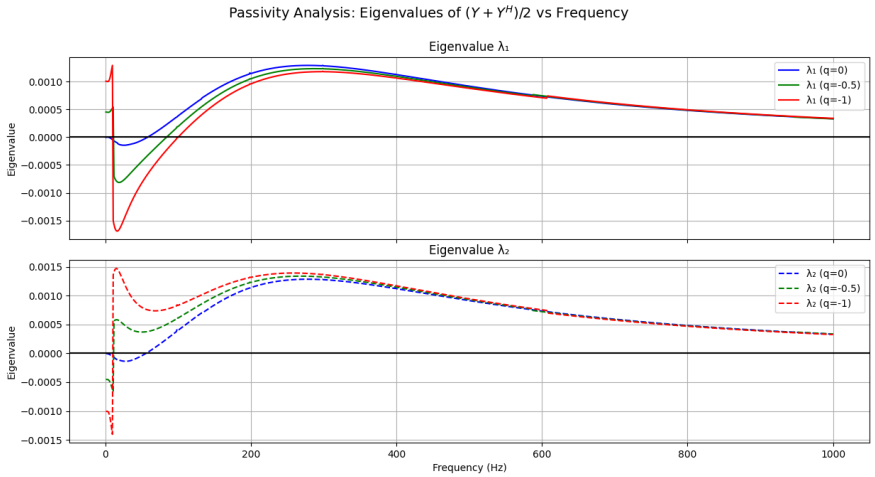

Figure A.3: Plot of the eigenvalues of $Y + Y^H$ for a 20 km long line using the thesis tool

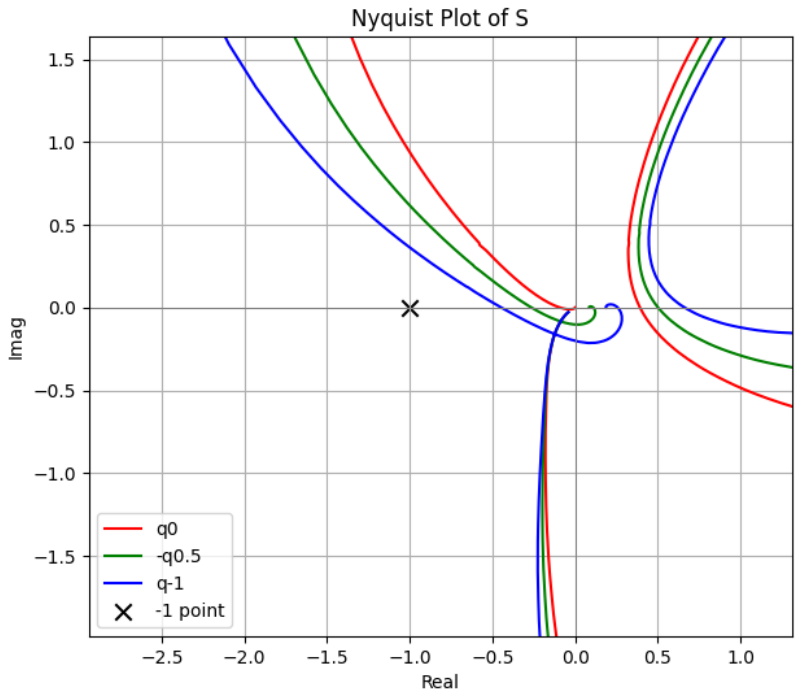

Figure A.4: Nyquist plot for the case of 20 km long line using the thesis tool

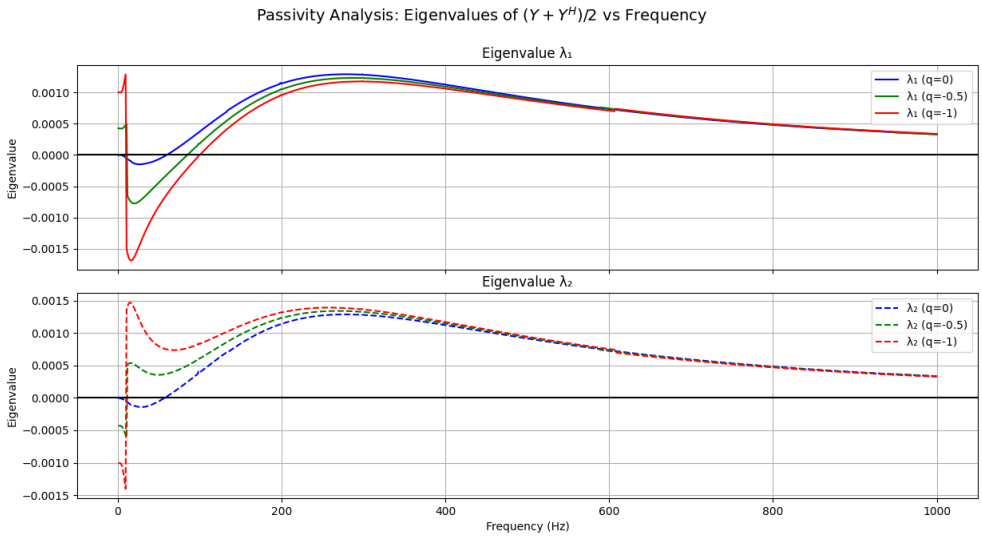

Figure A.6: Plot of eigenvalues of $Y + Y^H$ of a 30 km long line

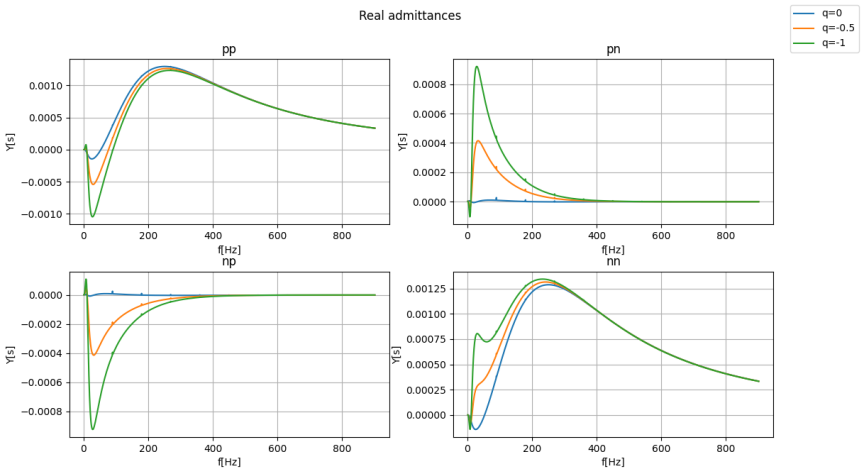

Figure A.5: Real admittance characteristics of the DUT for the different power flow settings

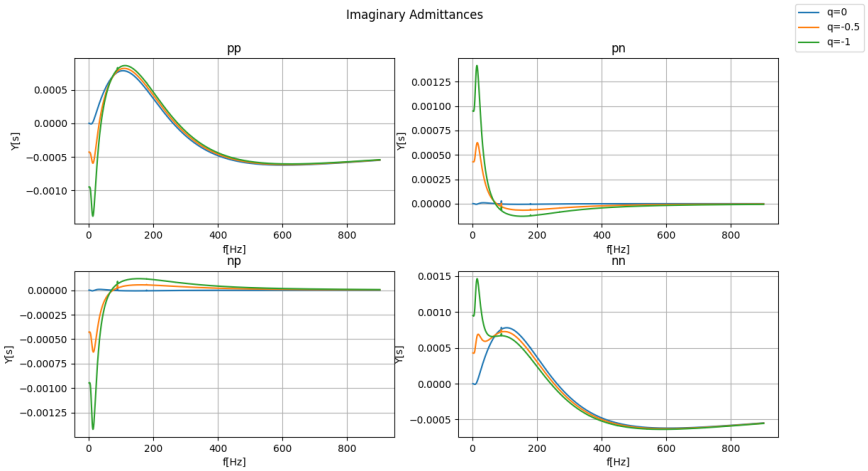

Figure A.7: Imaginary admittance characteristics of the DUT for the different power flow settings

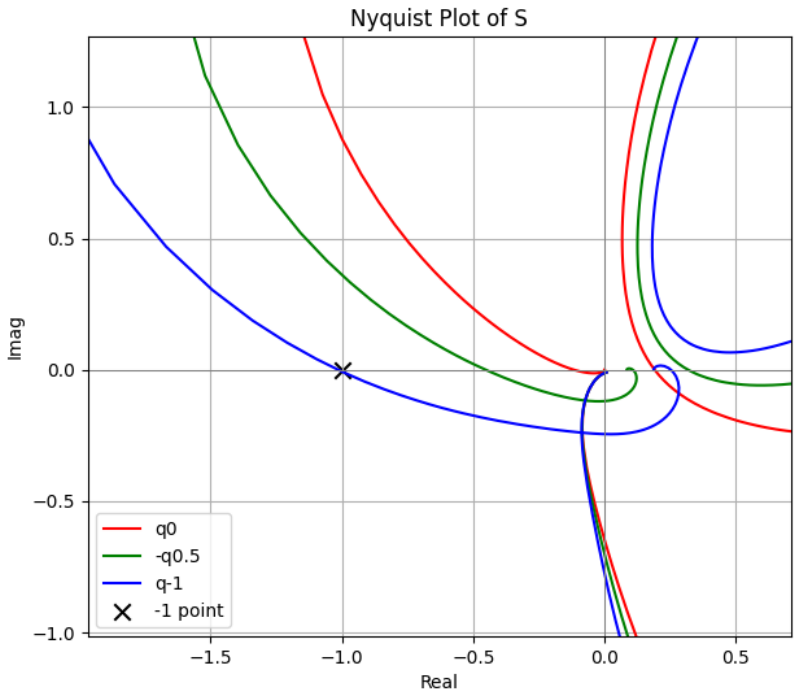

Figure A.8: Nyquist plot generated by ADMeasure for 30 km line length

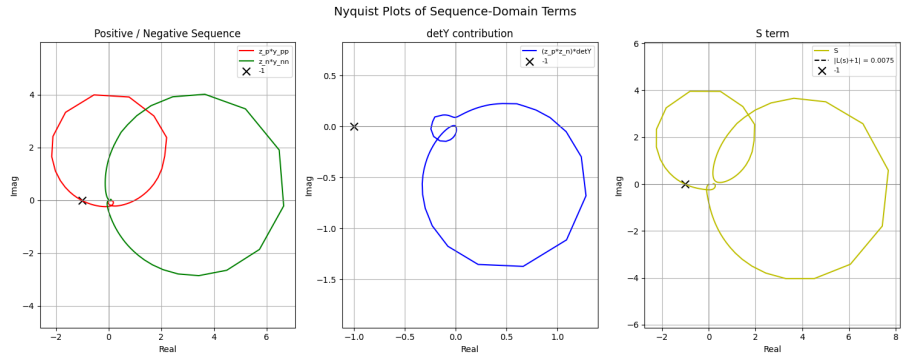

Figure A.9: Nyquist plot from the thesis tool of sequence components for q=-1, 30 km cable.

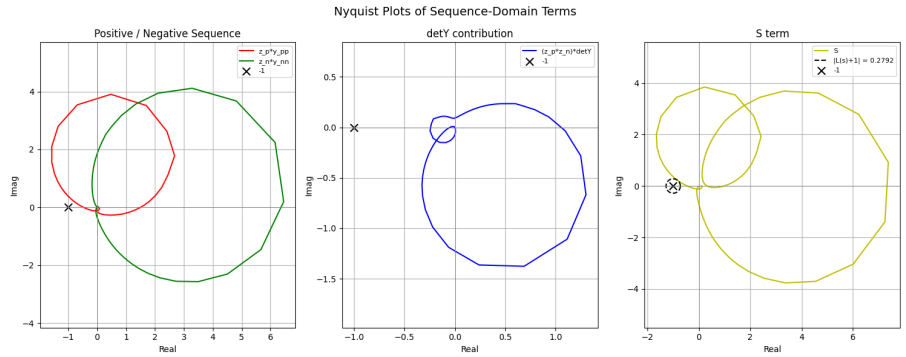

Figure A.10: Nyquist plot from the thesis tool of sequence components for q=-0.5, 30 km cable

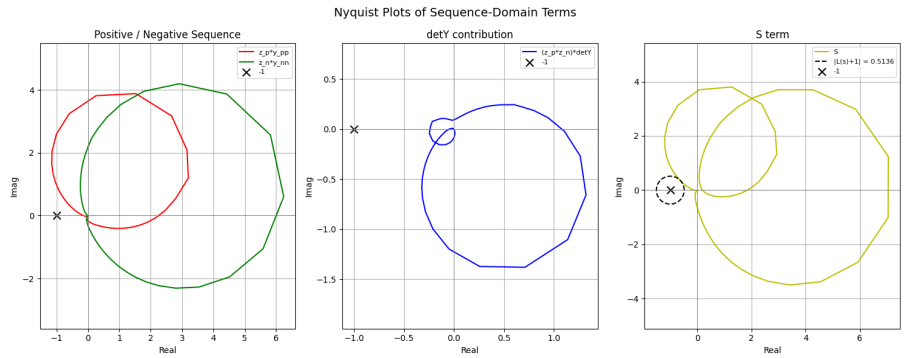

Figure A.11: Nyquist plot from the thesis tool of sequence components for q-0, 30 km cable

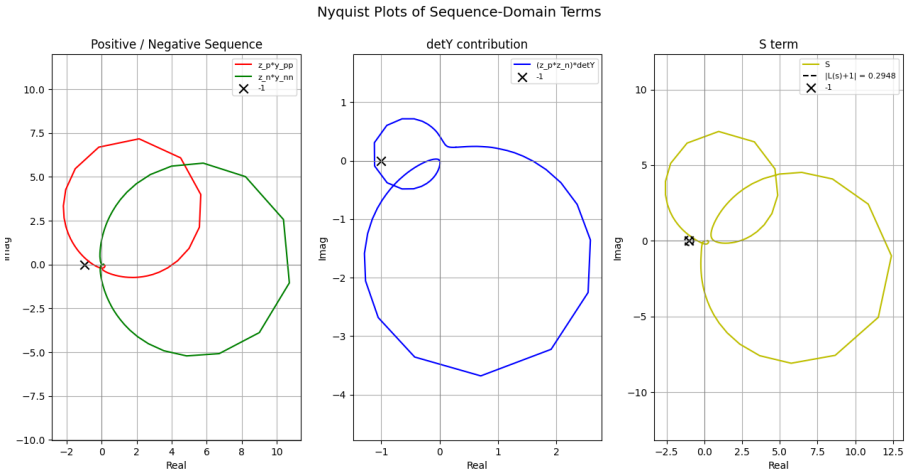

Figure A.12: Nyquist plot from the thesis tool of sequence components for q=-1, 20 km cable.

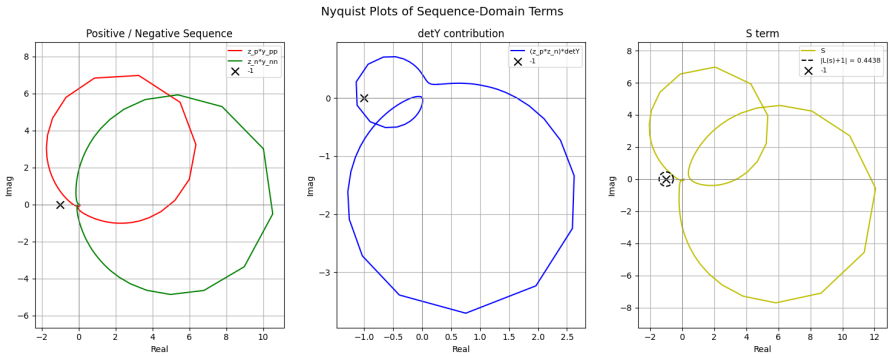

Figure A.13: Nyquist plot from the thesis tool of sequence components for q=-0.5, 20 km cable

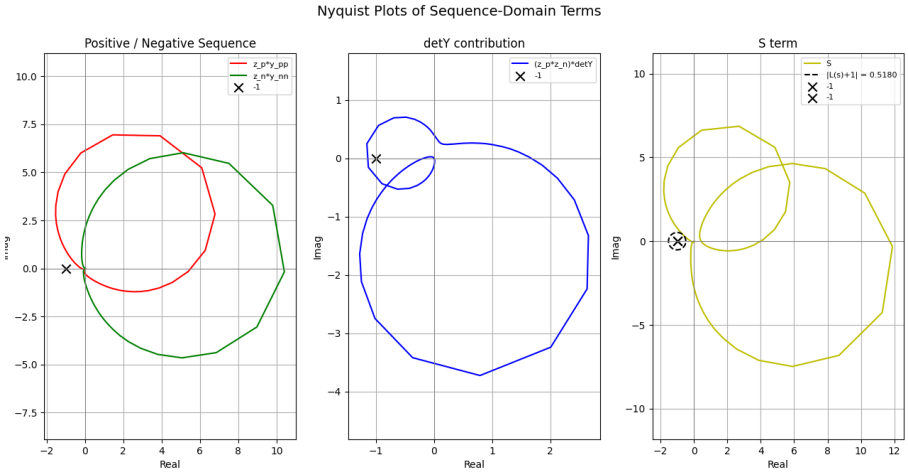

Figure A.14: Nyquist plot from the thesis tool of sequence components for q=0, 20 km cable

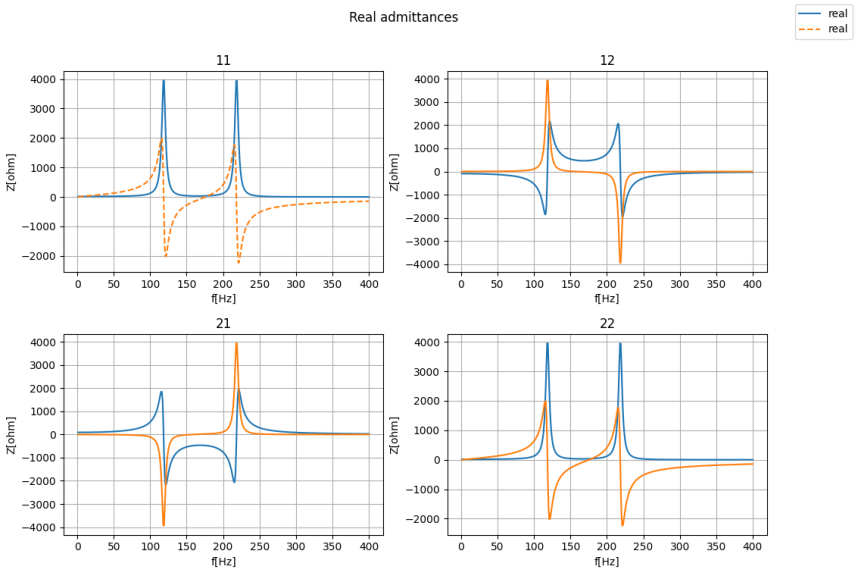

Figure A.15: Grid side impedance characteristics captured by IMTB for a 20km line

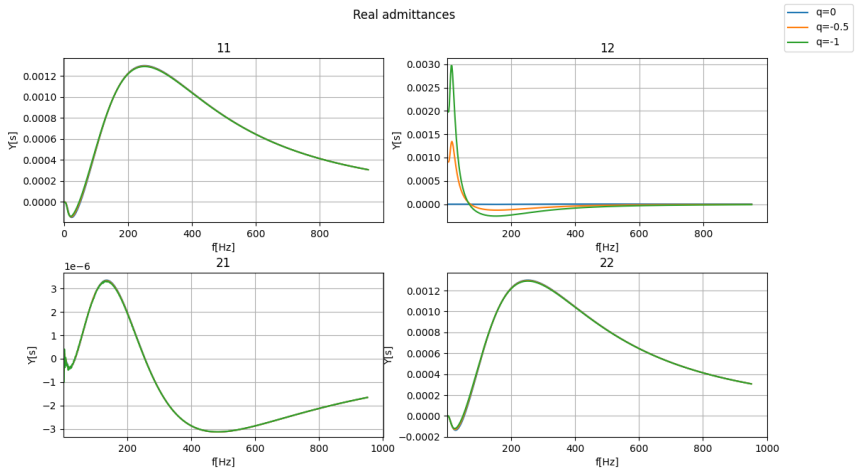

Figure A.16: Real dq admittance characteristics captured by IMTB for a 20km long line

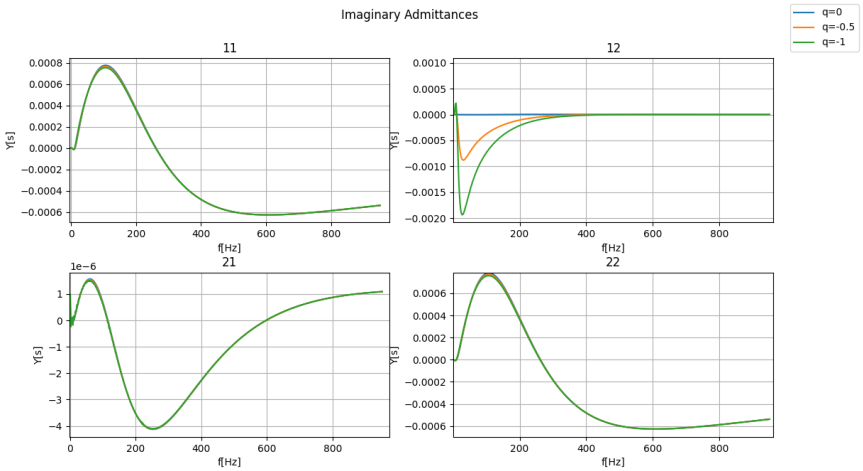

Figure A.17: Imaginary dq admittance characteristics captured by IMTB for a 20km long line

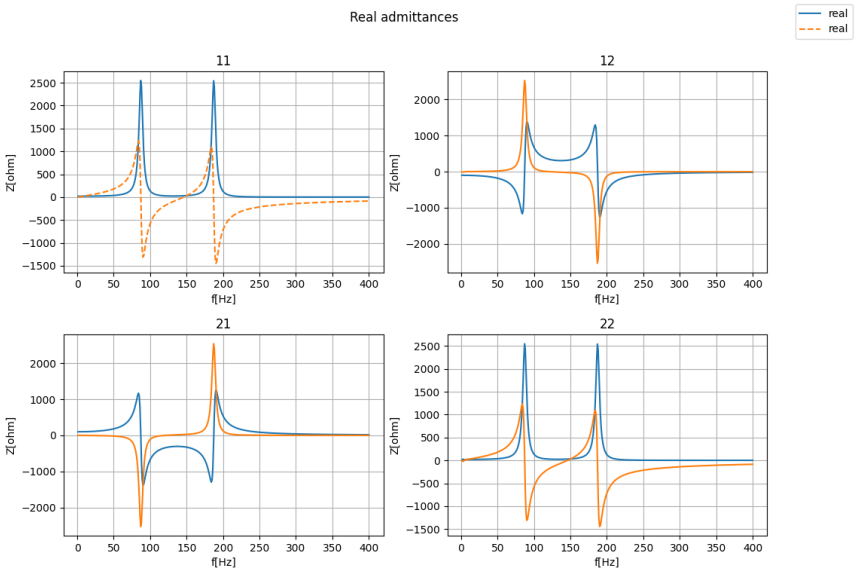

Figure A.18: Grid side impedance characteristics captured by IMTB for a 30km line

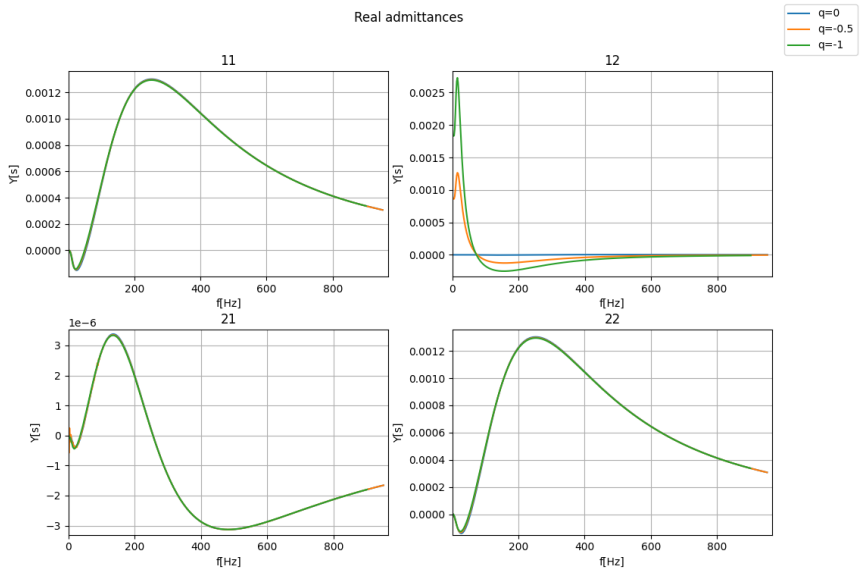

Figure A.19: Real dq admittance characteristics captured by IMTB for a 30km long line

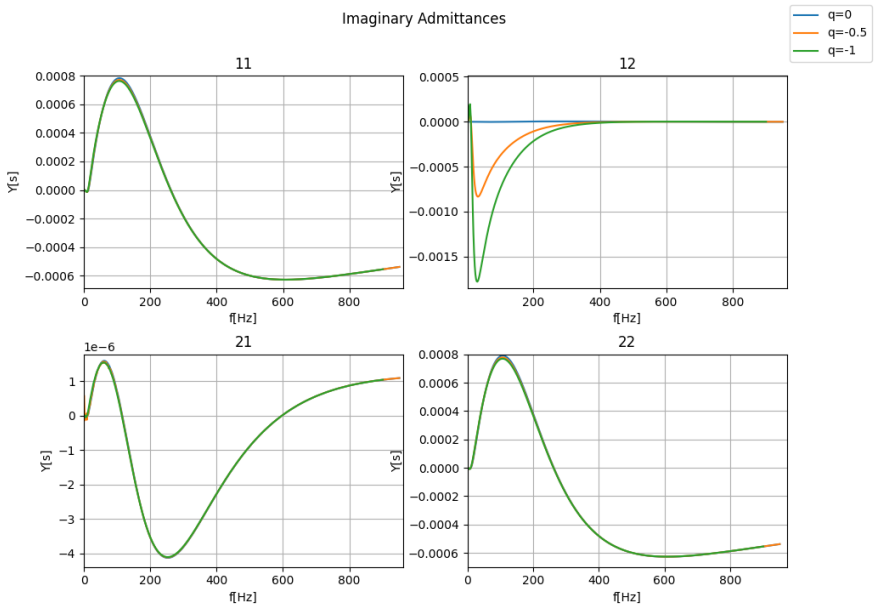

Figure A.20: Imaginary dq admittance characteristics captured by IMTB for a 30km long line

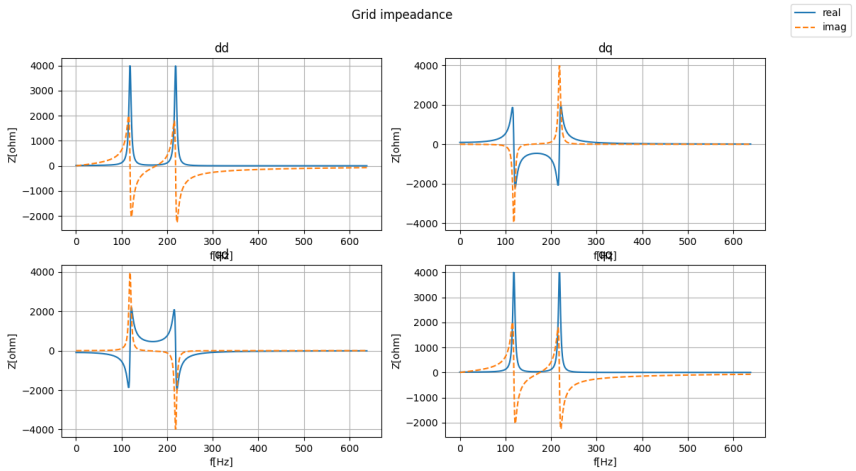

Figure A.21: Grid dq Characteristic measurement result from Z-tool for a 20 km line

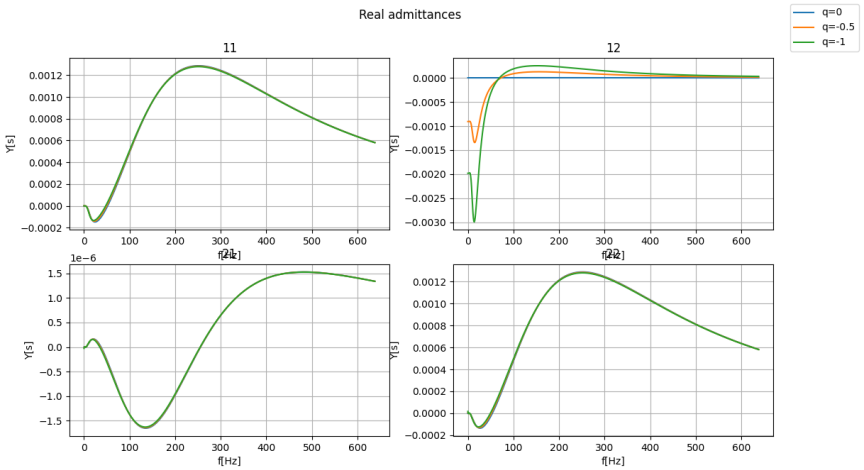

Figure A.22: Real dq admittance characteristic from Z-tool for a 20 km line

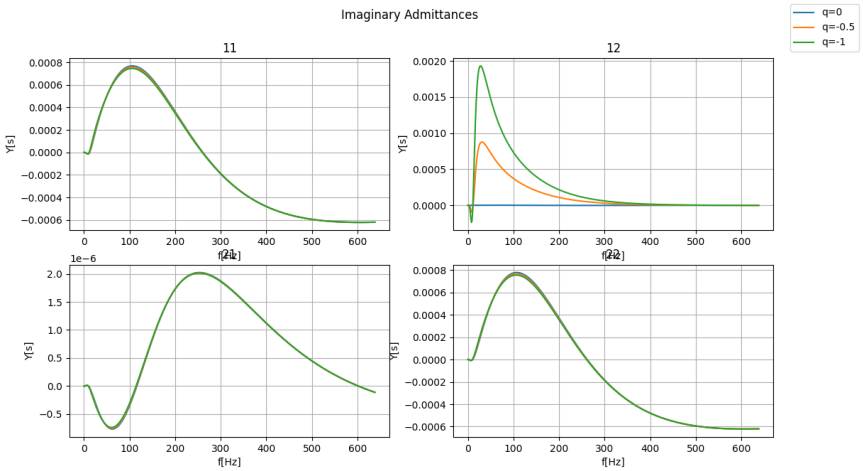

Figure A.23: Imaginary dq admittance characteristic for a 20km line

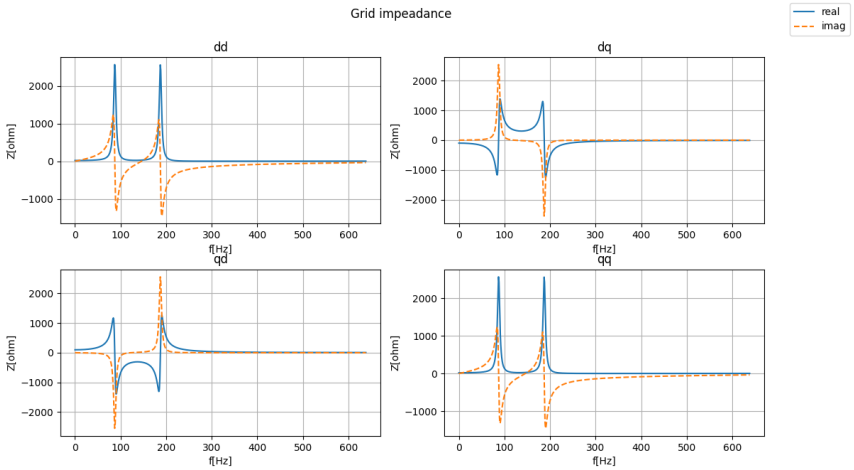

Figure A.24: Grid dq Characteristic measurement result from Z-tool for a 30 km line

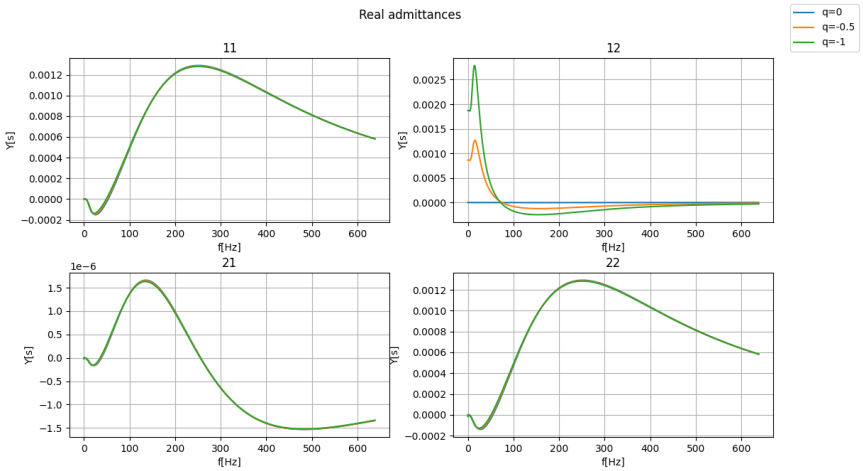

Figure A.25: Real dq admittance characteristic from Z-tool for a 30 km line

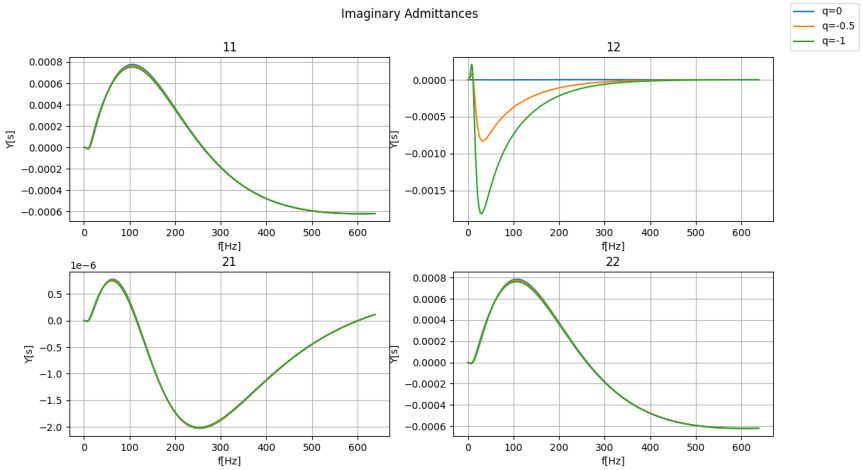

Figure A.26: Imaginary dq admittance characteristic from Z-tool for a 30km line

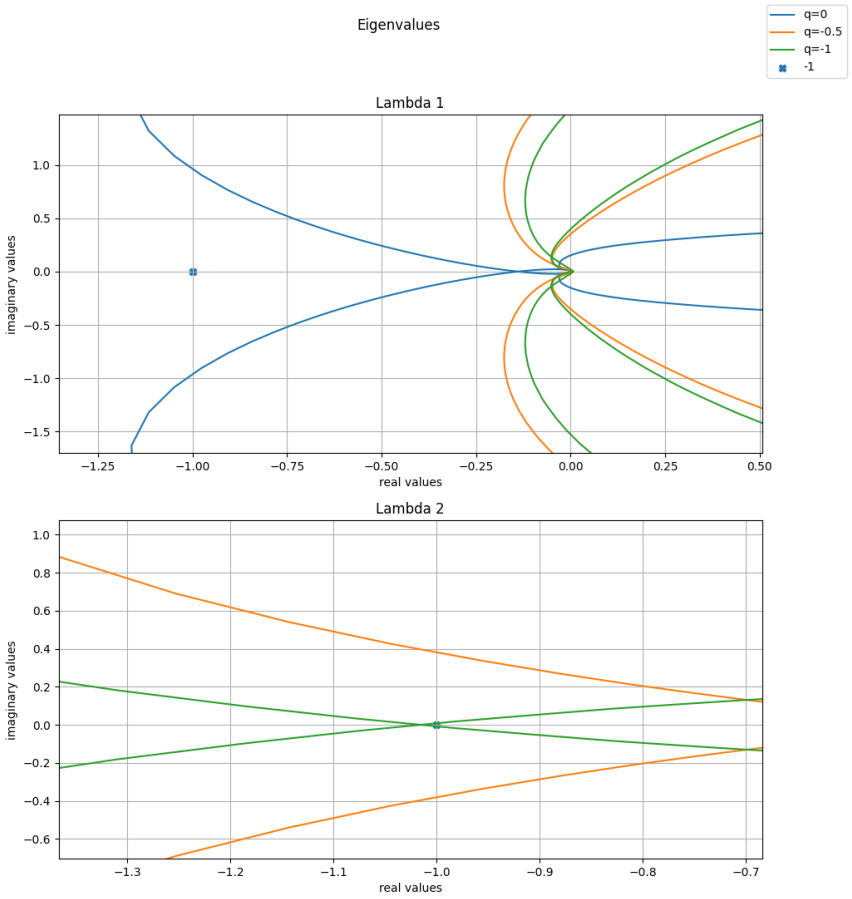

Figure A.27: Nyquist values provided from Z-tools gnc function, zoomed in at around -1

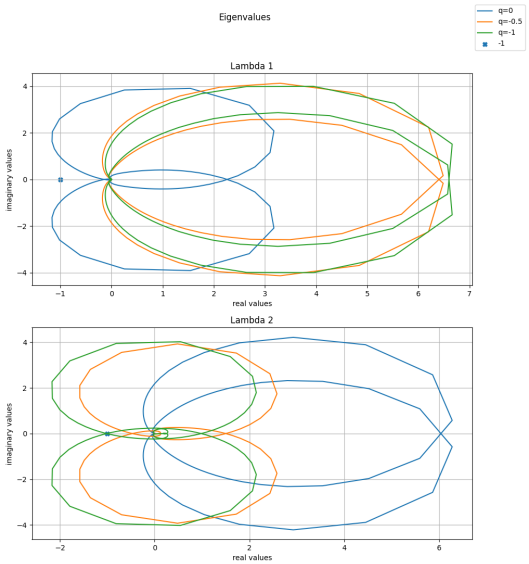

Figure A.28: Full nyquist plot from the 30km z-tool case

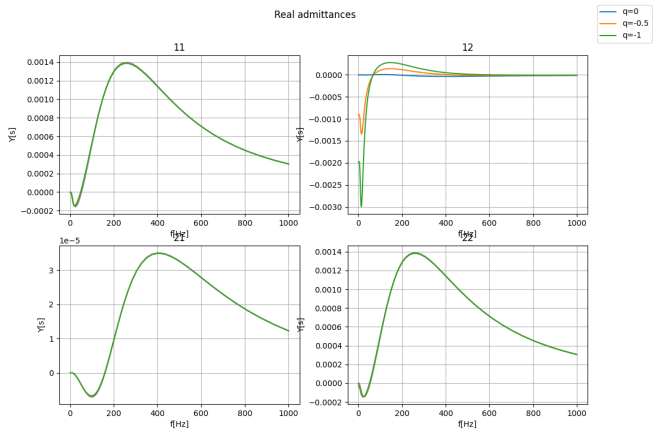

Figure A.29: Real admittance plot from SIAD for a 20 km line

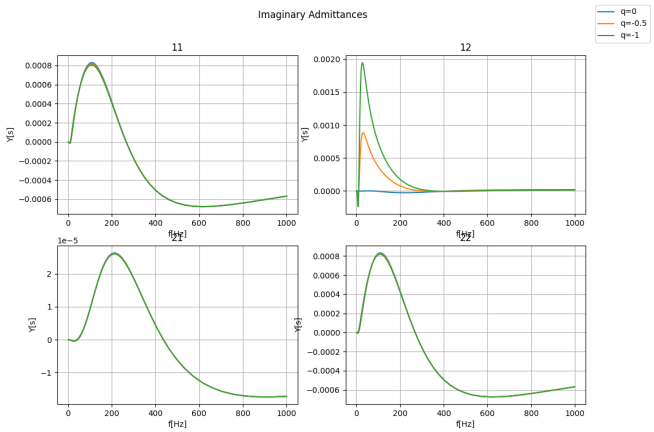

Figure A.30: Imaginary admittance plot from SIAD for a 20 km line

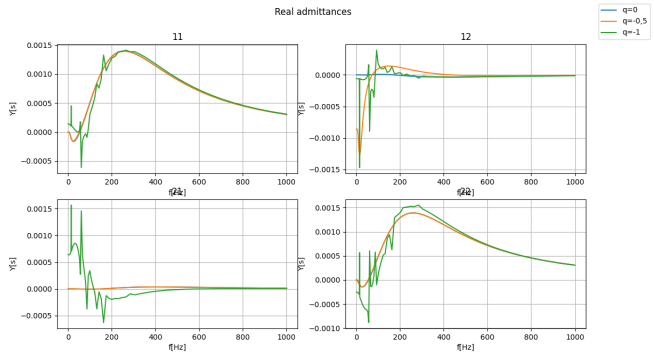

Figure A.31: Real admittance plot from SIAD for a 30 km line

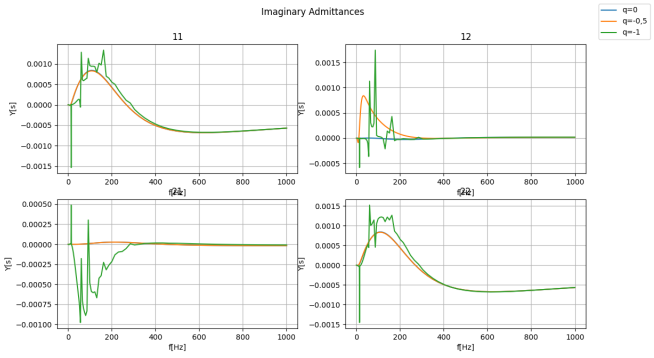

Figure A.32: Imaginary admittance plot from SIAD for a 30 km line

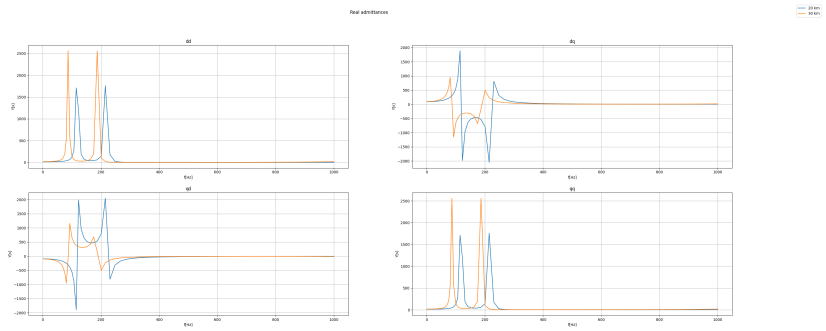

Figure A.33: Plot of real impedances from the SIaD tool for the 20 and 30 km cases.

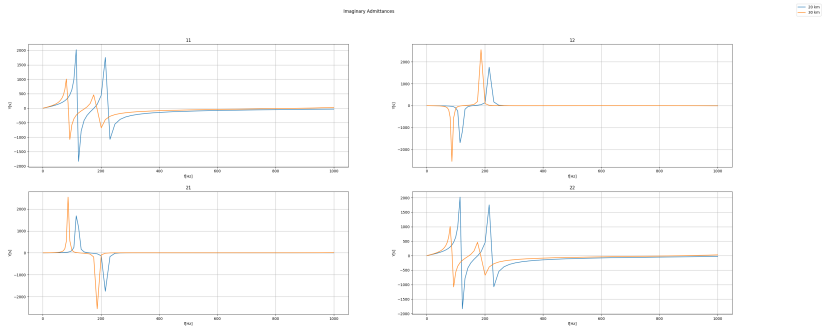

Figure A.34: Plot of imaginary impedances from SIaD tool for the 20 and 30 km cases.

DEPARTMENT OF SOME SUBJECT OR TECHNOLOGY
CHALMERS UNIVERSITY OF TECHNOLOGY
Gothenburg, Sweden
www.chalmers.se

CHALMERS
UNIVERSITY OF TECHNOLOGY